

**RICCATI GENERALIZED SOLITARY WAVE SOLUTIONS
OF NONLINEAR EQUATIONS**

A Thesis
Submitted to the
FACULTY OF SCIENCE
PANJAB UNIVERSITY, CHANDIGARH
for the degree of
DOCTOR OF PHILOSOPHY

2014

SHALLY LOOMBA

DEPARTMENT OF PHYSICS
CENTRE OF ADVANCED STUDY IN PHYSICS
PANJAB UNIVERSITY
CHANDIGARH, INDIA

Dedicated to my parents.

Acknowledgement

First and foremost, I would like to express my gratitude to my supervisor Prof. C. Nagaraja Kumar, Professor, Department of Physics, Panjab University, Chandigarh for his encouragement, continuous support, generous and expert guidance throughout the course of my research work. Without his knowledge and assistance, this study would not have been possible.

I am also grateful to Dr. T. Solomon Raju and Mr. M. S. Mani Rajan for their co-operation and useful suggestions at various times.

I express my sincere thanks to the Chairman, Department of Physics, Panjab University for providing me the required facilities in the department. I am also thankful to all the staff members of Department of Physics, Panjab University for their help during this work.

I would like to acknowledge my fellow labmates Mr. Amit Goyal, Mr. Vivek Sharma, Ms. Rama Gupta, Ms. Harleen Kaur, and Mr. Kanchan Kumar De for their contribution in the accomplishment of various research projects. I sincerely thank Ms. Rama Gupta for the stimulating discussions and her valuable suggestions that helped me a lot to tackle the problems, arisen during the course of research work.

I am deeply indebted to my father Mr. Anil Kumar Loomba and mother Mrs. Meenu Loomba for all the accomplishments in my life. I am also grateful to the family of my parents and my in-laws for their blessings and support. My heartfelt thanks goes to my loving sisters Shweta, Swati and my brother-in laws for their inspiration, constant affection and care.

I owe a special thanks to my husband Mr. Gaurav Sharma for his motivation, support and helpful advice. This thesis would not have been completed without his continuous co-operation and endless encouragement.

Above all, I am humbly grateful to Almighty for granting me the strength to undertake this research work and helping me overcome all obstacles.

I am bound to have missed expressing my gratitude to some deserving names whom I have forgotten to include here. Nonetheless, I sincerely thank each and every one of them as each major and minor interaction with them helped mould and guide this work in its own measure.

Date:

Shally Loomba

Abstract

We study the nonlinear localized solutions and their Riccati generalization for the variants of inhomogeneous generalized nonlinear Schrödinger equation. In this regard, we consider two different fields: (i) nonlinear fiber optics (ii) Bose-Einstein condensates (BECs). In both the cases, the nonlinear excitations arise due to the balancing of dispersive and nonlinearity terms.

There has been a surge of interest for investigating rogue wave propagation through different nonlinear optical fibers and waveguides due to their possible applications in carrying large amount of energy. The governing model for these physical systems is the inhomogeneous generalized nonlinear Schrödinger equation (GNLSE). We have obtained the optical rogue wave solutions for GNLSE with the aid of self-similarity transformation and investigated the interesting features of rogue waves as they travel through dispersion increasing and decreasing fibers. To overcome the inherent losses experienced by the pulses during propagation, we have discussed the role of doping of the fiber core with erbium atoms. We have then studied the rogue waves propagation through the erbium doped fiber system and predicted a mechanism to get their controllable recurrence and annihilation characteristics. Additionally, we have made use of the analogy between “dispersion in time” for fibers and “diffraction in space” for waveguides to analyse the optical rogue wave propagation through tapered graded-index nonlinear waveguide in different management regimes. For the nonlinearity management regime we investigate the effects of modulated tapering profiles on the intensity of optical rogue waves. This is accomplished by invoking isospectral Hamiltonian technique, which enables us to identify a large manifold of allowed tapering profiles. It reveals that the intensity of rogue waves can be made very large for specific choices of tapering profile and thus paves the way for experimental realization of highly energetic waves in nonlinear optics.

We have further explored tapered graded-index nonlinear waveguides for optical similaritons. Optical similaritons are self-similar waves which adjust themselves in accordance with the system parameters and hence are of great practical relevance. Consequently, we have examined the nonlinear tunneling properties of optical similaritons for different cases and predicted a way which allows us to get the optical similaritons of desired width at desired location. The results obtained

may be useful to study nonlinear optical devices based on similaritons.

We have also studied rogue waves for quasi-one-dimensional Gross-Pitaevskii (GP) equation, with space and time dependent trapping potential, which describes the wave propagation in BECs. We have shown the controllable dynamics of rogue waves for the cases where the condensate is subjected to different forms of external potential. This analysis shows the possibility of studying rogue waves in various experimentally relevant systems. By employing self-similarity transformation, we have also studied the controllable self-similar matter waves for the special case of quasi-one-dimensional GP equation where the condensate is under the influence of expulsive parabolic trapping potential. In this regard, we present a systematic analytical approach to generate the class of nonlinearity parameter by using Riccati generalization for a given trapping potential, within the integrability framework of GP equation. This enables us to control the intensity profiles of self-similar matter waves by tuning the Riccati parameter.

Contents

Acknowledgement	iii
Abstract	v
List of Figures	xi
1 Introduction	1
1.1 The nonlinear Schrödinger equation and its solutions	3
1.2 Inhomogeneous NLSE and self-similar nonlinear waves	13
1.3 Riccati generalization	15
1.4 Outline of thesis	19
Bibliography	21
2 Controlling rogue waves in nonlinear optical fibers and waveguides	29
2.1 Introduction	29
2.2 Optical Waveguides and Fibers	30
2.3 Nonlinear waveguides	33
2.4 Rogue waves in nonlinear optical fibers	34
2.4.1 Model equation	35
2.4.2 Similarity transformation	36
2.4.3 Self-similar first and second-order rogue waves	38
2.5 Signal attenuation in optical fiber	43
2.6 Erbium doped fiber amplifiers (EDFA)	44
2.6.1 Background and Motivation	46
2.6.2 Bright and dark rogue waves in an inhomogeneous erbium doped fiber system	48

2.6.3	Controlling bright and dark rogue waves in a periodically distributed system	52
2.7	Tapered graded-index nonlinear waveguide	55
2.7.1	Optical rogons in a tapered graded-index nonlinear waveguide	56
2.7.2	Management of optical rogons	58
2.7.3	Riccati parameterized optical rogons in a tapered graded-index nonlinear waveguide	62
2.8	Conclusion	65
	Bibliography	67
3	Nonlinear tunneling of optical similaritons in a tapered graded-index nonlinear waveguide	75
3.1	Introduction	75
3.2	Nonlinear tunneling	75
3.3	Optical similaritons	77
3.4	Nonlinear tunneling of optical similaritons	77
3.4.1	Bright and Dark similariton solutions	79
3.4.2	Nonlinear tunneling of optical similaritons with constant background	81
3.4.3	Nonlinear tunneling of optical similaritons with exponential background	86
3.4.4	Cascade compression	90
3.5	Conclusion	92
	Bibliography	93
4	Controlling self-similar matter waves in Bose-Einstein condensates	97
4.1	Introduction	97
4.2	Bose-Einstein condensate (BEC)	98
4.3	Controlling matter rogue waves in BEC	99
4.3.1	Methodology and rogue wave solutions	100
4.3.2	Management of matter rogue waves	102
4.4	Controlling matter waves by tailoring nonlinearity parameter . . .	106
4.4.1	Analytical solutions	107

4.4.2	Construction of a family of $R(t)$ ($\widehat{R}(t)$) through Riccati parameterization	109
4.4.3	Riccati parameterized self-similar matter waves in BEC	110
4.5	Conclusion	115
	Bibliography	117
5	Summary and conclusions	121
	List of publications	127
	Reprints	129

List of Figures

1.1	Intensity profile of (a) bright soliton with $a = v = 1$. (b) dark soliton with $u_0 = 1, \phi = \pi/6$	8
1.2	Intensity profile of 2-bright soliton for (a) in-phase collision $\delta\phi = 0$ (b) out-of-phase collision $\delta\phi = \pi/2$. The other parameters are $a = 1/4, b = 0.1$	9
1.3	Intensity profile of 2-dark soliton with $\beta_1 = \beta_2 = 1, \alpha_1 = -\alpha_2 = 1.2, x_{10} = 0, x_{20} = 10$	10
1.4	Intensity profiles for ABs of the NLSE for modulation parameter: (a) $a = 0.25$ and (b) $a = 0.45$	11
1.5	Intensity profiles for (a) first-order, and (b) second-order rogue waves of the NLSE.	13
1.6	The isospectral oscillator potentials $V_\lambda(x)$	16
1.7	Spectra strictly isospectral to harmonic oscillator.	17
2.1	The profile of $\Gamma(Z)$ for $D(Z) = R(Z) = a \cos(\kappa Z), \kappa = \sqrt{2}$ and $w = 1, a = 1, \rho_0 = 0, c_0 = 1.5$	40
2.2	Intensity profile (a) for first-order rogue waves of Eq. (2.12) (b) for second-order rogue waves of Eq. (2.12) with $D(Z) = R(Z) = a \cos(\kappa Z), \kappa = \sqrt{2}$ and $w = 1$	40
2.3	The profile of $\Gamma(Z)$ for (a) dispersion increasing fiber case with $c_0 = -2$ and $\sigma = 0.1$ (b) dispersion decreasing fiber case with $c_0 = 1$ and $\sigma = -0.1$. The other parameters are $\kappa = 1$ and $\gamma = 0.5$	41
2.4	Intensity profile in dispersion increasing fiber (a) for first-order rogue waves of Eq. (2.12) (b) for second-order rogue waves of Eq. (2.12) with $c_0 = -2, \kappa = 1, \gamma = 0.5$ and $\sigma = 0.1$	41

2.5	Intensity profile in dispersion decreasing fiber (a) for first-order rogue waves of Eq. (2.12) (b) for second-order rogue waves of Eq. (2.12) with $c_0 = 1, \kappa = 1, \gamma = 0.5$ and $\sigma = -0.1$	42
2.6	Energy-level diagram of erbium ions in silica fiber.	45
2.7	(a) Intensity profile of bright rogue waves ($ q ^2$) (b) Intensity profile of dark rogue waves ($ p ^2$) (c) Dark rogue waves properties of η of Eq. (2.40). The parameters are $d = 1, b = \frac{3}{2}, \omega_0 = \frac{1}{2}, l_1 = 1$ and $l_2 = 2$	52
2.8	(a) Recurrence (b) annihilation of bright rogue waves of Eq. (2.40) $ q ^2$. The parameters are $w = d_{10} = r_0 = \rho_0 = 1$ with (a) $\kappa = 0.8$ and (b) $\kappa = 6$	53
2.9	(a) Recurrence (b) annihilation of dark rogue waves of Eq. (2.40) $ q ^2$. The parameters are $w = d_{10} = r_0 = \rho_0 = 1$ with (a) $\kappa = 0.7$ and (b) $\kappa = 5$	54
2.10	Sectional view of Recurrence (black) for $\kappa = 0.8$ and annihilation (red) for $\kappa = 6$ for (a) bright rogue waves at $\tau = 0.2$ (b) dark rogue waves at $\tau = 1$ of Eq. (2.40).	54
2.11	Intensity profile of rogons for Eq. (2.68) (a) for $D(Z) = a \operatorname{sech} Z$ (b) for $D(Z) = 1 + a \cos Z$ with $a = 0.2$	60
2.12	Intensity profile of rogons for Eq. (2.68) (a) for $R(Z) = b \cosh Z$ (b) for $R(Z) = 1 + a \cos \Omega Z$ with $b = 1, a = 0.1$ and $\Omega = 0.5$. . .	60
2.13	Intensity profile of rogons for Eq. (2.68) with $w(Z) = 1 + \operatorname{sech} Z$ (a) for $R(Z) = \operatorname{sech} Z$ (b) for $R(Z) = 1 + c_0 \sin Z$ (c) for $R(Z) = \exp(-c_0 Z) \cosh Z$ with $c_0 = 0.5$	61
2.14	The profiles of (a) width (b) tapering (c) nonlinearity parameter. Each plot is drawn for the absence of Riccati generalization (black), for $\lambda = 0.1$ (red), for $\lambda = 1$ (green), for $\lambda = 10$ (blue). . .	63
2.15	The intensity profiles of rogue waves (a) in the absence of Riccati generalization, (b) for $\lambda = 0.1$, (c) for $\lambda = 1$, (d) for $\lambda = 10$	64
3.1	(a) The tapering profile $F(Z)$ given by Eq. (3.25) (b) The gain profile $\Gamma(Z)$ given by Eq. (3.26) solid line (for DW) and dashed (for DB). The chosen parameters are $\epsilon = 1, R_0 = 1, h = 5$ for DB and $h = -0.5$ for DW, $Z_0 = 8$	83

3.2 Intensity plots of (a) bright similariton For DB (b) DW with $\alpha_1 = -0.8, \beta_1 = 0.2$ (c) Intensity plot for 2-bright similariton for DB with $\beta_2 = -0.1$ (d) For DW with $Z_0 = 8, \beta_2 = -1.5$. The other parameters are $\beta_1 = 0.1, \alpha_1 = -1.1, \alpha_2 = 1$. The remaining parameters are same as in Fig. 3.1 83

3.3 Intensity plots of (a) dark similariton for DB with $\alpha_1 = \beta_1 = 0.6$ (b) DW with $\alpha_1 = 0.8, \beta_1 = 0.2$, (c) Intensity plot for 2-dark similariton for DB (d) For DW $\chi_{10} = -\chi_{20} = 20, \beta_1 = 0.45, \beta_2 = 0.35, \alpha_1 = -0.01, \alpha_2 = 0.6$. The remaining parameters are same as in Fig. 3.1 85

3.4 Intensity plots of (a) bright similariton for NB (b) NW with $\alpha_1 = 1, \beta_1 = 0.2$ (c) Intensity plot for 2-bright similariton for NB with $D_0 = 0.5$ (d) For NW $D_0 = 1$. The other parameters are $\beta_1 = -0.9, \beta_2 = -0.5, \alpha_1 = 2, \alpha_2 = -2.1, Z_0 = 5$. The remaining parameters are same as in Fig. 3.1. 86

3.5 Intensity plots of (a) dark similariton for NB (b) NW with with $\epsilon = \beta_1 = 1, \alpha_1 = 0.8$ (c) Intensity plot for 2-dark similariton for DB (d) For DW $\chi_{10} = -\chi_{20} = 10, \beta_1 = -0.5, \beta_2 = -0.4, \alpha_1 = -0.58, \alpha_2 = 0.38, Z_0 = 5$. The remaining parameters are same as in Fig. 3.1. 87

3.6 Intensity profile of 2-bright similariton (a) for nonlinearity barrier case (b) for nonlinearity well case for $D_0 = 1$ (Blue), $D_0 = 0.3$ (Green), $D_0 = 0.1$ (Red). The other parameters are the same as depicted in Fig. 3.4 88

3.7 (a) The tapering profile $F(Z)$ given by Eq. (3.30) (b) The gain profile $\Gamma(Z)$ given by Eq. (3.31) solid line (for DW) and dashed (for DB). The chosen parameters are $\epsilon = 1, R_0 = 1, h = 5$ for DB and $h = -0.1$ for DW, $Z_0 = 8$ 88

3.8 Intensity plots of 1-bright similariton (a) DB with $h = 5$ (b) DW with $h = -0.5, \alpha_1 = 0.5, \beta_1 = 0.2$.Intensity plots of 2-bright similaritons with (c)DB (d) DW with $\alpha_1 = 1.21, \alpha_2 = 1.19, \beta_1 = -0.2, \beta_2 = -0.3$. The remaining parameters are $r_0 = 0.08, \epsilon = 2, Z_0 = 8$ 89

3.9	Intensity plots of 1-bright similariton through DB (a) $r_0 = -0.014$ (b) $r_0 = 0.164$. The evolution of the pulse before (red) at $Z = 7$ and after crossing (blue) the barrier at $Z = 20$. The other parameters are the same as depicted in Fig. 3.8.	90
3.10	(a) Intensity plot 2-bright similariton profile through DB (b) The corresponding contour plot with $h = 3$. (c) Intensity plot 2-bright similariton profile through DW (d) The corresponding contour plot with $h = -1$. The other parameters are $\alpha_1 = 1.21$, $\beta_1 = -0.2$, $\alpha_2 = 1.19$, $\beta_2 = -0.3$, $\epsilon = 2$ $r_0 = 0.08$	91
4.1	(a) The profile of potential for Eq. (4.29) (b) Intensity profile of first-order rogue wave for the parameters $D = 3 \cos t$, $k_1 = 1.1$, $k_2 = \sin^2 t$, $\mu_0 = k_{10} = 1$, $\chi_0 = 0$	103
4.2	Intensity profile of rogue waves with a periodic background (a) shows the periodic background and the rogue wave (b) Detailed local profile of rogue wave. The parameters are $k_1 = 1.1 + \cos t$, $k_2 = 1$, $D = 1$ $\mu_0 = k_{10} = 1$, $\chi_0 = 0$	104
4.3	(a) The profile of periodic potential (b) Intensity plot of rogue wave for the parameters $k_2 = \sin t$, $\mu_0 = k_{10} = 1$, $\chi_0 = 0$	105
4.4	Profile of nonlinearity control parameter: Curve A is for $R(t)$ given by Eq. (4.55). Curve B is for $\widehat{R}(t)$ given by Eq. (4.58) and $\lambda = 0.37$. $\gamma = 3$ for both the curves.	111
4.5	Intensity plots corresponding to $R(t)$ for (a) bright soliton (b) dark soliton (c) 2-soliton (d) AB (e) rogue waves. The parameter $\gamma = 3$ for all of these plots.	112
4.6	(a) Variation of nonlinearity control parameter: Curve A shows $R(t)$ given by Eq. (4.59), Curve B and C are the plots for $\widehat{R}(t)$ given by Eq. (4.62) with $\lambda = 0.8$ and $\lambda = 2$, respectively (b) plot of trapping potential, given by Eq. (4.60), of both the plots, $\gamma = 2$	113
4.7	Intensity profiles corresponding to $R(t)$ are shown in (a),(c),(e) for bright soliton, dark soliton, 2-solitons, respectively. Profiles corresponding to $\widehat{R}(t)$ for bright ((b) with $\lambda = 0.9$), dark ((d) with $\lambda = 0.7$), 2-soliton ((f)with $\lambda = 0.7$, $\eta_1 = 2$, $\eta_2 = 1.8$, $\kappa_1 = 1$, $\kappa_1 = 0.5$). The parameter $\gamma = 1$ in all these plots.	114

-
- 4.8 Intensity profiles corresponding to $R(t)$ are shown in (a),(c) (i) for ABs and rogue wave. Profiles corresponding to $\widehat{R}(t)$ for AB ((b) with $\lambda = 1$), rogue waves ((d)with $\lambda = 0.7$). The parameter $\gamma = 1$ in all these plots. 115

Chapter 1

Introduction

Modern theories of nonlinear sciences have been widely developed over the last half century as it is believed that they are the important element for understanding nature [1]. They cover almost all branches of science such as plasma physics, hydrodynamics, mechanics, biology, chemistry, etc. Various nonlinear phenomena are encountered in our daily life such as the stock market, population growth, weather forecast, planetary systems, etc. In general, the nature of a physical system depends on the nature of the forces acting on it and on the initial conditions. A system is said to be nonlinear if it is subjected to nonlinear forces and its behaviour is significantly dependent on the initial conditions. These nonlinear systems are quite complex and a small change in the initial input conditions can bring a drastic change in their output. Hence, for these systems output is not directly proportional to the input. In contrast, linear systems are generally gradual, smooth and regular and are involved in slowly flowing streams, engines working at low power, slowly reacting chemicals, etc. Nonlinear systems comprise of regular as well as complicated and irregular behaviours. Strictly, almost all systems can behave as a nonlinear system if the input is large enough. In case of dielectric media, if the strength of electric field is small, the refractive index of the medium remains constant and the polarization varies linearly with electric field. For sufficiently large electric fields, the linear response of polarization towards the electric field switches to a nonlinear response and varies as the higher power of electric field. In case of a simple pendulum, if the initial displacement is large then the system exhibits nonlinear response in contrast to the linear motion for a small initial displacement. The dynamics of nonlinear systems are well described by the set of nonlinear evo-

lution equations (NLEEs). The exact solutions of these NLEEs gives a deeper insight to understand the behaviour of a nonlinear system. To find the exact solutions of NLEEs is a challenging enterprise as mathematical tools like Fourier and Laplace transform, Greens function, superposition principle hold for linear systems only and can not be applied here. Since analytical solutions are easier to interpret, hence with time various analytical methods like inverse scattering transform (IST), Painlevé analysis, Darboux transformation, ansatz method, factorization method have been developed to find the exact solutions and the integrability of the nonlinear systems. These NLEEs are known to possess various types of solutions like solitary waves, periodic solutions, shock waves, exponentially growing and decaying solutions, etc. Nowadays a vast amount of research is taking place in this area due to the advancement of high-speed computers, mathematical softwares and the development of new analytical methods to solve NLEEs. The well known NLEEs which are used to model various physical phenomenon are Sine-Gordon equation, Korteweg de-Vries (KdV) equation, nonlinear reaction diffusion equation (NLRD), nonlinear Schrödinger equation (NLSE), etc. The sine-Gordon equation has been thoroughly exploited to study the properties of Josephson junctions, charge density waves, etc. The KdV equation finds application in studying the properties of many physical systems which are weakly dispersive and weakly nonlinear such as blood pressure waves, internal waves in oceanography, etc. The NLRD equation plays a vital role in understanding the flow in porous media, heat combustion in plasma, image processing, chemical reactions, etc. The NLSE and its variants appear in many fields such as nonlinear optics, condensed matter physics, plasma physics, etc. Due to the wide applicability of NLSE and its variants, they have been thoroughly employed to study the various nonlinear phenomenon occurring in different areas.

The thesis involves the study of NLSE and its variants in two different contexts: (i) nonlinear optics (ii) Bose-Einstein condensates (BECs). We report the exact self-similar solutions like similaritons and their pairs, Akhmediev breathers, rogue waves, etc. which helps in understanding the pulse propagation in various nonlinear optical fibers, tapered graded-index waveguides and BECs. It is worth mentioning that the stability analysis of the self-similar solutions of generalized NLSE (GNLSE) which we have obtained can be performed by using the standard meth-

ods. Few such cases have been considered in [2] where the stability of optical rogons against the periodic perturbation and noise have been discussed. In order to understand the pulse propagation properties modelled by GNLSE, we provide a brief introduction of standard NLSE and the various analytical solutions exhibited by it.

1.1 The nonlinear Schrödinger equation and its solutions

In the standard form, NLSE can be written as

$$i\frac{\partial\psi}{\partial t} + \frac{1}{2}\frac{\partial^2\psi}{\partial x^2} + \sigma|\psi|^2\psi = 0, \quad (1.1)$$

where ψ represents the complex field envelope. The first term describes the pulse evolution with time. The second term represents the group velocity dispersion (GVD) and the third term describes the nonlinearity. The parameter σ denotes the self-focusing ($\sigma = +1$) or self-defocusing ($\sigma = -1$) nature of nonlinearity. In the context of nonlinear fiber optics, in Eq. (1.1), t denotes propagation distance ($t \rightarrow z$) and x represents either retarded time (for pulses in optical fibers) or transverse spatial co-ordinate (for beams in a waveguide). In 1972, the complete integrability of the NLSE has been shown in [3] by Zakharov and Shabat. They have used inverse scattering transform method which was originally developed by Gel'fand et al. in the quantum theory of scattering [4, 5]. In general, NLSE possesses bright and dark soliton solutions, kink and double-kink type solutions, fractional transform solutions, breathers solutions, Peregrine-soliton/rogue wave solutions, etc. The exact solutions help to understand the nonlinear phenomena in a better way. We describe some of these solutions of NLSE, which will be used further in the thesis.

Solitary waves and solitons

Solitary wave: A solitary wave is a non-singular and localized wave which propagates without change of its properties like shape, velocity, etc. It arises due to the delicate balance between the nonlinear and dispersive effects of a medium. The term *solitary wave* has been given to them because they often occur as a single

entity. The existence of stable solitary waves was first observed experimentally by J. Scott Russell [6] while conducting experiments to determine the most efficient design for canal boats. He found that these waves propagate for miles before being lost in the meanders of the canal and called them *Great Wave of Translation*. He reported his observations to the British Association in his 1844 *Report on Waves* in the following words:

"I believe I shall best introduce the phenomenon by describing the circumstances of my own first acquaintance with it. I was observing the motion of a boat which was rapidly drawn along a narrow channel by a pair of horses, when the boat suddenly stopped not so the mass of water in the channel which it had put in motion; it accumulated round the prow of the vessel in a state of violent agitation, then suddenly leaving it behind, rolled forward with great velocity, assuming the form of a large solitary elevation, a rounded, smooth and well-defined heap of water, which continued its course along the channel apparently without change of form or diminution of speed. I followed it on horseback, and overtook it still rolling on at a rate of some eight or nine miles an hour, preserving its original figure some thirty feet long and a foot to a foot and a half in height. Its height gradually diminished, and after a chase of one or two miles I lost it in the windings of the channel.

Scott Russell immediately realized that the distinct features of this wave are longevity and the capability to possess finite non-zero energy. He then performed some laboratory experiments to generate these waves in order to study the phenomena more carefully. He successfully demonstrated solitary waves by dropping a weight at one end of a water channel and made two key discoveries:

1. The laboratory existence of solitary waves which are long and shallow water waves of permanent profile.
2. The speed of propagation v of a solitary wave in a channel given by

$$v = \sqrt{g(h + a)},$$

where a is the amplitude of the wave, h is the undisturbed depth of water and g is the acceleration due to gravity.

In 1895, the theoretical explanation of the formation of solitary wave was given by the two Dutch physicists Korteweg and de Vries [7]. They deduced the famous

wave equation, which is responsible for the Scott Russell phenomenon and now known as the KdV equation. Soon the solitary wave solution was rediscovered as a solution of KdV equation.

Solitons: The solitons are the special case of solitary waves which retain their identity even after undergoing collisions and maintain their shape while travelling at their original speed. The discovery of the solitons took place when Russell had observed the interactions of nonlinear waves and found that these nonlinear waves can interact strongly and then continue thereafter as if there had been no interaction at all. The persistence of these waves demonstrates the particle-like character and led Zabusky and Kruskal to coin the name “soliton”. The suffix “on” represents the particle nature as in photon, proton, etc. We can say that the soliton is a localized self-reinforcing solitary wave solution of a NLEE, which is stable against the mutual collisions with other solitons and retains its identity but undergoes a phase shift after collisions. Many NLEEs which possess similar properties exhibit solitary wave/soliton solutions. Though the distinction between the solitons and solitary waves is clear, the former being a restricted subset of the latter, yet in much of the literature the solitary waves are usually referred to as solitons. After the experimental and theoretical investigation of solitary waves/solitons, numerical studies took place in order to understand their characteristic properties. In 1965, Zabusky and Kruskal solved KdV equation numerically for a nonlinear lattice and found that the solitons interact elastically with one another.

After the acceptance of the soliton concept, a great amount of research took place to employ different mathematical methods to obtain the soliton solutions. Soon afterwards, Gardner et al. reported the existence of multi-soliton solutions of KdV equation by using inverse scattering transform (IST) [8]. Lax generalized these results and proposed the concept of Lax pair [9]. With time the same method had been employed to work out the soliton solutions of various NLEEs. In 1972, this method had been applied to obtain the exact solutions of NLSE [3]. It immediately implied that the IST method is not restricted to KdV alone but it has wider applicability. Hirota proposed a new method, known as the Hirota method, to obtain the exact solution for the KdV equation for the case of multiple collisions of solitons having different amplitudes [10]. Moreover, the analysis done by

Zakharov and Shabat clearly suggested that the soliton property is a more comprehensive phenomenon possessed by a class of nonlinear dispersive systems. It gave a tremendous motivation to other scientists to look for nonlinear equations which exhibit soliton solutions. In 1974, Ablowitz et al. [11] revealed that the IST is the nonlinear counterpart of the Fourier transform method applicable to linear dispersive systems and is used to solve a wide range of NLEEs such as the modified KdV equation, NLSE, and the classical sine-Gordon equation. These techniques stimulated the study of solitons and they have been widely investigated in various fields such as in nonlinear optics, condensed matter physics, biophysics, hydrodynamics, etc. Now we present the explicit mathematical expressions of exact bright, dark solitons, 2-solitons, Akhmediev breathers (ABs) and rogue wave solutions of Eq. (1.1).

1-soliton solutions

Solitons are mainly categorised into two types:

Bright soliton

For self-focusing case ($\sigma = +1$), Eq. (1.1) possess bright soliton solution which appears as a localized intensity peak on a constant background and in the general form can be express as

$$\psi(x, t) = a \operatorname{sech}[a(x - vt)] e^{i(vx + (a^2 - v^2)t/2)}, \quad (1.2)$$

where a and v represent the amplitude and the velocity of the propagating soliton. At $v = 0$ the bright soliton has a simplified structure and referred to as a fundamental bright soliton and can be expressed as [3]

$$\psi(x, t) = a \operatorname{sech}[a(x)] e^{ia^2t/2}. \quad (1.3)$$

The intensity of bright soliton I_{B1} corresponding to Eq. (1.2) is given as

$$I_{B1} = |\psi(x, t)|^2 = a^2 \operatorname{sech}^2[a(x - vt)]. \quad (1.4)$$

The typical intensity profile is shown in Fig. 1.1(a).

Dark soliton

For self-defocusing case ($\sigma = -1$), Eq. (1.1) admits dark soliton solution which appears as a localized dip on a constant background [12]. The dark soliton can be expressed as [13]

$$\psi(x, t) = u_0 [B \tanh(u_0 B(x - Au_0 t)) + iA] e^{-iu_0^2 t}, \quad (1.5)$$

where u_0 is the amplitude of constant background, and A and B satisfy the relation $A^2 + B^2 = 1$. We are introducing a parameter ϕ such that $A = \sin \phi$ and $B = \cos \phi$. Now instead of two parameters A and B we are now dealing with a single parameter ϕ which corresponds to the total phase shift across the dark soliton i.e 2ϕ . The intensity expression for dark soliton will take the form

$$I_{D1} = u_0^2 [\cos^2 \phi \tanh^2(u_0 \cos \phi(x - u_0 \sin \phi t)) + \sin^2 \phi]. \quad (1.6)$$

Hence, $u_0 \sin \phi$ represents the velocity of the dark soliton and $\cos^2 \phi$ gives the magnitude of the dip at the center. The evolution of dark soliton for NLSE is shown in Fig. 1.1(b) for typical values of u_0 and ϕ . It should be noted that for $\phi = 0$, the velocity of dark soliton becomes zero i.e. it is a stationary soliton and at the dip center ($x = 0$) intensity also drops to zero and hence it is called as black soliton. For $\phi \in (0, \pi)$, the intensity of soliton does not drop to zero and these are referred as gray solitons.

2-soliton solutions

These second-order solutions are of utmost importance because they describe the collisions between two solitons. Thus, they will help in determining if the basic fundamental solution deserves the name of solitons.

2-bright soliton

For self-focusing case ($\sigma = +1$), Eq. (1.1) possesses two-bright soliton solution of the form [14]

$$\psi = -8iab \frac{A + iB}{D} e^{-2i(a^2 + b^2)t + i(\phi_1 + \phi_2)}, \quad (1.7)$$

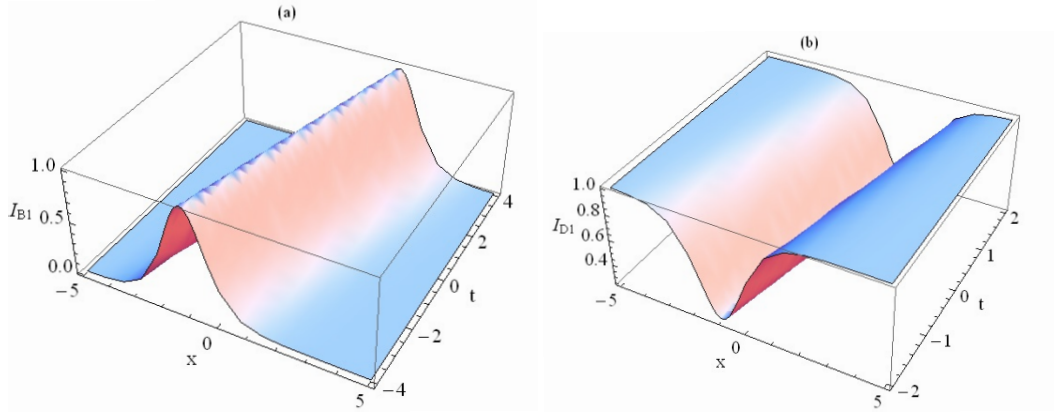


Figure 1.1: Intensity profile of (a) bright soliton with $a = v = 1$. (b) dark soliton with $u_0 = 1$, $\phi = \pi/6$.

with

$$\begin{aligned}
 A &= \cosh(4abt)[a \cosh(2bx) \cos(2ax + \delta\phi) - b \sinh(2bx) \sin(2ax + \delta\phi)], \\
 B &= \sinh(4abt)[a \sinh(2bx) \sin(2ax + \delta\phi) + b \cosh(2bx) \cos(2ax + \delta\phi)], \\
 D &= a^2 \cosh(4bx) + (a^2 + b^2) \cosh(8abt) - b^2 \cos(4ax + 2\delta\phi) \quad (1.8)
 \end{aligned}$$

where $\delta\phi = 2(\phi_1 - \phi_2)$ is the phase difference between the two solitons. For the sake of simplicity, the two-bright soliton solution has been written by considering that the two solitons have equal amplitude b and have velocities a which are equal in magnitude but opposite in sign. The intensity of two-bright soliton I_{B2} corresponding to Eq. (1.7) is given as

$$I_{B2} = \frac{64a^2b^2}{D^2}[A^2 + B^2], \quad (1.9)$$

where A , B and D are given by Eq. (1.8).

The intensity plots of two-bright solitons are plotted in Fig. 1.2. Fig. 1.2(a) depicts the collision process of solitons when they are in phase and Fig. 1.2(b) displays the collisions of out-of-phase solitons.

2-dark soliton

For self-defocusing case ($\sigma = -1$), Eq. (1.1) admits 2-dark soliton solution of the

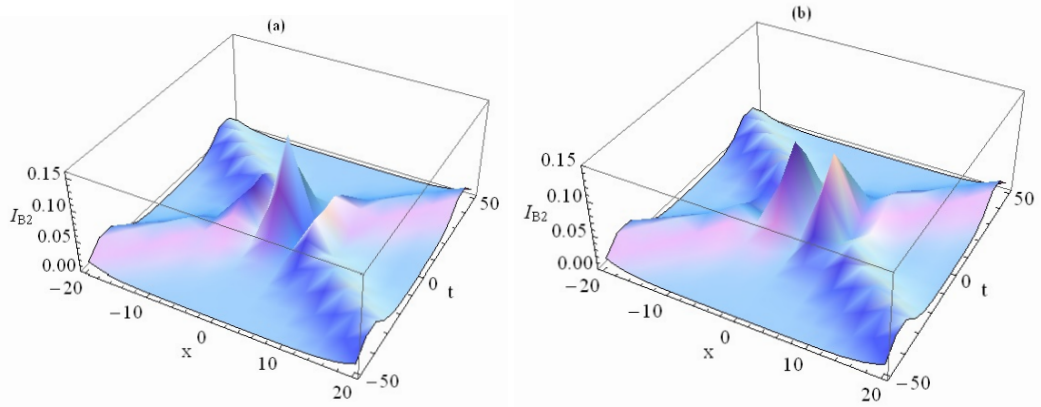


Figure 1.2: Intensity profile of 2-bright soliton for (a) in-phase collision $\delta\phi = 0$ (b) out-of-phase collision $\delta\phi = \pi/2$. The other parameters are $a = 1/4$, $b = 0.1$.

form

$$\psi(x, t) = \mu e^{i(\zeta(x, t))} \left(1 + \frac{A_1}{B_1}\right), \quad (1.10)$$

where

$$A_1 = 4\mu(\omega_1 + \omega_2 - 2\mu) - 4i \frac{\lambda_1 + \lambda_2}{(\beta_1 + \beta_2)} \eta \quad (1.11)$$

$$B_1 = 4\mu^2 \left(\frac{\lambda_1 + \lambda_2}{\beta_1 + \beta_2}\right)^2 \eta, \quad \eta = (\omega_1 - \mu)(\omega_2 - \mu),$$

$$\omega_j = \frac{(\alpha_j - i\beta_j)(\alpha_j + i\beta_j \tanh(\delta_j))}{\mu},$$

$$\delta_j = \beta_j [x - x_{j0} - (\Omega + \alpha_j)t],$$

$$\zeta = -\left(\mu^2 + \frac{\Omega^2}{2}\right)t - \Omega x - \zeta_0, \quad \mu = |\lambda_j|.$$

Here, λ_j represents the complex spectral parameter

$$\lambda_j = \alpha_j + i\beta_j,$$

where $j = 1, 2$ for 2-soliton solution. The parameters α_j and β_j with $j = 1, 2$ depict the velocity and the amplitude of the first and second dark soliton, respectively. The initial position and initial phase are related with the parameters x_{j0} and ζ_0 . The typical intensity profile of 2-dark soliton is plotted in Fig. 1.3.

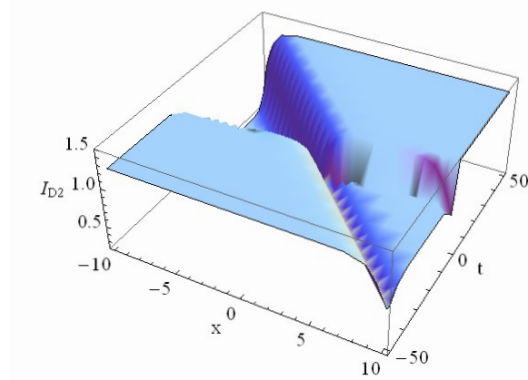


Figure 1.3: Intensity profile of 2-dark soliton with $\beta_1 = \beta_2 = 1$, $\alpha_1 = -\alpha_2 = 1.2$, $x_{10} = 0$, $x_{20} = 10$.

Breathers

The breathers are nonlinear waves which can carry energy in a localized and oscillatory fashion. In contrast to solitons which are localized in x the breathers are localized in t and oscillating in x . These solutions increase their amplitude either exponentially or according to a power law in t . They achieve their maximum value and finally decay symmetrically to disappear forever. The mathematical proof of the existence of breathers was given by MacKay and Aurbay [15]. The breathers are not only a mathematical concept but they have also been realized experimentally in different systems such as in BEC [16], dispersion managed optical waveguides and fibers [17] and Josephson arrays [18]. Consequently, these breather solutions have been obtained for various NLEEs like KdV [19], Gardner equation [20], modified-KdV [21] and NLSE. In the context of NLSE, the spatially periodic solutions are termed as Akhmediev breathers (ABs) [22]. For the self-focusing case AB solution of NLSE can be expressed as

$$\psi(x, t) = \frac{(1 - 4a) \cosh(\beta t) + \sqrt{2a} \cos(px) + i\beta \sinh(\beta t)}{\sqrt{2a} \cos(px) - \cosh(\beta t)} e^{it}, \quad (1.12)$$

where a is a free parameter and is known as the modulation parameter. The coefficients β and p are related to a by: $\beta = \sqrt{8a(1 - 2a)}$ and $p = 2\sqrt{1 - 2a}$. The characteristics of AB depends on a . To demonstrate the role of a we have plotted the intensity profiles of ABs for different values of a in Fig. 1.4. Clearly, as the value of a increases, the separation between adjacent peaks increases and the

width of each individual peak decreases.

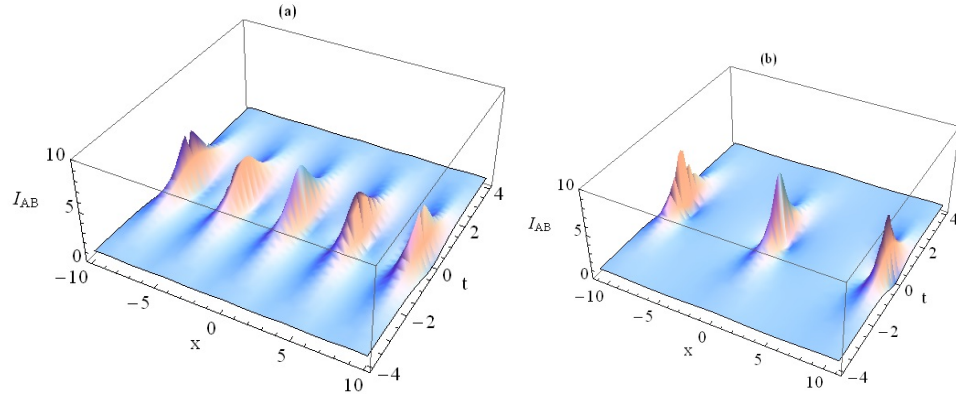


Figure 1.4: Intensity profiles for ABs of the NLSE for modulation parameter: (a) $a = 0.25$ and (b) $a = 0.45$.

In addition of ABs which are space periodic, the other kind of breather solutions also exist which are periodic in time and termed as Ma-solitons (MS) [23]. Initially, it was predicted that the rational solutions or rogue wave solutions can be obtained as the limiting cases of either periodic Ma solitons (MS) or ABs [24]. The analysis made in [23] reveals that MS are created directly from the initial conditions consisting of the background plane wave and solitons. It means that the MS must exist in the wave field from the very beginning. On the other hand, the rational solutions and ABs belong to the class of excitations which appear from nowhere [22, 25]. ABs arise due to modulational instability [26] and in the limit when $a \rightarrow 0.5$, it reduces to the rational solution which is known as rogue wave solution.

Rogue waves

In 1983, the rational solutions of NLSE was first given by Peregrine and are so known as Peregrine solitons [27]. The hierarchy of rational solutions have been presented by using Darboux transformation [28] for the self-focusing NLSE. The rational solutions are of utmost importance to study high amplitude rogue waves in deep ocean [29, 30] and in optical fibers [28]. Akhmediev et al. suggested that the collisions of two or more ABs results into the formation of high amplitude rogue

waves [22] which offer the possibility of high energy concentration in space and time. These doubly localized solutions (localized in space and time) are known as rogue waves. The occurrence of rogue waves from the collision of two ABs has been demonstrated experimentally by controlling their phases and velocities [31]. The general form of the rational solution is given as

$$\psi(x, t) = \left[1 - \frac{K + iH}{D} \right] e^{it}, \quad (1.13)$$

where K , H and D are the polynomials in x and t . For the limiting case $a \rightarrow 1/2$ in AB solution given by Eq. (1.12), the first-order rogue wave solution has been obtained by choosing $K = 4$, $H = 8t$ and $D = 1 + 4t^2 + 4x^2$. The exact solution reads

$$\psi(x, t) = \left[1 - 4 \frac{1 + 2it}{1 + 4t^2 + 4x^2} \right] e^{it}. \quad (1.14)$$

The intensity expression for first-order rogue wave is given by

$$I_{R_1} = 1 + 8 \frac{1 + 4t^2 - 4x^2}{(1 + 4t^2 + 4x^2)^2}. \quad (1.15)$$

The second-order rogue wave solution has the form given in Eq. (1.13), where the polynomials K , H and D have the following form

$$\begin{aligned} K &= \left(x^2 + t^2 + \frac{3}{4} \right) \left(x^2 + 5t^2 + \frac{3}{4} \right) - \frac{3}{4}, \\ H &= t \left(t^2 - 3x^2 + 2(x^2 + t^2)^2 - \frac{15}{8} \right), \\ D &= \frac{1}{3} (x^2 + t^2)^3 + \frac{1}{4} (x^2 - 3t^2)^2 + \frac{3}{64} (12x^2 + 44t^2 + 1). \end{aligned} \quad (1.16)$$

The intensity expression for second-order rogue waves takes the form

$$I_{R_2} = \left(\frac{D - K}{D} \right)^2 + \left(\frac{H}{D} \right)^2. \quad (1.17)$$

The intensity plots for first and second-order rogue waves are shown in the Fig. 1.5.

Here, we have presented the explicit expressions till second-order rogue waves. The higher order rogue waves for Eq. (1.1) have been obtained and the explicit analytical expressions of rogue waves from first to fourth order are given in [28].

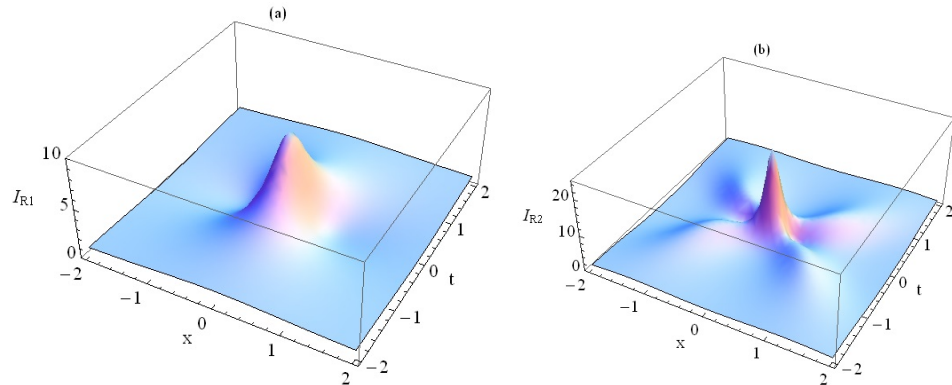


Figure 1.5: Intensity profiles for (a) first-order, and (b) second-order rogue waves of the NLSE.

The higher order rogue waves have not only been predicted theoretically but up to fifth-order these rogue waves have been observed experimentally [30]. We have already mentioned that NLSE exhibits both bright and dark solitons in the self-focusing and self-defocusing regime, respectively. The next question is whether the dark rogue waves exist for the defocusing NLSE. In general, unlike the bright rogue waves which appear as a single peak hump with two dips, the dark rogue wave has one down dominant peak and two small lumps. In contrast to solitons we can not get dark rogue waves for the defocusing NLSE because of the singularity of the solution in this regime [32, 33]. However, the bright and dark rogue wave solutions of the coupled nonlinear equations system such as in Manakov [34] and erbium doped fiber system [35] have been obtained. Very recently, the N-order bright and dark rogue wave solutions of the erbium doped optical fiber system have been presented by using Darboux transformation method [36].

1.2 Inhomogeneous NLSE and self-similar nonlinear waves

So far, we have discussed the constant-coefficient standard NLSE and its various analytical solutions. The constant coefficient NLSE represents the physical phenomenon under highly ideal conditions. But in realistic systems some sort of inhomogeneities are always present in the system e.g in optical fibers inhomogeneities

are due to the manufacturing defects and the density variations in the fiber core, in NLRD system inhomogeneities are due to the fluctuations in the environmental conditions, in BECs inhomogeneities are associated with the bosonic interactions, etc. Such realistic nonlinear phenomenon are governed by variable coefficient NLEEs. In this thesis we are considering variable coefficient NLSE (vcNLSE) due to its applicability in nonlinear fiber optics and in BECs. In the context of nonlinear optics, the coefficients of NLSE are z dependent and we call the system as inhomogeneous system and the governing equation is the inhomogeneous NLSE or generalized NLSE (GNLSE). In the context of BECs, the coefficients of NLSE are t dependent and we call the system as nonautonomous system, where time appears explicitly and the governing equation is the nonautonomous NLSE.

In general, the variable coefficient NLEEs are not integrable and hence, cannot be solved directly by using integrable techniques. Serkin et al. have deduced the integrability conditions for the GNLSE with varying dispersion, nonlinearity and gain term and discussed the soliton management regimes [37, 38]. In the context of BEC they have deduced the integrability conditions for the nonautonomous NLSE in the presence of external trap [39]. Subsequently, this model equation has been explored thoroughly to understand the nonautonomous solitons and their interactions in the presence of linear and expulsive harmonic trap [40]. Recently, a new mathematical technique known as “symmetry reduction” has been developed to obtain the exact solutions of variable coefficient NLEEs. It involves the use of similarity transformation which maps the dynamics of the system at one time onto the dynamics of the system at some other time by invoking a suitable scaling. This similarity transformation led to the discovery of new class of solutions which are called self-similar solutions. These solutions obey the scaling laws in such a way that their evolution can be regarded as self similar [41]. For a highly nonlinear media, these solutions correspond to the self-similar wave, retains their shape but change their width and the amplitude in accordance with the system parameters such as nonlinearity, dispersion and gain [42, 43]. In comparison to solitons which become unstable at high power, self-similar waves are more robust with increasing intensity [44].

These days there is a surge of interest to study the properties of self-similar nonlinear waves. Kruglov et al. have obtained the self-similar solutions for GNLSE

[42] and studied their propagation in optical fiber amplifiers [45]. Their characteristics have been investigated in optical waveguide amplifiers [46], in dispersion decreasing fibers [47] and even in the femtosecond regime [48]. Zhao et al. have studied their propagation in a slab waveguide amplifier with spatial inhomogeneity, inhomogeneous nonlinearity and gain or loss parameters [49]. These waves have also been reported for the cubic-quintic NLSE [50]. Like the solitary wave solutions are termed as solitons, the bright and dark self-similar waves are known as bright and dark similaritons, respectively. The first experimental observation of similaritons was reported by Ferman et al. in nonlinear fiber amplifiers [51]. These waves have not only been explored in the context of nonlinear optics but also been explored in the context of BECs. Yan et al. have studied these waves in BECs with harmonic and gaussian potentials [52]. In the BEC framework they have been investigated for quintic NLSE [53] and cubic-quintic NLSE [54] with time and space modulated nonlinearities and potentials. From the theoretical analysis of self-similar waves, it is expected that these solutions will also find applications from experimental and industrial point of view.

1.3 Riccati generalization

Despite powerful integrability methods such as Lie group, Painlevé analysis, and inverse scattering transform it is in general a very difficult task to obtain solutions of second-order NLEEs. Truncated WTC method, generalized Tanh method, ansatz method, auxiliary equation method, similarity-transformations are a few tools successfully employed to obtain solutions for non-integrable PDEs. Rosu and his collaborators developed factorization method to find the solutions for the class of equations having polynomial non-linearities. For nonlinear and dispersive systems governed by NLEEs, the superposition principle does not hold and so it is quite difficult to generalize solutions of NLEEs from a known simple solution. In Quantum Mechanics Riccati generalization has already been known to obtain a class of solutions since the work of Infeld and Hull [55]. It was exploited by Mielnik [56] in 1984 to find potentials which are isospectral to the simple harmonic oscillator potential as shown in Fig. 1.6 and 1.7.

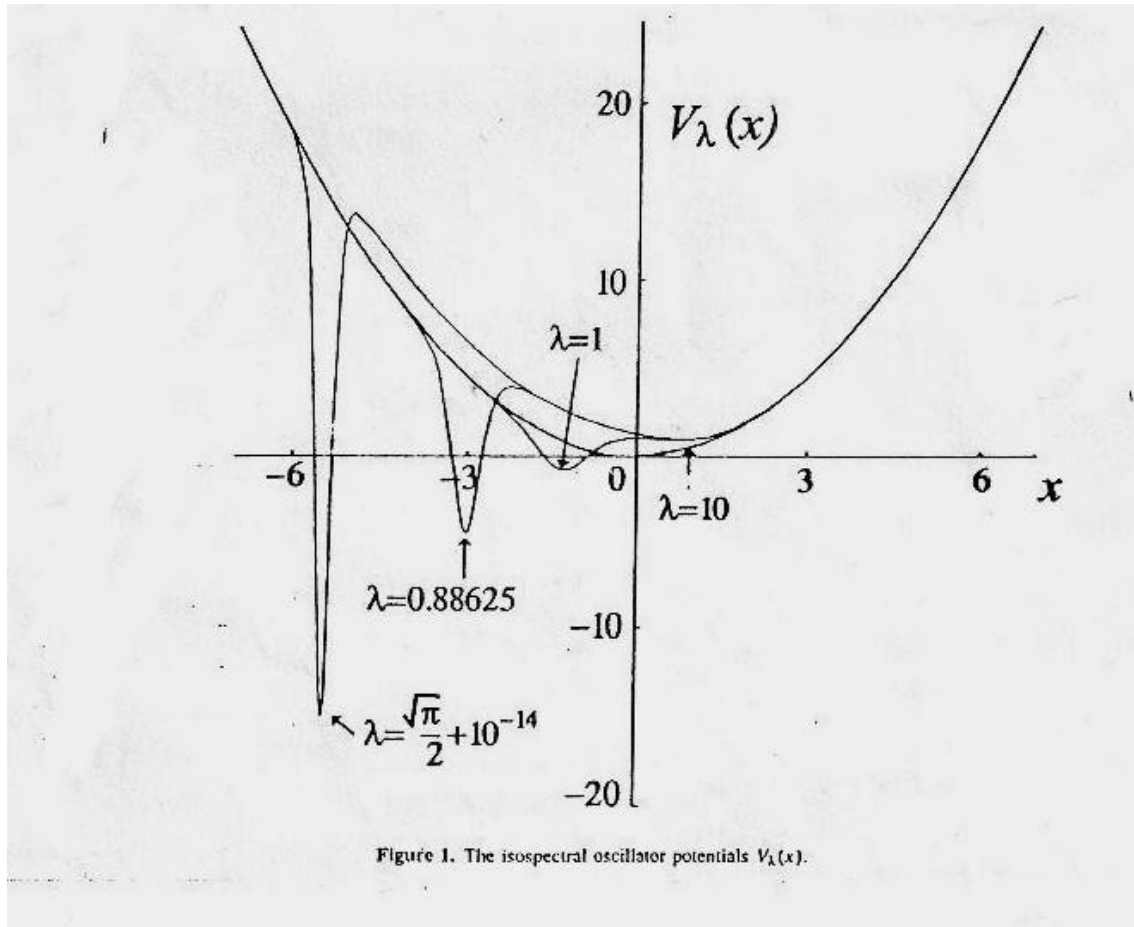


Figure 1.6: The isospectral oscillator potentials $V_\lambda(x)$

. This method can be used not only to define the interdependence between different spectral subspaces but also to transform one Hamiltonian into another. The new Hamiltonian is having different potential, wave function, moments, transition amplitudes but the same energy spectra as that of the initial one. In the mathematical form we can express it as:

$$H_1 = -\frac{1}{2} \frac{d^2}{dx^2} + V_1(x) = a^\dagger a, \quad (1.18)$$

where

$$a = \frac{d}{dx} + W(x), \quad a^\dagger = -\frac{d}{dx} + W(x). \quad (1.19)$$

STRICTLY ISOSPECTRAL:

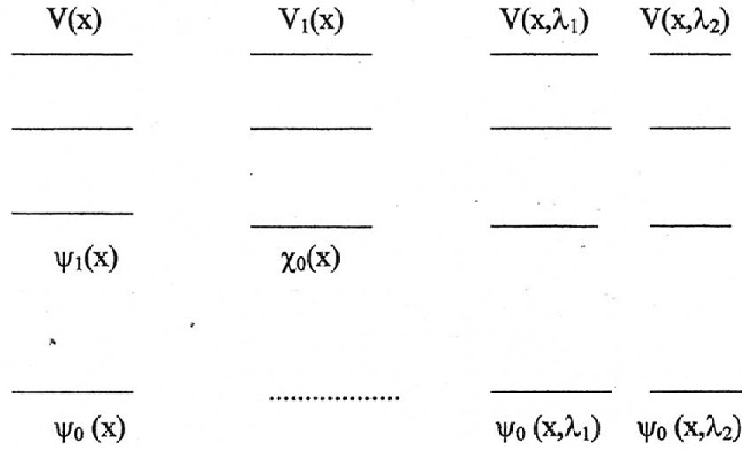


Figure 1.7: Spectra strictly isospectral to harmonic oscillator.

Here, $W(x)$ is the super potential and is given by

$$W = -\frac{d}{dx}[\log \psi_0], \tag{1.20}$$

such that

$$V_1(x) = W^2 - W', \quad H_2 = aa^\dagger, \quad V_2(x) = W^2 + W'. \tag{1.21}$$

Removing a bound state and re-inserting it results in solving a Riccati equation. This introduces a parameter 'λ' known as Riccati parameter and the resultant potential reads [56]

$$\hat{V}_1(x, \lambda) = V_1(x) - 2\frac{d^2}{dx^2}[\ln I(x) + \lambda], \tag{1.22}$$

where, $I(x) = \int_{-\infty}^x \Psi_0^2(x')dx'$. The normalized ground state wave function corresponding to the potential \hat{V}_1 reads,

$$\hat{\psi}_0(x, \lambda) = \frac{\sqrt{(\lambda(1 + \lambda))}}{I(x) + \lambda} \Psi_0(x). \tag{1.23}$$

One could obtain a large class of exactly solvable quantum mechanical potentials by factorizing the second-order Schrödinger equation into the product of two first-order operators and using super symmetric (SUSY) Quantum mechanics techniques described above [57]. This formalism has also proved advantageous in studying various physical situations, such as in determining a spectra of a charged particle in a wide class of nonuniform magnetic fields which are related to the uniform magnetic field [58], in the stability analysis of Sine-Gordon model [59]. It has also been shown that given a kink bearing Hamiltonian, this methodology can be used to generate new sets of Hamiltonian which also admit kink solutions [60].

This method was further extended by Rosu and his co-workers [61, 62] in the context of differential equations. If a non-linear second-order differential equation can be factorized into two first-order differential operators then it is easy to find the particular solution of the problem. They considered the nonlinear equation of the type:

$$\phi_{\xi\xi} + g(\phi)\phi_{\xi} + F(\phi) = 0. \quad (1.24)$$

The above equation can be factorized in the following form

$$[D - u_2(\phi)][D - u_1(\phi)]\phi = 0. \quad (1.25)$$

which implies the following conditions on the function u

$$-(u_1 + u_2 + \phi \frac{du_1}{d\phi}) = g(\phi), F(\phi) = u_1 u_2 \phi. \quad (1.26)$$

One can easily obtain the solution of equation (1.24) by solving the following first-order equation

$$[D - u_1(\phi)]\phi = 0. \quad (1.27)$$

Using this technique, solutions of various nonlinear equations like Modified Emden equation, Generalized Lienard equation, Convective Fisher equation, etc. have been obtained [62]. If the factorization is of a particular type such that $u_1 = p + q\phi$, then Eq. (1.27) is a Riccati equation.

$$\phi_{\xi} = p\phi + q\phi^2, \quad (1.28)$$

One can find its general solution as

$$\phi_{\lambda,q} = \phi_1 + \frac{e^{I_1}}{\lambda - qI_2}, \quad (1.29)$$

where

$$\begin{aligned} I_1(\xi) &= \int_{\xi_0}^{\xi} (2q\phi_1(\xi') + p) d\xi', \\ I_2(\xi) &= \int_{\xi_0}^{\xi} e^{I_1(\xi')} d\xi', \end{aligned} \quad (1.30)$$

λ is known as Riccati parameter which is to be chosen in such a way so as to avoid singularities. It is also called ‘growth parameter’ in the sense that it takes solutions from ϕ_1 to $\phi_{\lambda,q}$.

This method plays an important role in generalizing the solution of NLEEs of physical interest. Recently, this method has been used to obtain a class of solitary wave solutions for nonlinear dynamics of DNA [63]. We shall apply the Riccati generalization formalism to obtain the class of analytical solutions for the GNLSE in two different frameworks involving nonlinear fiber optics and BECs.

1.4 Outline of thesis

The layout of the thesis is as follows:

In Chapter 2, we have studied the propagation of controllable rogue waves through different nonlinear systems in the context of nonlinear fiber optics. The chapter begins with the introduction of optical fibers, nonlinear waveguides and rogue waves. We have then obtained the rogue wave solutions for inhomogeneous GNLSE and investigated their properties for a periodic choice of system parameters, through dispersion increasing fibers, and through dispersion decreasing fibers. Further, we have presented the bright and dark rogue wave solutions for the erbium doped optical fiber system which is governed by the inhomogeneous coupled nonlinear Schrödinger equation and Maxwell-Bloch equation. By making use of the obtained solutions we have presented a mechanism which allows us to get the controllable propagation of rogue waves through a periodically distributed fiber system. Additionally, we have also predicted the recurrence and annihilation characteristics of rogue waves. The chapter then proceeds with the study of optical rogons in a tapered graded-index nonlinear waveguide. Here we have dis-

discussed three different management regimes of optical rogons namely, diffraction management, nonlinearity management and combined nonlinearity and diffraction management. In case of nonlinearity management we have found that the tapering function resembles with the linear Schrödinger equation of quantum mechanics and thus enables us to generate a class of tapering functions by introducing the Riccati parameter. We have also revealed the effect of Riccati parameter on the intensity profile of optical rogons as they propagate through a tapered graded-index nonlinear waveguide.

In Chapter 3, we have studied the nonlinear tunneling properties of optical similaritons through a tapered graded-index nonlinear waveguide. We have analysed it for two cases: nonlinear tunneling with constant background; and nonlinear tunneling with exponential background followed by cascade pulse compression. Here we have demonstrated that by suitable adjusting the barrier's height and location we can get optical similaritons of desired widths at the desired locations.

Chapter 4 deals with the study of self-similar matter waves for the quasi-one-dimensional Gross-Pitaevskii (GP) equation with space and time dependent external potential which governs the dynamics of waves in a cigar shaped BEC. We have obtained the matter rogue wave solutions and exemplified their controllable dynamics for different choices of the parameters. Then we have discussed the special case of quasi-one-dimensional GP equation which describes the scenario when the condensate is subjected to expulsive parabolic trap. For this case we have presented a systematic analytical approach to construct the family of self-similar matter waves including bright and dark solitons, 2-solitons, Akhmediev breathers (ABs) and rogue waves. This is achieved by generating the class of nonlinearity parameter for a given trapping potential through Riccati generalization procedure. Additionally, the role of Riccati parameter on the intensity profile of self-similar matter waves has also been discussed.

Chapter 5 describes the results obtained in the preceding chapters and provides a summary of the significant findings of our work.

Bibliography

- [1] J A Krumhansl. Unity in the Science of Physics. *Physics Today*, 44(3): 33-38, 1991.
- [2] S Loomba, R Gupta, C N Kumar, and D Milovic. Optical rogons for inhomogeneous nonlinear Schrödinger equation with inter modal dispersion. *Applied Mathematics and Computation*, 225: 318-325, 2013.
- [3] A B Shabat, and V E Zakharov. Exact theory of two-dimensional self-focusing and one-dimensional self-modulation of waves in nonlinear media. *Soviet Physics JETP*, 34: 6269, 1972.
- [4] I M Gel'fand, and B M Levitan. On the determination of a differential equation from its spectral function. *American Mathematical Society*, 1: 253-304, 1955.
- [5] L D Fadeev. The inverse problem in the quantum theory of scattering. *Uspekhi Matem. Nauk*, 14: 57-90, 1959. English translation *Journal of Mathematical Physics*, 4: 72, 1963.
- [6] J S Russell. Report on waves. 14th meeting of the British Association for the Advancement of Science, 311: 390, 1844.
- [7] D J Korteweg, and G de Vries. Xli. on the change of form of long waves advancing in a rectangular canal, and on a new type of long stationary waves. *The London, Edinburgh, and Dublin Philosophical Magazine and Journal of Science*, 39(240): 422-443, 1895.
- [8] C S Gardner, J M Greene, M D Kruskal, and R M Miura. Method for solving the Korteweg-de Vries equation. *Physical Review Letters*, 19: 1095-1097, 1967.

- [9] P D Lax. Integrals of nonlinear equations of evolution and solitary waves. *Communications on Pure and Applied Mathematics*, 21(5): 467-490, 1968.
- [10] R Hirota. Exact solution of the Kortewegde Vries equation for multiple collisions of solitons. *Physical Review Letters*, 27(18): 1192-1194, 1971.
- [11] M J Ablowitz, D J Kaup, A C Newell, and H Segur. The inverse scattering transform-fourier analysis for nonlinear problems. *Studies in Applied Mathematics*, 53: 249-315, 1974.
- [12] V E Zakharov, and A B Shabat. Interaction between solitons in a stable medium. *Soviet Physics JETP*, 37(5): 823-828, 1973.
- [13] Y S Kivshar, and B L Davies. Dark optical solitons: physics and applications. *Physics Reports*, 298(2): 81-197, 1998.
- [14] P Mandel, and M Tlidi. *Introduction to Soliton Theory*. Universit Libre de Bruxelles, 2006.
- [15] R S MacKay, and S Aubry. Proof of existence of breathers for time-reversible or Hamiltonian networks of weakly coupled oscillators. *Nonlinearity*, 7(6): 1623, 1994.
- [16] A Trombettoni, and A Smerzi. Discrete solitons and breathers with dilute Bose-Einstein condensates. *Physical Review Letters*, 86(11): 2353, 2001.
- [17] J N Kutz, and S G Evangelides. Dispersion-managed breathers with average normal dispersion. *Optics Letters*, 23(9): 685-687, 1998.
- [18] E Trias, J J Mazo, and T P Orlando. Discrete breathers in nonlinear lattices: Experimental detection in a josephson array. *Physical Review Letters*, 84(4): 741, 2000.
- [19] K W Chow, R H J Grimshaw, and E Ding. Interactions of breathers and solitons in the extended Kortewegde Vries equation. *Wave Motion*, 43(2): 158-166, 2005.

- [20] A V Slyunyaev. Dynamics of localized waves with large amplitude in a weakly dispersive medium with a quadratic and positive cubic nonlinearity. *Journal of Experimental and Theoretical Physics*, 92(3): 529-534, 2001.
- [21] K G Lamb, O Polukhina, T Talipova, E Pelinovsky, W Xiao, and A Kurkin. Breather generation in fully nonlinear models of a stratified fluid. *Physical Review E*, 75(4): 046306, 2007.
- [22] N Akhmediev, A Ankiewicz, and M Taki. Waves that appear from nowhere and disappear without a trace. *Physics Letters A*, 373(6): 675-678, 2009.
- [23] Ya-C Ma. The perturbed plane-wave solutions of the cubic Schrödinger equation. *Studies in Applied Mathematics*, 60: 43-58, 1979.
- [24] N Akhmediev, and A Ankiewicz. *Solitons, Nonlinear Pulses, and Beams*. Chapman and Hall, London, 1997.
- [25] V V Voronovich, V I Shrira, and G Thomas. Can bottom friction suppress freak waveformation? *Journal of Fluid Mechanics*, 604: 263-296, 2008.
- [26] T B Benjamin, and J E Feir. The disintegration of wave trains on deep water Part 1. Theory. *Journal of Fluid Mechanics* 27(3): 417-430, 1967.
- [27] D H Peregrine. Water waves, nonlinear Schrödinger equations and their solutions. *The Journal of the Australian Mathematical Society*, 25(01): 1643, 1983.
- [28] N Akhmediev, A Ankiewicz, and J M Soto-Crespo. Rogue waves and rational solutions of the nonlinear Schrödinger equation. *Physical Review E*, 80(2): 026601, 2009.
- [29] A Chabchoub, N Hoffmann, M Onorato, and N Akhmediev. Super rogue waves: observation of a higher-order breather in water waves. *Physical Review X*, 2(1): 011015, 2012.
- [30] A Chabchoub, N Hoffmann, M Onorato, A Slunyaev, A Sergeeva, E Pelinovsky, and N Akhmediev. Observation of a hierarchy of up to fifth-order rogue waves in a water tank. *Physical Review E* 86(5): 056601, 2012.

- [31] B Frisquet, B Kibler, and G Millot. Collision of Akhmediev Breathers in Nonlinear Fiber Optics. *Physical Review X*, 3(4): 041032, 2013.
- [32] G Neugebauer, and R Meinel. General N -soliton solution of the AKNS class on arbitrary background. *Physics Letters A*, 100(9): 467-470, 1984.
- [33] V B Matveev, and M A Salle. *Darboux Transformations and Solitons*. Springer, Berlin, 1991.
- [34] F Baronio, A Degasperis, M Conforti, and S Wabnitz. Solutions of the vector nonlinear Schrödinger equations: evidence for deterministic rogue waves. *Physical Review Letters*, 109: 044102, 2012.
- [35] J He, S Xu, and K Porsezian. New types of rogue wave in an erbium-doped fibre system. *Journal of the Physical Society of Japan* 81(3): 033002, 2012.
- [36] J He, S Xu, and K Porsezian. N-order bright and dark rogue waves in a resonant erbium-doped fiber system. *Physical Review E*, 86(6): 066603, 2012.
- [37] V N Serkin and A Hasegawa. Soliton management in the nonlinear Schrödinger equation model with varying dispersion, nonlinearity, and gain. *Journal of Experimental and Theoretical Physics Letters*, 72(2): 8992, 2000.
- [38] V N Serkin and A Hasegawa. Exactly integrable nonlinear Schrödinger equation models with varying dispersion, nonlinearity and gain: Application for soliton dispersion. *IEEE Journal of Selected Topics in Quantum Electronics*, 8(3): 418- 431, 2002.
- [39] V N Serkin, A Hasegawa, and T L Belyaeva. Nonautonomous matter-wave solitons near the Feshbach resonance. *Physical Review A*, 81(2): 023610, 2010.
- [40] V N Serkin, A. Hasegawa, and T L Belyaeva. Solitary waves in nonautonomous nonlinear and dispersive systems: nonautonomous solitons. *Journal of Modern Optics*, 57(14-15): 1456-1472, 2010.
- [41] A C Peacock. *Applications of light propagation in novel photonic devices*. PhD thesis, University of Southampton, 2004.

- [42] V I Kruglov, A C Peacock, and J D Harvey. Exact self-similar solutions of the generalized nonlinear Schrödinger equation with distributed coefficients. *Physical Review Letters*, 90(11): 113902, 2003.
- [43] S A Ponomarenko, and G P Agrawal. Do solitonlike self-similar waves exist in nonlinear optical media? *Physical Review Letters*, 97(1): 013901, 2006.
- [44] J M Dudley, C Finot, D J Richardson, and G Millot. Self-similarity in ultra-fast nonlinear optics. *Nature Physics*, 3(9): 597603, 2007.
- [45] V I Kruglov, A C Peacock, J M Dudley, and J D Harvey. Self-similar propagation of high power parabolic pulses in optical fiber amplifiers. *Optics Letters*, 25(24): 1753-1755, 2000.
- [46] S A Ponomarenko, and G P Agrawal. Optical similaritons in nonlinear waveguides. *Optics Letters*, 32(12): 1659-1661, 2007.
- [47] C Q Dai, Y Y Wang, Q Tian, and J F Zhang. The management and containment of self-similar rogue waves in the inhomogeneous nonlinear Schrödinger equation. *Annals of Physics*, 327(2): 512-521, 2012.
- [48] C Q Dai, G Q Zhou, and J F Zhang. Controllable optical rogue waves in the femtosecond regime. *Physical Review E, Statistical, nonlinear, and soft matter physics* 85(1): 016603, 2012.
- [49] L H Zhao, and C Q Dai. Self-similar cnoidal and solitary wave solutions of the (1+ 1)-dimensional generalized nonlinear Schrödinger equation. *The European Physical Journal D*, 58(3): 327-332, 2010.
- [50] C Dai, Y Wang, and C Yan. Chirped and chirp-free self-similar cnoidal and solitary wave solutions of the cubic-quintic nonlinear Schrödinger equation with distributed coefficients. *Optics Communications*, 283(7): 1489-1494, 2010.
- [51] M E Fermann, V I Kruglov, B C Thomsen, J M Dudley, and J D Harvey. Self-similar propagation and amplification of parabolic pulses in optical fibers. *Physical Review Letters*, 84(26): 6010, 2000.

- [52] Z Yan, and D Jiang. Matter-wave solutions in Bose-Einstein condensates with harmonic and Gaussian potentials. *Physical Review E*, 85(5): 056608, 2012.
- [53] J Belmonte-Beitia, and G F Calvo. Exact solutions for the quintic nonlinear Schrödinger equation with time and space modulated nonlinearities and potentials. *Physics Letters A*, 373(4): 448-453, 2009.
- [54] J Belmonte-Beitia, and J Cuevas. Solitons for the cubic-quintic nonlinear Schrödinger equation with time-and space-modulated coefficients. *Journal of Physics A: Mathematical and Theoretical*, 42(16): 165201, 2009.
- [55] L Infeld, and T E Hull. The factorization method. *Reviews of Modern Physics*, 23(1): 21, 1951.
- [56] B Mielnik. Factorization method and new potentials with the oscillator spectrum. *Journal of Mathematical Physics*, 25: 3387, 1984.
- [57] F Cooper, A Khare, and U Sukhatme. *Supersymmetry in quantum mechanics*. World Scientific Publishing Company, 2001.
- [58] A Khare, and C N Kumar. Landau level spectrum for charged particle in a class of non-uniform magnetic fields. *Modern Physics Letters A*, 8(6): 523529, 1993.
- [59] B Dey, and C N Kumar. New sets of kink-bearing Hamiltonians. *International Journal of Modern Physics A*, 9(15): 26992705, 1994.
- [60] C N Kumar. Isospectral hamiltonians: Generation of the soliton profile. *Journal of Physics A: Mathematical and General*, 20(15): 53975401, 1987.
- [61] M A Reyes, and H C Rosu. Riccati-parameter solutions of nonlinear second-order ODEs. *Journal of Physics A: Mathematical and Theoretical*, 41(28): 285206, 2008.
- [62] O Cornejo-Pérez, and H C Rosu. Nonlinear second order ode's: Factorizations and particular solutions. *Progress of Theoretical Physics*, 114(3): 533-538, 2005.

-
- [63] W Alka, A Goyal, and C N Kumar. Nonlinear dynamics of DNA-Riccati generalized solitary wave solutions. *Physics Letters A*, 375(3): 480-483, 2011.

Chapter 2

Controlling rogue waves in nonlinear optical fibers and waveguides

2.1 Introduction

These days a great amount of theoretically as well as experimental research is taking place on the study of rogue waves. This is because rogue waves are large amplitude waves and are capable of transmitting highly intense signals through nonlinear optical fibers. This opens up the flood gates for their use in digital communication. These waves have also been explored in space plasma [1, 2] and are related with the supercontinuum generation in a fiber [3, 4]. Thus, it is quite interesting to study the dynamics of rogue waves through different nonlinear media. In this chapter we study for different nonlinear optical systems the propagation of self-similar rogue waves which adjust themselves with the modulating system parameters. The entire chapter is divided into two parts: The first part involves the study and management of self-similar rogue waves in nonlinear optical fiber systems such as dispersion increasing and decreasing fibers, erbium doped fibers, periodic systems while the second part involves the propagation of rogue waves in the tapered graded-index nonlinear optical waveguides where we discuss the various management regimes of rogue waves and also study the effect of tapering of waveguides on the intensity of rogue waves by invoking Riccati generalization scheme. The concluding remarks are given in the end. Before presenting the main work we give a brief introduction of nonlinear optical fibers and waveguides and show that nonlinear Schrödinger equation (NLSE) is the governing model equation

to understand the dynamics of pulses in a nonlinear dispersive medium.

2.2 Optical Waveguides and Fibers

The dramatic reduction of transmission loss in optical fibers coupled with the developments in the area of light sources has resulted in a phenomenal growth of nonlinear fiber optics industry. Recent developments in optical amplifiers and wavelength division multiplexing (WDM) are paving the way to a communication system with almost zero loss and infinite bandwidth. To understand a nonlinear optical system, it is important to study the propagation of electromagnetic wave through an optical waveguide. An optical waveguide guides the propagation of electromagnetic pulse in the optical spectrum. They can be classified in accordance with their geometry, the form of refractive index and the nature of the material. In general they comprise of a high refractive index region (core) which is surrounded by a low refractive index dielectric material (cladding). The pulse propagates in the core region through the process of total internal reflections. Like all electromagnetic processes, Maxwell's equations are used to study the propagation of optical fields in a nonlinear medium. In the international system of units, these equations in vector form are given as

$$\nabla \times \mathbf{E} = -\frac{\partial \mathbf{B}}{\partial t}, \quad (2.1)$$

$$\nabla \times \mathbf{H} = \mathbf{J} + \frac{\partial \mathbf{D}}{\partial t}, \quad (2.2)$$

$$\nabla \cdot \mathbf{D} = \rho, \quad (2.3)$$

$$\nabla \cdot \mathbf{B} = 0, \quad (2.4)$$

where \mathbf{E} and \mathbf{H} are the vector electric and magnetic fields. The corresponding electric and magnetic flux densities are represented by \mathbf{D} and \mathbf{B} , respectively. The vector \mathbf{J} and ρ stand for the free current and charge densities. For a nonmagnetic dielectric medium such as optical fibers, \mathbf{J} and ρ become zero and the relation between the flux densities and the fields is given as

$$\mathbf{D} = \epsilon_0 \mathbf{E} + \mathbf{P}, \quad (2.5)$$

$$\mathbf{B} = \mu_0 \mathbf{H}, \quad (2.6)$$

where \mathbf{P} is the induced electric polarization in the medium, ϵ_0 and μ_0 are the permittivity and permeability of free space, respectively.

In order to study the pulse propagation in nonlinear dispersive media it is necessary to incorporate the nonlinear effects in \mathbf{P} and it takes the following form:

$$\mathbf{P}(\mathbf{r}, \mathbf{t}) = \mathbf{P}_L(\mathbf{r}, \mathbf{t}) + \mathbf{P}_{NL}(\mathbf{r}, \mathbf{t}), \quad (2.7)$$

where $\mathbf{P}_L(\mathbf{r}, \mathbf{t})$ indicates the linear contribution of polarization vector and $\mathbf{P}_{NL}(\mathbf{r}, \mathbf{t})$ arises due to the third-order nonlinear effect governed by the third-order susceptibility $\chi^{(3)}$. This in turn leads to nonlinear intensity dependent refractive index n of the medium which is given as

$$n = n_0 + n_2|E|^2, \quad (2.8)$$

where n_0 and n_2 characterize the linear and nonlinear (due to Kerr nonlinearity) response, respectively. At very high intensities, obtained by using lasers, the refractive index deviates from the linear response and in the generalized form can be written as

$$n = n_0 + n_{nl}(I), \quad (2.9)$$

where n_{nl} represents the variation in refractive index due to the intensity dependence of light ($I = |E|^2$). For a Kerr medium Eq. (2.9) becomes Eq. (2.8).

To simplify the calculations $\mathbf{P}_{NL}(\mathbf{r}, \mathbf{t})$ is treated as a small perturbation to the total induced polarization $\mathbf{P}(\mathbf{r}, \mathbf{t})$ and represents the weak Kerr nonlinearity. The next important step is to use the wave envelope function $\mathbf{E}(\mathbf{r}, \mathbf{t})$ which is slowly varying in time and can be expanded in the Fourier space by using $\Delta\omega = \omega - \omega_0$. This signifies a small frequency shift of the side band from the carrier frequency ω_0 , which in turn induces a shift in the carrier wave number as $\Delta k = k - k_0$. The expansion of the wave number $k(\omega)$ around k_0 can be given as follows:

$$k - k_0 = k_{\omega}|_{\omega=\omega_0} (\omega - \omega_0) + \frac{1}{2}k_{\omega\omega}|_{\omega=\omega_0} (\omega - \omega_0)^2 + \dots, \quad (2.10)$$

where the first derivative (k_{ω}) represents the group velocity and the second derivative ($k_{\omega\omega}$) stands for group velocity dispersion. Expanding the electric field envelope and combining the effects of group velocity dispersion and the weak Kerr nonlinearity, the following nonlinear equation is obtained [5]

$$iA_z + i\frac{\alpha}{2}A - \frac{\beta_2}{2}A_{TT} + \gamma|A|^2A = 0, \quad (2.11)$$

where $A(z, t)$ represents the complex amplitude of the electric field envelope \mathbf{E} , z is the normalized distance along the fiber and T is the retarded time which is measured in the reference frame moving along the fiber with group velocity. Also, α is the gain/loss term, β_2 stands for group velocity dispersion parameter and γ signifies self phase modulation parameter. For $\alpha = 0$, Eq. (2.11) is known as standard NLSE, which is used to describe ultrashort pulse propagation in a nonlinear system. It is completely integrable by inverse scattering transform method and is known to exhibit soliton solutions [6]. Although Eq. (2.11) has been successful in explaining a large number of nonlinear phenomena, it needs to be modified depending on the experimental conditions. If the peak power of the incident pulse is above than a certain threshold value then the higher order nonlinear effects in the system such as stimulated Raman scattering (SRS), self-steepening, third order dispersion, etc. need to be incorporated in the model equation. To study the pulse propagation in silica fibers, Eq. (2.11) is used and refer as cubic-NLSE. However, the fibers doped with highly nonlinear materials like organic dyes and semiconductors show the dependence on the fifth powers of the amplitude at $1\text{GW}/\text{cm}^2$ incident power intensity. To study the pulse propagation in these fibers, the effect of the fifth powers of the amplitude is included by quintic term and the resulting equation is known as cubic-quintic NLSE. This analogy is further extended and the model equation is refer as extended or higher order NLSE. It should be noted that Eq. (2.11) has constant coefficients and the constant coefficients NLSE describe the pulse propagation in a homogenous fiber. In realistic situations, fibers are not homogeneous due to manufacturing defects and density variations. Moreover, the longitudinal homogeneities drastically affect the pulse propagation. Hence, it is quite relevant to investigate the pulse behaviour in an inhomogeneous fiber. To introduce the effects of inhomogeneity of the fibers, the coefficients of NLSE are considered as space dependent and the governing equation is known as generalized NLSE (GNLSE). The variants of GNLSE have been studied in different contexts [7]. Surprisingly, if we replace the variable T with a spatial coordinate then the same equation governs the propagation of continuous wave beams in a planar waveguide. The β_2 term represents diffraction in the plane of the waveguide instead of dispersion in time. Therefore, the same equation governs the underlying physics for nonlinear fibers and waveguides. The analogy between “diffraction in

space” and “dispersion in time” can be exploited to understand the pulse propagation in waveguides and fibers. A brief discussion on nonlinear waveguides is provided in the next section.

2.3 Nonlinear waveguides

It is known that both the fibers and the waveguides support bright and dark soliton propagation. For fibers, they are termed as temporal solitons and for waveguides, they are known as spatial solitons. In case of optical fibers the GVD vanishes at a wavelength of about $1.3\mu m$ and is positive at large wavelengths and negative at short wavelengths [8]. The silica optical fibers always have positive Kerr coefficient and two different signs of GVD: positive (normal dispersion regime) and negative (anomalous dispersion regime), which in turn support two different kinds of solitons, dark in the first case and bright in the second case. A similar situation arises for self-guided beams or spatial solitons for waveguides. Here, the dispersion role in fibers is replaced by diffraction and the nonlinearity can be either positive or negative characterising the self-focusing or self-defocusing nature of the nonlinear medium. This is in contrast to the optical fibers where the nonlinearity (Kerr) can only take positive values. The two choices of the nonlinearity parameter again gives rise to two distinct types of solitons, bright and dark, respectively. Due to this spatio-temporal analogy in wave propagation, it is considered that the stationary beam propagation in planar waveguides is similar to the pulse propagation in fibers. This implies that the propagation coordinate is treated as the evolution variable and the spatial beam profile along the transverse direction (for waveguides) is similar to the temporal pulse profile (for fibers). This analogy has been explored by many researchers, by using the simple fact that both the phenomena are described by the NLSE [9].

We shall also exploit this analogy and discuss the propagation and management of rogue waves in different nonlinear fibers and tapered graded-index waveguide.

2.4 Rogue waves in nonlinear optical fibers

Rogue waves have become a subject of intense research owing to their potential applications in highly intense signal transmission through nonlinear optical systems. They are also going by the name of freak waves, monster waves, giant waves, etc. as they appear when certain conditions are met and then disappear without a trace. They appear in the ocean and cause vast destruction [10]. Their amplitude is two to three times larger than the amplitude of the average wavelets. The nonlinear theories provide a tool to understand the cause behind their generation as their occurrence is a nonlinear phenomena. Their possible nonlinear mechanisms are nonlinear focusing via modulation instability in one-dimensional and two-dimensional crossing, nonlinear spectral instability, focusing with caustic currents and anomalous wind excitation [11, 12]. While nobody wishes their emergence in the oceans due to their capability of carrying large amount of energy to cause vast destruction, experimentalists were excited to create these waves in a laboratory so that they can harness their properties for various practical purposes. Solli et al. successfully demonstrated these waves in an optical system, based on a microstructured optical fiber [13]. Since then, there was a surge of interest to understand the dynamics of rogue waves experimentally and theoretically. Various studies took place in this regard and these waves were extensively investigated in different contexts. Just like solitary waves are called as solitons, the term rogons is coined for rogue waves as they appear virtually unaffected in their size and shape after undergoing collisions [14]. The corresponding terminologies of oceanic rogons, optical rogons and matter wave rogons are used in the field of hydrodynamics, nonlinear optics and Bose-Einstein condensates (BECs), respectively. The NLSE admits modulation instability and hence is used as a model equation for rogue waves. Interestingly, it is also the governing model to describe pulse propagation in nonlinear optical systems and matter waves in BECs. Hence, nonlinear fiber optics and BECs provide a good platform to study rogue waves. Here we study the propagation of rogue waves through different nonlinear optical systems. The study of rogue waves in the context of BECs will be presented in Chapter 4.

As mentioned, the rogue waves are high amplitude pulses which make them

capable of transmitting highly intense signals through optical fibers and opens the flood gates for their use in digital communication. Consequently, their utility in telecommunication data streams has been revealed in [15]. Dai et al. have discussed the management and control of optical rogue waves as they propagate through nonlinear fibers [16, 17]. In addition to analytical investigations, numerical studies have also been carried out to study the generation and validity of optical rogue waves by including higher order terms like third order dispersion, self-steepening and self-frequency shift [18, 19, 20]. Very recently, J. Zamora-Munt and his coworkers predicted rogue waves in an optically injected laser [21]. The intriguing developments made in the field of rogue waves have motivated us to understand their behaviour analytically.

2.4.1 Model equation

We consider the model which is given by Serkin and Hasegawa to formulate the effect of varying dispersion with external harmonic oscillator potential, by using a methodology based on the generalized inverse scattering transform (IST) concept [22]

$$i\frac{\partial U}{\partial Z} + \frac{D(Z)}{2}\frac{\partial^2 U}{\partial \tau^2} + R(Z)|U|^2U + i(\alpha(Z) + \delta D(Z)P(Z)\tau)\frac{\partial U}{\partial \tau} - \frac{i}{2}\Gamma(Z)U = 0 \quad (2.12)$$

where $U(\tau, Z)$ represents the normalized slowly varying complex envelope of the pulse, τ and Z are the retarded time and the normalized propagation distance in the nondimensional form, respectively. $D(Z)$, $R(Z)$, $P(Z)$ and $\Gamma(Z)$ are real functions and account for the varying dispersion corresponding to which it has a harmonic oscillator potential form, varying nonlinearity, nonlinear focus length and gain/loss respectively. The parameter $\alpha(Z)$ denotes the velocity of propagation. In the above equation it is mandatory that the radius of curvature of the wavefront must be an oscillating function of the propagating distance in order to have the oscillating self-focusing light beam in nonlinear Kerr-like media. We would like to mention that the model Eq. (2.12) is nonautonomous in nature due to the explicit presence of time τ . It has been used to study the various aspects of dispersion management of solitons and their interactions pertaining to in-phase

and off-phase injection with equal and unequal amplitudes [23, 24]. Now we have to find the exact analytical rogue wave solutions for Eq. (2.12) and to discuss their controllable propagation for different choices of dispersion parameter.

2.4.2 Similarity transformation

In general, the inhomogeneous NLSE with distributive coefficients is not integrable and hence can not be solved directly by using integrable techniques. These days a very effective mathematical tool, known as similarity transformation is used to find the exact solutions of NLEEs with distributive coefficients. The similarity transformation involves the mapping of distributive coefficients NLEEs to their respective constant coefficient NLEE. Then, by borrowing the known solutions of constant coefficient NLEEs and by doing the back transformation the exact solutions of distributive NLEEs can be obtained. The advantage of this method is that it ensures the stability or instability of the solutions as they are obtained from the respective counterparts of the constant coefficient NLEEs. If the solution of the constant coefficient NLEE is stable then the solution of the distributive coefficient will be stable, worked out by similarity transformation and vice-versa. This technique has been successfully employed to obtain the exact solution of (1+1)-dimensional and (2+1)-dimensional GNLSE [25, 26]. Dai et al. have adopted this method to obtain the solutions of GNLSE with linear potential term [27]. Various researchers have applied this method to study the similaritons, similariton pairs and the class of self-similar nonlinear waves as they propagate through a tapered graded-index nonlinear waveguide [28, 29, 30]. Raju and Panigrahi have investigated the optical similaritons through a tapered graded-index nonlinear waveguide amplifier by including external source term [31]. This method has not only been applied in nonlinear optics but has also been used in the context of BECs to study the dynamics of nonautonomous bright-dark matter wave solitons [32].

In order to work out the exact solution of Eq. (2.12) we are choosing the following similarity transformation

$$U(\tau, Z) = A(Z)\psi[\chi(\tau, Z), \rho(Z)]e^{i\Phi(\tau, Z)}, \quad (2.13)$$

with

$$\chi(\tau, Z) = \frac{\tau - \tau_c(Z)}{w}, \quad (2.14)$$

where the amplitude $A(Z)$, the similarity variable $\chi(\tau, Z)$, the phase $\Phi(\tau, Z)$, dimensionless pulse width w and the position of the rogue wave center $\tau_c(Z)$ are real functions and $\psi(\chi, \rho)$ is a complex function. Explicitly, the form of quadratically chirped phase can be considered as

$$\Phi(\tau, Z) = C(Z)\frac{\tau^2}{2} + B(Z)\tau + d_1(Z), \quad (2.15)$$

where $C(Z)$, $B(Z)$ and $d_1(Z)$ are parameters related to the phase-front curvature, the frequency shift, and the phase offset, respectively.

For the given $D(Z)$, $R(Z)$ and $\alpha(Z)$ the gain $\Gamma(Z)$ and the nonlinear focus length $P(Z)$ can be obtained by using the following integrability conditions

$$\Gamma(Z) = \left(\frac{W[R, D]}{RD} - \delta PD \right), \quad (2.16)$$

with

$$\begin{aligned} W[R, D] &= RD_Z - DR_Z, \\ P_Z &= -\delta P^2 D. \end{aligned} \quad (2.17)$$

The functional form of the parameters $R(Z)$ and $D(Z)$ must be chosen in such a way so that the gain $\Gamma(Z)$ does not become singular. On inserting the transformation given in Eq. (2.13) and Eq. (2.14) in Eq. (2.12) along with the phase Φ , it reduces to the standard NLSE

$$i\frac{\partial\psi}{\partial\rho} + \frac{1}{2}\frac{\partial^2\psi}{\partial\chi^2} + |\psi|^2\psi = 0. \quad (2.18)$$

where $\rho(Z)$ represents the effective propagation distance and is given as

$$\rho(Z) = \frac{\int_0^Z D(S)dS}{w^2}, \quad (2.19)$$

It is worth mentioning here that the form of ρ is governed by the dispersion parameter $D(Z)$ as w represents the width of the pulse which is constant.

The rogue wave center $\tau_c(Z)$ is given as follows

$$\tau_c(Z) = \left(\tau_0 + C_{02} \int_0^Z (\alpha(S) + D(S)B(S))dS \right), \quad (2.20)$$

where τ_0 and C_{02} are constants. The parameters $A(Z)$, $B(Z)$, $C(Z)$ and $d_1(Z)$ are obtained by collecting the similar terms after the substitution of Eq. (2.13) and Eq. (2.14) in Eq. (2.12) along with the phase Φ and demanding the coefficients of real and imaginary parts of each term to be separately equal to zero. In the explicit form they can be defined as

$$\begin{aligned} A(Z) &= \frac{1}{w} \sqrt{\frac{D}{R}}, \quad B(Z) = \int_0^Z \delta P(S) dS, \quad C(Z) = -\delta P(Z), \\ d_1(Z) &= - \int (\alpha(Z)B(Z) + \frac{D(Z)B(Z)^2}{2}) dZ. \end{aligned} \quad (2.21)$$

The nonlinear focus length $P(Z)$ can be obtained by using Eq. (2.17) as

$$P(Z) = - \frac{1}{(c_0 - \delta \int_0^Z D(Z') dZ')}, \quad (2.22)$$

where c_0 is an integration constant and has to be chosen in such a way so that $P(Z)$ is non singular.

2.4.3 Self-similar first and second-order rogue waves

We can obtain the exact solutions of Eq. (2.12) by reducing it to standard NLSE through the transformation given in Eq. (2.13) for the conditions given in Eqs. (2.16) and (2.17). Through this methodology, one can obtain the known solutions of the standard NLSE such as single soliton or multisoliton, breathers, rogue wave solutions, etc. (discussed in Section 1.1) for Eq. (2.12). Here, we are interested in obtaining first and second order rogue wave solutions because of their capability to carry large amounts of energy. The first-order (U_1) and the second-order (U_2) rogue wave solution of Eq. (2.12) can be given as [17]

$$U_1(Z, \tau) = \frac{1}{w} \sqrt{\frac{D}{R}} \left[1 - \frac{4(1 + 2i(\rho - \rho_0))}{1 + 4((\rho - \rho_0)^2 + 4\chi^2)} \right] e^{i(\rho - \rho_0)}, \quad (2.23)$$

$$U_2(Z, \tau) = \frac{1}{w} \sqrt{\frac{D}{R}} \left[1 - \frac{k + ih_1}{l} \right] e^{i(\rho - \rho_0)}, \quad (2.24)$$

The corresponding intensities of first (I_1) and second (I_2) order rogue waves read

$$I_1 = |U_1|^2 = \frac{1}{w^2} \frac{D}{R} \left[1 + 8 \frac{1 + 4(\rho - \rho_0)^2 - 4\chi^2}{(1 + 4(\rho - \rho_0)^2 + 4\chi^2)^2} \right]. \quad (2.25)$$

$$I_2 = |U_2|^2 = \frac{1}{w^2} \frac{D}{R} \left[\frac{(l-k)^2}{l^2} + \frac{h_1^2}{l^2} \right], \quad (2.26)$$

where

$$l = \frac{1}{3}[\chi^2 + (\rho - \rho_0)^2]^3 + \frac{1}{4}[\chi^2 - 3(\rho - \rho_0)^2]^3 + \frac{3}{64}12\chi^2 + 44(\rho - \rho_0)^2 + 1, \quad (2.27)$$

$$k = \left(\chi^2 + (\rho - \rho_0)^2 + \frac{3}{4} \right) \left(\chi^2 + 5(\rho - \rho_0)^2 + \frac{3}{4} \right) - \frac{3}{4}, \quad (2.28)$$

$$h_1 = \rho \left(-3\chi^2 + (\rho - \rho_0)^2 + 2(\chi^2 + (\rho - \rho_0)^2)^2 - \frac{15}{8} \right). \quad (2.29)$$

Here ρ_0 is an arbitrary constant. The effective propagation distance ρ and the similarity variable χ can be obtained from Eq. (2.19) and Eq. (2.14), respectively.

In order to understand the pulse propagation, various forms of distributed parameters can be chosen according to the specific problem. Here, we are exemplifying it for two cases: one corresponds to $W[R, D] = 0$ and the other one for $W[R, D] \neq 0$.

Case(i) Wronskian $W[R, D] = 0$

Consider the following forms of nonlinearity and dispersion parameter

$$R(Z) = D(Z) = a \cos[\kappa Z]. \quad (2.30)$$

For these periodic choices of the parameters, the corresponding $P(Z)$ and $\Gamma(Z)$ can be obtained by using Eq. (2.22) and Eq. (2.16). Clearly, the above choice of parameters yields the zero value of Wronskian $W[R, D]$.

The profile of $\Gamma(Z)$ is plotted in Fig. 2.1. It reveals that the gain/loss parameter $\Gamma(Z)$ is periodic in nature and possesses a constant amplitude. So the pulse does not suffer any broadening and compression but an overall phase change, which is depicted in Fig. 2.2(a) and Fig. 2.2(b) for first and second order rogue waves, respectively.

The periodic choice of dispersion and nonlinearity parameters is of practical relevance as it has been used to study nonautonomous solitons in external potentials [34] and indicates the improved stability of solitons [35]. In particular, periodic form of dispersion finds applications in enhancing the signal to noise ratio,

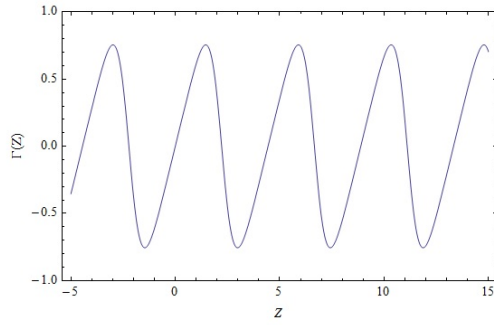


Figure 2.1: The profile of $\Gamma(Z)$ for $D(Z) = R(Z) = a \cos(\kappa Z)$, $\kappa = \sqrt{2}$ and $w = 1$, $a = 1$, $\rho_0 = 0$, $c_0 = 1.5$.

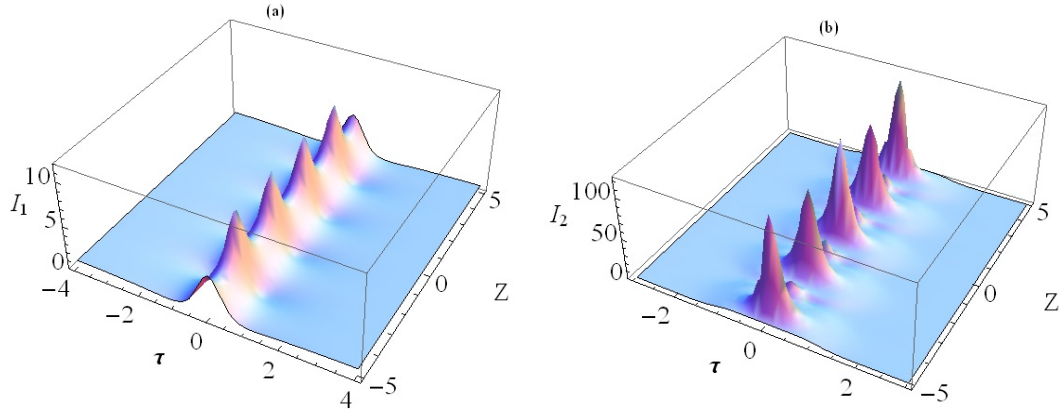


Figure 2.2: Intensity profile (a) for first-order rogue waves of Eq. (2.12) (b) for second-order rogue waves of Eq. (2.12) with $D(Z) = R(Z) = a \cos(\kappa Z)$, $\kappa = \sqrt{2}$ and $w = 1$.

reducing Gordon Haus time jitter and in suppressing the phase matched condition for four wave mixing in single mode optical fibers [36].

Case(ii) Wronskian $W[R, D] \neq 0$

For this case we have taken the nonlinearity and dispersion parameters as follow

$$R(Z) = \gamma \cos(\kappa Z), \quad D(Z) = \frac{\gamma}{d_0} \cos(\kappa Z) \exp(\sigma Z), \quad (2.31)$$

where the parameters κ and d_0 are related to Kerr nonlinearity and the initial peak power in the system, respectively. The parameter σ can take positive and negative values. The positive (negative) value of σ stands for dispersion increasing (de-

creasing) fibers. For these choices of the parameters, the corresponding nonlinear focus length $P(Z)$ and the gain/loss function $\Gamma(Z)$ can be obtained by using Eq. (2.22) and Eq. (2.16), respectively. The profile of $\Gamma(Z)$ for the dispersion increasing and dispersion decreasing fiber case has been plotted in Fig. 2.3 which demonstrates that the gain/loss parameter $\Gamma(Z)$ increases with propagation distance Z for dispersion increasing fiber, and decreases with Z for dispersion decreasing fiber.

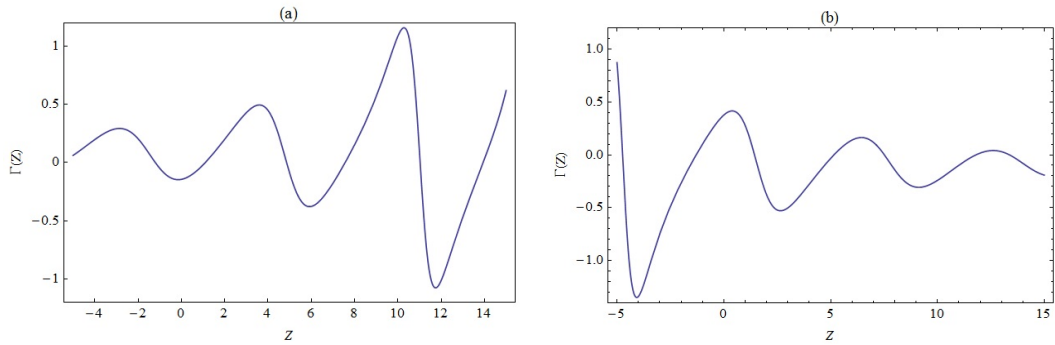


Figure 2.3: The profile of $\Gamma(Z)$ for (a) dispersion increasing fiber case with $c_0 = -2$ and $\sigma = 0.1$ (b) dispersion decreasing fiber case with $c_0 = 1$ and $\sigma = -0.1$. The other parameters are $\kappa = 1$ and $\gamma = 0.5$.

We have plotted the intensity profiles for first and second order rogue waves for both dispersion increasing and decreasing fibers in Fig. 2.4(a), Fig. 2.4(b), Fig. 2.5(a) and Fig. 2.5(b), respectively.

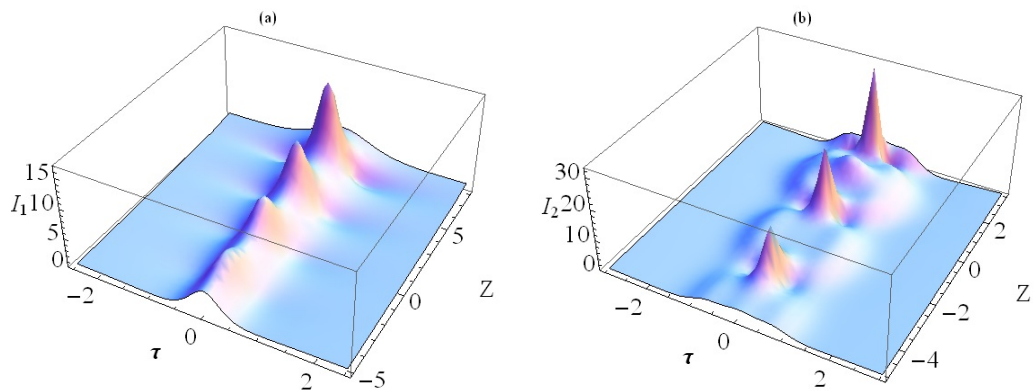


Figure 2.4: Intensity profile in dispersion increasing fiber (a) for first-order rogue waves of Eq. (2.12) (b) for second-order rogue waves of Eq. (2.12) with $c_0 = -2$, $\kappa = 1$, $\gamma = 0.5$ and $\sigma = 0.1$

Clearly the amplitude of the pulse changes as it propagates through the fiber while its width remains constant. In case of dispersion increasing fiber, the amplitude of the rogue wave increases while the opposite happens for dispersion decreasing fiber case. This is because the dispersion increasing (decreasing) fiber is under the influence of the gain parameter $\Gamma(Z)$ whose amplitude increases (decreases) with Z , as depicted in Fig. 2.3. This is in contrast to the other known results where the increase in the amplitude occurs at the cost of the width of the pulse.

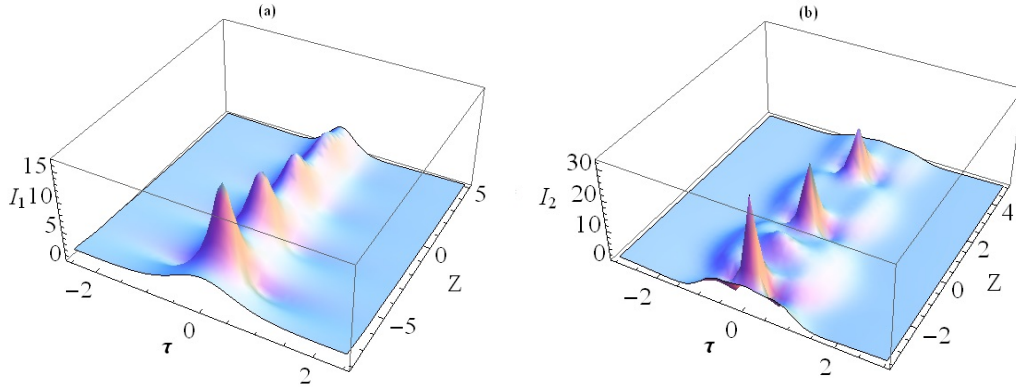


Figure 2.5: Intensity profile in dispersion decreasing fiber (a) for first-order rogue waves of Eq. (2.12) (b) for second-order rogue waves of Eq. (2.12) with $c_0 = 1$, $\kappa = 1$, $\gamma = 0.5$ and $\sigma = -0.1$

A similar analysis of rogue waves has been reported in [37] by using lens-type transformation. However while studying the dynamical properties of the system in [37], the gain term is explicitly made zero whereas in our study the gain/loss parameter $\Gamma(Z)$ is Z dependent which corresponds to more realistic systems. Consequently, our results hold greater practicality. Additionally, we have also obtained the rogue wave solutions for GNLSE by including an approximate form of self-induced Raman effect and have revealed that their interactions can be tuned by properly choosing the system parameters [38].

2.5 Signal attenuation in optical fiber

We have discussed the rogue wave propagation through different nonlinear optical fiber systems by using GNLSE and by employing self-similarity transformation. In general, when the pulse propagates through a nonlinear optical fiber system it gets attenuated or even sometimes vanishes due to the inherent absorption and scattering processes. The typical transmission loss exhibited by silica fiber is $0.2\text{dB}/\text{Km}$ near $1.55\mu\text{m}$. To measure the power loss during transmission, a fiber parameter is introduced, known as attenuation constant. It is a measure of total losses from all the sources. It is expressed in units of dB/Km . If the power launched at the input of the fiber length L is P_0 and the transmitted power is P_T then the attenuation parameter $\alpha_{1\text{dB}}$ is given as

$$\alpha_{1\text{dB}} = -\frac{10}{L} \log\left(\frac{P_T}{P_0}\right). \quad (2.32)$$

The fiber losses depend on the wavelength of the light. Several factors contribute to the spectrum loss but the major contribution towards the spectrum loss are the material absorption and Rayleigh scattering.

Absorption losses

The absorption losses are caused by the presence of impurities such as traces of metal ions and hydroxyl ions. Optical power is absorbed in the molecular excitation of these impurities in the glass in the vicinity of definite wavelength which corresponds to the natural oscillation frequencies and their harmonics of the particular material. In modern fibers, the absorption losses are almost entirely present due to hydroxyl ions which has a fundamental vibrational absorption peak at $\approx 2.7\mu\text{m}$. To minimize the losses due to absorption special precautions need to be taken during the manufacturing of the fibers to ensure that the hydroxyl ion level should not exceed one part in one hundred million [39]. These losses virtually disappear in the so called “dry” fibers [40]. Such fibers which show low losses in the spectral regime $1.3\mu\text{m} - 1.6\mu\text{m}$ are considered suitable for fiber optic communication. Unlike scattering losses which are wideband effects, absorption losses due to each type of impurity behave like a band suppression filter which show absorption peak at well defined wavelengths.

Scattering losses

On the other hand, despite careful manufacturing techniques, fibers are inhomogeneous in nature and have disordered structures. The scattering losses are caused by the imperfections present in the core material and the irregularities between the core-cladding interface [41]. These inhomogeneities result in the fluctuation of the refractive index. If the scale of these fluctuations is on the order of $1/10$ or less, each irregularity acts as a scattering center. This form is known as Rayleigh scattering and is characterized by an effective absorption coefficient that varies as λ^{-4} and are dominant at shorter wavelengths. These losses are not localized and can even be caused by the tiny dielectric inconsistencies in the glass. They can be minimized by having low thermodynamic density fluctuations.

Modern fibers exhibit a loss of $\approx 0.2dB/Km$ near $1.55\mu m$. These losses can be compensated by doping the core of the fiber with erbium atoms. We now discuss the basics of erbium doped fibers and then demonstrate the rogue wave propagation and their management through the erbium doped fiber system.

2.6 Erbium doped fiber amplifiers (EDFA)

It is well known that the optical soliton pulses which arise due to the delicate balance between the GVD (in the anomalous regime) and the Kerr nonlinearity propagate in an optical fiber. Their propagation is governed by NLSE of the following form [42]

$$U_Z = i\left(\frac{1}{2}U_{\tau\tau} + |U|^2U\right). \quad (2.33)$$

As these pulses propagate along the fiber they get attenuate and can vanish due to the above mentioned losses inherently present in the system. To overcome this problem it is necessary to incorporate some medium which can provide continuous amplification to the pulse. This is achieved by doping the silica fiber core with a two-level resonant medium. The amplifier properties such as operative wavelength and the gain bandwidth are determined by the dopants rather than the silica fiber which plays the role of a host medium. For this purpose, many rare earth elements such as erbium, holmium, neodymium, samarium, ytterbium, etc.

have been used to realize fiber amplifiers operating at different wavelengths ranging from $500\text{nm} - 3500\text{nm}$. Among all, erbium atoms have gathered significant attention because they operate in the wavelength region near 1550nm which is suitable for optical telecommunication. The EDFA is pumped from a laser at a wavelength of 980nm or 1480nm and exhibits gain at the 1550nm region. These transitions are shown in Fig. 2.6

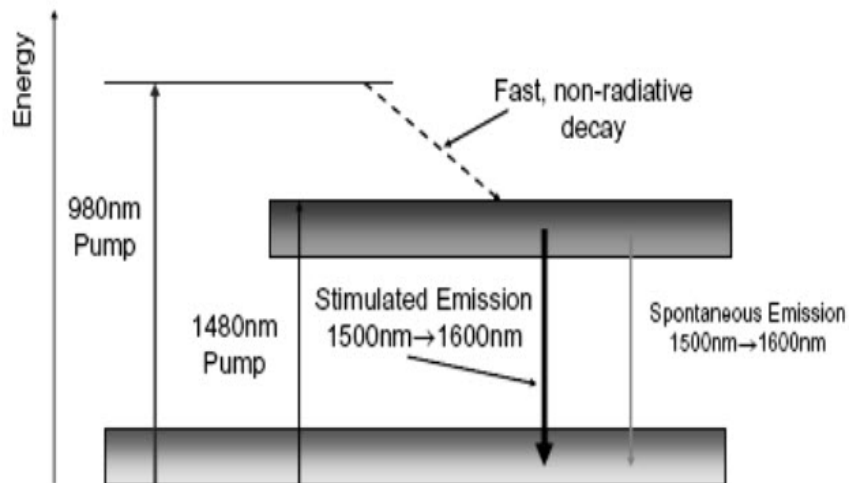


Figure 2.6: Energy-level diagram of erbium ions in silica fiber.

The two-level resonant medium like erbium atoms support soliton kind of pulse propagation known as self-induced transparency (SIT). The SIT arises when the ultrashort optical pulse of central frequency ω propagates in a two-level resonant medium with the frequency separation close to ω . The coherent interaction between the optical field and the two-level erbium atoms makes the medium optically transparent at resonance [43]. These coherent interactions arise due to resonant absorption and control the optical losses in the fiber medium.

2.6.1 Background and Motivation

McCall and Hahn proposed that the coherent pulse propagation (SIT) is described by Maxwell-Bloch (MB) equations [44]. The MB equations are given as

$$\begin{aligned} U_Z &= \langle p \rangle, \\ p_\tau &= i\omega p - fU\eta, \\ \eta_\tau &= 2f(Up^* + U^*p), \end{aligned} \quad (2.34)$$

where $p = v_1 v_2^*$, $\eta = |v_2|^2 - |v_1|^2$ and f describes the interaction between the propagating field and the two-level resonant atoms. Here v_1 and v_2 stand for the wavefunctions in a two-level system, ω is the frequency and $\langle p \rangle$ represents the averaging with respect to inhomogeneous broadening of the resonant frequency;

$$\langle p(Z, \tau; \omega) \rangle = \int_{-\infty}^{\infty} p(Z, \tau; \omega) g(\omega) d\omega, \quad (2.35)$$

with

$$\int_{-\infty}^{\infty} g(\omega) d\omega = 1. \quad (2.36)$$

Here, $g(\omega)$ is a distribution function and is a measure of the uncertainty in the energy level of resonant atoms.

In general, the optical fibers support two types of solitons. One type have been predicted by Hasagawa that arise due to the delicate balance between dispersion and the nonlinear term and are governed by well the known NLSE [42]. The other type are due to the presence of erbium atoms in the fiber core which causes the coherent absorption and re-emission of light from the atoms and are governed by MB equations. From a practical point of view, Eq. (2.33) represents the soliton propagation in an impurity-free optical fiber but despite powerful manufacturing techniques it is not possible to get impurity-free fibers. These impurities contribute to radiation absorption and lead to inhomogeneous broadening of the impurity energy levels. There is always a group of energy levels that are in resonance with the radiation transmitted through the fiber. This will make the system contribute to SIT. The impurities can be added in the form of erbium atoms which will result in the amplification of optical pulses which tend to decay during the course of their propagation. The dynamics of optical pulses in an erbium doped fiber system are

described by coupled nonlinear Schrödinger-Maxwell-Bloch (NLS-MB) equation of the form

$$\begin{aligned} U_Z &= iDU_{\tau\tau} - iR|U|^2|U| + \langle p \rangle, \\ p_\tau &= i\omega p - fU\eta, \\ \eta_\tau &= 2f(Up^* + U^*p). \end{aligned} \quad (2.37)$$

The solitons supported by Eq. (2.37) are termed as NLS-MB solitons. The model Eq. (2.37) was predicted by Maimistov and Manykin to treat the ultra-short pulse propagation in a light pipe with a two-level resonant medium with Kerr nonlinearity [45]. Nakazawa et al. have observed SIT solitons experimentally in an erbium doped silica fiber waveguide [46]. In their experiment, they cooled the fiber to 4.2 K and the corresponding dipole-dephasing time was of the order of nanoseconds. The resulting SIT solitons which were generated this way were short enough to be in the coherent photon-atom interaction regime. The co-existence of NLS and SIT soliton has also been confirmed in [47, 48]. The experimental observation of NLS-MB soliton stimulated the research on EDFA. Soon afterwards, Painléve analysis and Lax pair [49] had been carried out to study the integrability of the system and even the soliton solutions of the coupled NLS-MB model have been reported [50]. Nakkeeran investigated the optical solitons in erbium doped fibers by including higher order terms and pumping effects [51, 52]. With time, an enormous amount of analytical research took place to study the integrability aspect [53], soliton propagation, their management and their properties in an inhomogeneous erbium doped fiber system which is governed by variable coefficient NLS-MB equations [54, 55]. Recently, the two soliton solutions for an inhomogeneous NLS-MB model have been constructed by using the Lax pair and Darboux transformation technique where interesting features of the solitons have been revealed [56, 57]. Moreover, the nonlinear tunneling properties of optical solitons in the inhomogeneous NLS-MB model have also been investigated [58]. In addition to analytical studies on EDFA, these fibers have also been exploited experimentally [59, 60, 61]. Very recently, He et al. have shown the existence of bright and dark rogue waves in a homogeneous optical fiber doped with erbium atoms [62]. They have further extended this study and obtained the N-order bright and dark rogue wave solutions for constant coefficient NLS-MB model equation using Darboux

transformation by assuming periodic seed solutions [63]. In realistic situations, fibers doped with erbium atoms are not homogeneous due to density variations and manufacturing defects and so it is quite relevant to work out the rogue wave solitons for the variable coefficient NLS-MB model equation which describes the pulse propagation in an inhomogeneous erbium doped fiber system. The next section of this chapter is devoted to obtain the bright and dark rogue wave solutions for the inhomogeneous NLS-MB model, followed by studying their characteristics for the hyperbolic choices of the parameters.

2.6.2 Bright and dark rogue waves in an inhomogeneous erbium doped fiber system

We are considering coupled generalized nonlinear Schrödinger-Maxwell-Bloch (GNLS-MB) equations of the form

$$\begin{aligned} iU_Z + \frac{D(Z)}{2}U_{\tau\tau} + R(Z)|U|^2U - \frac{i}{2}\Gamma(Z) - 2i\beta(Z)\langle p \rangle &= 0, \\ p_\tau &= 2i\omega p + 2f(Z)U\eta, \\ \eta_\tau &= -f(Z)(Up^* + U^*p). \end{aligned} \quad (2.38)$$

The parameter $\beta(Z)$ accounts for the interaction between silica and doped atoms and $\Gamma(Z)$ represents the gain/loss term.

For simplicity, we have chosen the distribution function $g(\omega)$ as a Dirac delta function at resonant frequency ω_0 i.e. an infinitely narrow line. So the averaging function given by Eq. (2.35) becomes

$$\begin{aligned} \langle p(Z, \tau; \omega) \rangle &= \int_{-\infty}^{\infty} p(Z, \tau; \omega)\delta(\omega - \omega_0)d\omega, \\ &= p(Z, \tau; \omega_0) \end{aligned} \quad (2.39)$$

Using this, Eq. (2.38) reads

$$\begin{aligned} iU_Z + \frac{D(Z)}{2}U_{\tau\tau} + R(Z)|U|^2U - \frac{i}{2}\Gamma(Z) - 2i\beta(Z)p &= 0, \\ p_\tau &= 2i\omega_0 p + 2f(Z)U\eta, \\ \eta_\tau &= -f(Z)(Up^* + U^*p). \end{aligned} \quad (2.40)$$

Now we are interested to obtain the exact bright and dark rogue wave solutions of Eq. (2.40). As we have used earlier, we will employ the same methodology that involves the mapping of the variable coefficient NLEE to its corresponding constant coefficient model equation to get the desired rogue wave solutions of Eq. (2.40). To do so we have chosen the ansatz for $U(Z, \tau)$ as

$$U(Z, \tau) = A(Z)\psi[\chi, \rho] \quad (2.41)$$

with $\chi = \chi(t)$ and $\rho = \rho(Z)$. Here ψ is a complex function and $A(Z)$ denotes the amplitude of the rogue waves.

We are setting χ of the form

$$\chi(\tau) = \frac{\tau}{w}. \quad (2.42)$$

The main task is to determine the concrete expressions for ρ and the various conditions among the parameters $R(Z)$, $D(Z)$, $A(Z)$, $f(Z)$, $\Gamma(Z)$ which reduces Eq. (2.40) to the following homogeneous equation

$$\begin{aligned} i\psi_\rho + \frac{1}{2}\psi_{\chi\chi} + |\psi|^2\psi - 2ip &= 0, \\ p_\chi &= 2i\omega p + 2\psi\eta, \\ \eta_\chi &= -(\psi p^* + \psi^* p). \end{aligned} \quad (2.43)$$

On substituting Eq. (2.41) along with Eq. (2.42) into Eq. (2.40), the explicit form of $\rho(Z)$ and the various conditions can be worked out by collecting the coefficients of similar terms. Then on demanding the coefficients of real and imaginary parts of each term to be explicitly zero, we get

$$\rho(Z) = \frac{\int_0^Z D(S)dS}{w^2}, \quad (2.44)$$

$$A(Z) = \sqrt{\frac{D(Z)}{R(Z)}} \frac{1}{w}. \quad (2.45)$$

with the following conditions among various equation parameters

$$\beta(Z) = R(Z)A^3, f(Z) = \sqrt{\frac{R(Z)}{D(Z)}}, \quad (2.46)$$

$$\Gamma(Z) = \frac{W[R, D]}{RD}. \quad (2.47)$$

Since Eq. (2.40) has been reduced to homogeneous NLS-MB system, hence by using Eqs. (2.41) and (2.42) we can present the exact rogue wave solutions for inhomogeneous GNLS-MB model as follows [62]

$$U(Z, \tau) = \frac{1}{w} \sqrt{\frac{D(Z)}{R(Z)}} \exp(is_1) \left[-d - \frac{4d \left(\frac{2ids_3(\rho - \rho_0)}{s_2} - 1 \right)}{\frac{4d^2(-s_2\chi + s_4(\rho - \rho_0))^2}{s_2^2} + 1 + \frac{4d^2s_3^2(\rho - \rho_0)^2}{s_2^2}} \right], \quad (2.48)$$

$$p = \frac{k_1}{k_2}, \quad (2.49)$$

$$\eta = -\frac{k_3}{k_2}, \quad (2.50)$$

Here,

$$\begin{aligned} k_1 = & [-64d^4s_5s_4s_3^2s_2\chi(\rho - \rho_0)^3 - 64d^4s_5s_4s_3^3\chi^3(\rho - \rho_0) - 64d^4s_5s_4^3s_2\chi(\rho - \rho_0)^3 \\ & + 16d^4s_5s_3^4(\rho - \rho_0)^4 + 16d^4s_5s_4^4(\rho - \rho_0)^4 + 16d^4s_5s_2^4\chi^4 + 32d^4s_5s_4^2s_3^2(\rho - \rho_0)^4 + \\ & 32d^4s_5s_3^2s_2^2(\rho - \rho_0)^2\chi^2 - 8d^2s_6s_4^2s_2^2(\rho - \rho_0)^2 - 8d^2s_6s_4^2\chi^2 \\ & - 8d^2\left(\frac{1}{2}b - \omega_0\right)^2 + 3d^2s_3^2s_2^2(\rho - \rho_0)^2 + 16d^2s_6s_4s_2^3(\rho - \rho_0)\chi + \\ & 96d^4s_5s_4^2s_2^2\chi^2(\rho - \rho_0)^2 + 32d^3s_4s_3\left(-\frac{1}{2}b + \omega_0\right)s_2^2(\rho - \rho_0)^2 - 32d^3s_3\left(-\frac{1}{2}b + \omega_0\right)s_2^3(\rho - \rho_0)\chi + \\ & (d^2 - 3\left(\frac{1}{2}b - \omega_0\right)^2)s_2^4 + 8is_7s_3^3s_2d(\rho - \rho_0)^3 + 8is_3s_3^3\left(\frac{1}{4}b^2 - d^2 - b\omega_0 + \omega_0^2\right)d(\rho - \rho_0) + \\ & 8ids_7s_3s_2^3(\rho - \rho_0)\chi^2 - 16ids_7s_4s_3s_2^2(\rho - \rho_0)^2\chi + 8i(db - 2d\omega_0)ds_2^4\chi - \\ & 8i(db - 2d\omega_0)d(\rho - \rho_0)s_2^3s_4 + 8is_7d(\rho - \rho_0)^3s_4^2s_3s_2] \exp(is_1)id, \end{aligned}$$

$$k_2 = (4d^2(s_2\chi - s_4(\rho - \rho_0))^2 + 4d^2s_3^2(\rho - \rho_0)^2 + s_2^2)^2 \left(\frac{1}{2}b - \omega_0\right)s_5, \quad (2.51)$$

$$\begin{aligned} k_3 = & -(16d^4s_8s_2^4\chi^4 - 64d^4s_8s_4s_2^3\chi^3(\rho - \rho_0) + ((32d^4s_8s_2^2s_3^2 + 96d^4s_8s_2^2s_4^2)(\rho - \rho_0)^2 + \\ & 8d^2s_9s_2^4)\chi^2 + ((-64d^4s_8s_2s_4^3 - 64d^4s_8s_4s_2s_3^2)(\rho - \rho_0)^3 + (-32d^5s_3s_2^3 - \\ & 16d^2s_9s_4s_2^3)(\rho - \rho_0))\chi + (16d^4s_8s_4^4 + 16d^4s_8s_3^4 + 32d^4s_8s_4^2s_3^2)(\rho - \rho_0)^4 + \\ & (32d^5s_4s_3s_2^2 + 8d^2\left(\frac{1}{8}b^3 + d^2\omega_0 - \omega_0^3 - \frac{3}{4}b^2\omega_0 + \frac{3}{2}b\omega_0^2 - \frac{1}{2}d^2b\right)s_2^2s_3^2 + \\ & 8d^2s_9s_4^2s_2^2)(\rho - \rho_0)^2 + \left(-\frac{3}{4}b^2\omega_0 + \frac{3}{2}b\omega_0^2 + \frac{1}{8}b^3 - \omega_0^3 - \frac{3}{2}d^2b + 3d^2\omega_0\right)s_2^4), \end{aligned}$$

with

$$s_1 = \frac{-b(\frac{1}{2}b - \omega_0)\chi + (2 + 2(\frac{1}{2}b - \omega_0)(\frac{1}{4}b^2 - \frac{1}{2}d^2))\rho}{-\frac{1}{2}b + \omega_0}, \quad (2.52)$$

$$s_2 = (-\frac{1}{2}b + \omega_0)((\frac{1}{2}b - \omega_0)^2 + d^2), \quad (2.53)$$

$$s_3 = -d\omega_0(d^2 + \omega_0^2) - \frac{3}{2}db\omega_0(\frac{1}{2}b - \omega_0) + \frac{1}{2}db(d^2 + \frac{1}{4}b^2) + d, \quad (2.54)$$

$$s_4 = -\frac{1}{2}b^2(d^2 + \frac{1}{4}b^2) + b\omega_0(d^2 + \omega_0^2) + \frac{3}{2}b^2\omega_0(\frac{1}{2}b - \omega_0) + \frac{1}{2}b - \omega_0, \quad (2.55)$$

$$s_5 = (\frac{1}{2}b - \omega_0)^2 + d^2, \quad (2.56)$$

$$s_6 = (\frac{1}{2}b - \omega_0)^2 - d^2, \quad (2.57)$$

$$s_7 = 4d^4 + 4d^2\omega_0^2 - 4d^2b\omega_0 + d^2b^2, \quad (2.58)$$

$$s_8 = \frac{1}{8}b^3 - d^2\omega_0 - \omega_0^3 - \frac{3}{4}b^2\omega_0 + \frac{3}{2}b\omega_0^2 + \frac{1}{2}d^2b, \quad (2.59)$$

$$s_9 = -3d^2\omega_0 + \frac{1}{8}b^3 + \frac{3}{2}d^2b - \frac{3}{4}b^2\omega_0 - \omega_0^3 + \frac{3}{2}b\omega_0^2. \quad (2.60)$$

Here $U(Z, \tau)$ represents bright rogue wave solution while p and η express dark rogue wave solutions. The results obtained here are in general valid for any form of $R(Z)$ and $D(Z)$, provided certain constraints are specified. To demonstrate the intensity profiles of rogue waves propagating through an inhomogeneous erbium doped optical fiber, we are considering the hyperbolic form of nonlinearity and dispersion parameter. We have chosen this specific form because it is practically feasible and was first used for soliton dispersion management in an optical fiber by Dianov's group [64]. Choosing

$$R(Z) = l_1 \operatorname{sech}(Z), \quad D(Z) = l_2 \operatorname{sech}(Z) \quad (2.61)$$

where l_1 and l_2 are constants associated with nonlinearity and GVD parameters. The intensity profile for bright rogue waves are plotted in Fig. 2.7(a), the maxima occurs at $Z = 0$ and $\tau = 0$ and is equal to 12.7 for the choices of parameters mentioned in the caption. By choosing different values of the parameters and different function form for various coefficients one can control the amplitude and the spatial distribution of the rogue waves and can set them as per the requirements of the system under study.

Fig. 2.7(b) depicts the dark rogue waves of $|p|^2$. In this case the maximum amplitude appears in the form of upper rings and is equal to 21 while the minimum

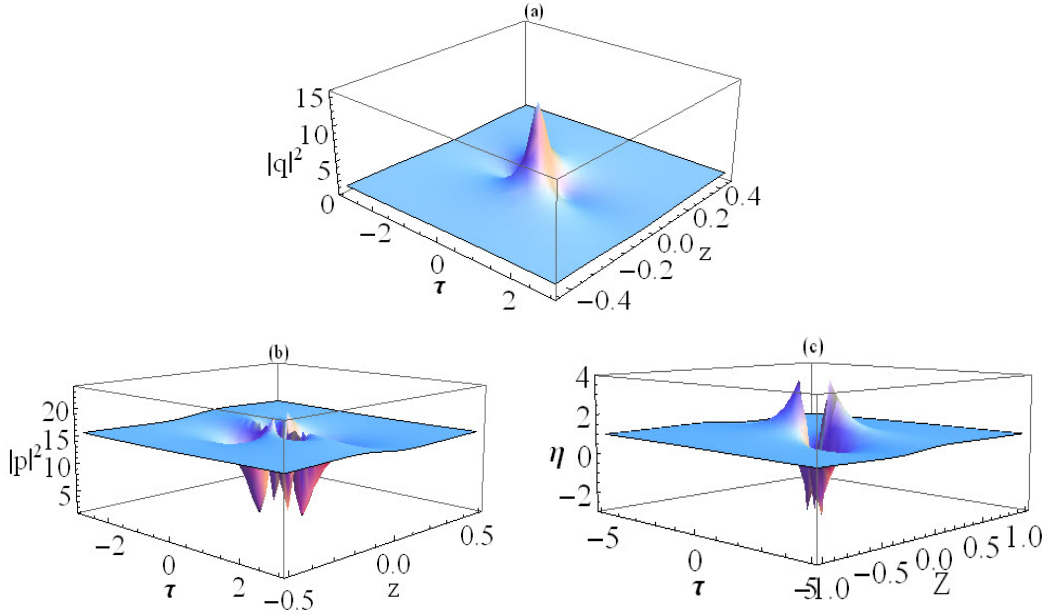


Figure 2.7: (a) Intensity profile of bright rogue waves ($|q|^2$) (b) Intensity profile of dark rogue waves ($|p|^2$) (c) Dark rogue waves properties of η of Eq. (2.40). The parameters are $d = 1$, $b = \frac{3}{2}$, $\omega_0 = \frac{1}{2}$, $l_1 = 1$ and $l_2 = 2$

amplitude equal to 1 appears in the form of four down peaks which are localized in the area of upper rings. Fig. 2.7(c) is plotted for η . For this case the maximum amplitude (approaches to 4) occurs in the form of two upper peaks and the minimum amplitude (approaches to -3) occurs in the form of two down peaks.

2.6.3 Controlling bright and dark rogue waves in a periodically distributed system

In the previous section, we have obtained the bright and dark rogue wave solutions for the coupled GNLS-MB equations. Now we discuss a mechanism which is used to control the dynamics of rogue waves as they propagate through a periodically distributed fiber system and will reveal their interesting features. In order to demonstrate controllable rogue waves for a periodically distributed system we consider the following form of dispersion and nonlinearity parameters

$$D(Z) = d_{10} \cos(\kappa Z), \quad R(Z) = r_0 \cos(\kappa Z), \quad (2.62)$$

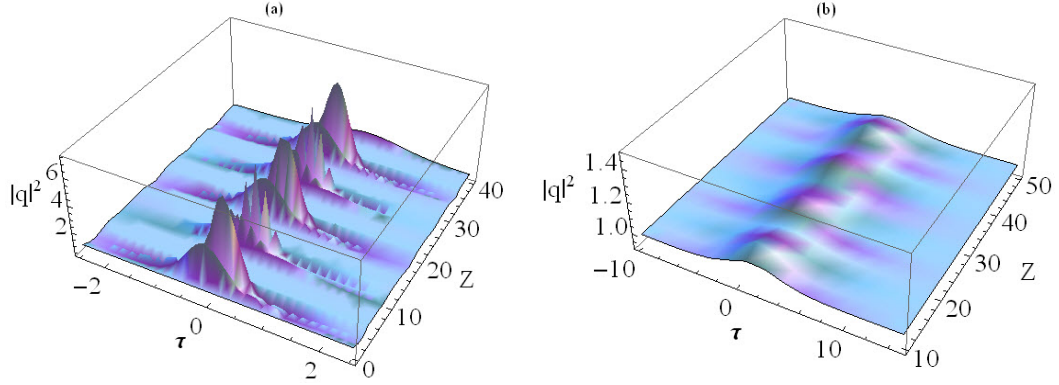


Figure 2.8: (a) Recurrence (b) annihilation of bright rogue waves of Eq. (2.40) $|q|^2$. The parameters are $w = d_{10} = r_0 = \rho_0 = 1$ with (a) $\kappa = 0.8$ and (b) $\kappa = 6$.

where the parameters d_{10} and r_0 are related with GVD and nonlinearity, respectively. To analyse the behaviour of rogue waves as they travel through a periodically distributed fiber system we concentrate on the relation between the effective propagation distance ρ and actual propagation distance Z . For the choice of parameters made in Eq. (2.62), an effective propagation distance comes out to be

$$\rho = \frac{d_{10}}{w^2\kappa} \sin(\kappa Z). \quad (2.63)$$

Clearly ρ is periodic and its maximum value ρ_{max} reads

$$\rho_{max} = \left| \frac{d_{10}}{w^2\kappa} \right|. \quad (2.64)$$

It is clear from Eq. (2.63) that effective propagation distance is confined to $-\frac{d_{10}}{w^2\kappa} \leq \rho \leq \frac{d_{10}}{w^2\kappa}$, while normalized propagation distance Z can take any value from zero to infinity. On closely observing the Fig. 2.8 we interpret that if $\left| \frac{d_{10}}{w^2\kappa} \right| > \rho_0$, the bright rogue waves get excited from their initial value at $Z = \frac{1}{\kappa} \arcsin\left(\frac{\rho_0 d_{10}}{\kappa}\right)$ and recur periodically while for $\left| \frac{d_{10}}{w^2\kappa} \right| < \rho_0$ the rogue waves do not have an appropriate propagation distance to get excited and get annihilated. So by properly regulating the values of ρ_{max} and ρ_0 we can control the rogue waves as they propagate through a nonlinear optical fiber. Similar behaviour is observed for dark rogue waves as shown in Fig. 2.9. It is worth mentioning that for this periodic system $W[R, D] = 0$ which implies that there is no gain in the fiber and as a result the pulse does not experience any compression or broadening during propagation

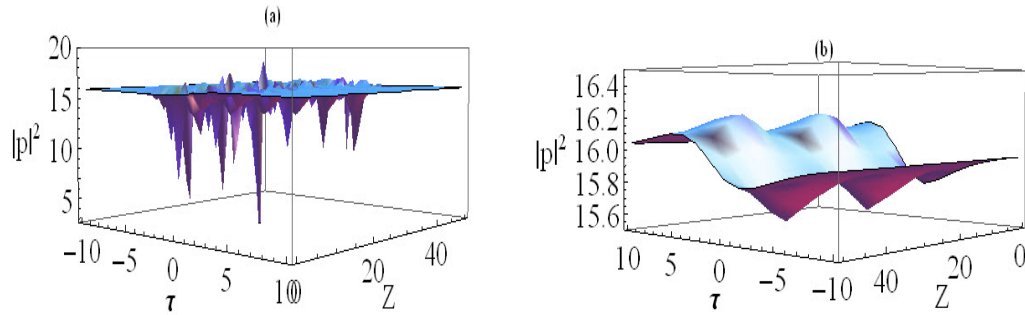


Figure 2.9: (a) Recurrence (b) annihilation of dark rogue waves of Eq. (2.40) $|q|^2$. The parameters are $w = d_{10} = r_0 = \rho_0 = 1$ with (a) $\kappa = 0.7$ and (b) $\kappa = 5$.

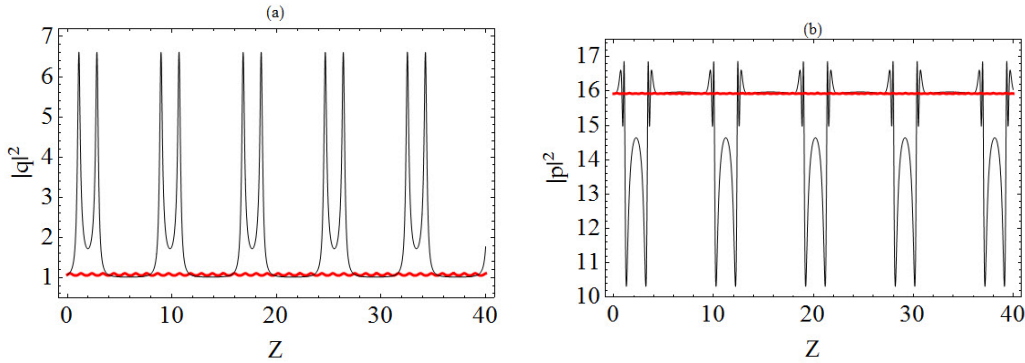


Figure 2.10: Sectional view of Recurrence (black) for $\kappa = 0.8$ and annihilation (red) for $\kappa = 6$ for (a) bright rogue waves at $\tau = 0.2$ (b) dark rogue waves at $\tau = 1$ of Eq. (2.40).

but an overall phase change. This behaviour is clearly depicted in sectional plots, shown in Fig. 2.10 for bright and dark rogue waves.

In the framework of Eq. (2.43) rogue wave appears from nowhere and disappear without a trace, while for the case of normalized propagation distance Z , bright and dark rogue waves exhibit periodic behaviour. This is happening because of the periodic functional form of the distributive parameters, which excites the rogue waves again and again after a particular interval of time. This kind of behaviour is not possible for the homogeneous optical fiber system, only an inhomogeneous system enables this new property of rogue waves.

2.7 Tapered graded-index nonlinear waveguide

So far we have discussed the rogue waves and their management in various nonlinear optical fibers. Now we make use of the analogy between “dispersion in time” and “diffraction in space” and study the rogue waves in the context of nonlinear waveguide. The study of pulse propagation through nonlinear waveguides is a hot topic of research these days. The basic principle of a waveguide is to guide a beam of light by using the variation of refractive index in the transverse direction. This allows the wave to propagate in a well defined channel. The variations of refractive index in the transverse direction can be continuous or discontinuous. The main feature is that the refractive index should be maximal in the channel along which the light is to be guided. There are different kinds of waveguides such as step-index, graded-index, birefringent, etc. which hold great practicality in communication. We are considering tapered graded-index waveguide because tapering is a tool that allows to add the desired form of inhomogeneity in a nonlinear system. It has various application such as maximizing the light coupled into optical fibers, integrated-optic devices and waveguides by reducing the reflection losses and mode mismatch [65]. It also finds application in the phenomena which require longitudinally varying waveguide properties such as in highly efficient Raman amplification [66].

The refractive index distribution in a nonlinear tapered graded-index waveguide can be written as [67]

$$n(x, z) = n_0 + n_1 F(z) x^2 + n_2 R(z) I(x, z), \quad (2.65)$$

where x is the spatial coordinate, z is the propagation distance and $I(x, z)$ is the beam intensity. The first two terms represent the linear contribution towards the linear refractive index and the third term is intensity dependent which arises due to Kerr type nonlinearity. Here we have assumed $n_1 > 0$ and the dimensionless tapering function $F(z)$ can be positive or negative, depending on whether the graded-index medium acts as a defocusing ($R(z) < 0$) or focusing ($R(z) > 0$) linear lens. The parameter n_2 can be positive or negative characterizing nonlinear self-focusing or self-defocusing and $R(z)$ is a dimensionless function which signifies the inhomogeneity of Kerr nonlinearity along the medium. It is worthwhile to mention that the shape of the taper $F(z)$ can be modelled appropriately depend-

ing upon the practical requirements. A taper can be made by heating one or more fibers up to the material softening point and then stretching it until a desired shape is obtained. Recently, the tapered graded-index waveguides have been explored to study dark solitons on a parabolic background [67], optical similaritons [31] and controllable rogue waves [68].

Under slowly varying envelope approximations, the nonlinear equation which governs the wave propagation in an inhomogeneous waveguide whose refractive index is given by Eq. (2.65) is GNLSE and can be written as

$$iQ_z + \frac{D(z)}{2k_0} Q_{xx} + \frac{k_0 n_2}{n_0} R(z) |Q|^2 Q - i\theta(z) Q_x + \frac{k_0 n_1}{n_0} F(z) x^2 Q = i \frac{\gamma(z)}{2} Q, \quad (2.66)$$

where $D(z)$ is diffraction parameter, $\theta(z)$ is related inversely with the group velocity of modes (a walk-off effect) [69, 70] and $\gamma(z)$ is the gain-loss coefficient. The wavenumber is $k_0 = 2\pi n_0/\lambda$ where λ is the wavelength of optical source generating the beam. Introducing the normalized variables as $U = (k_0 |n_2| L_D / n_0)^{\frac{1}{2}} Q$, $X = x/\omega_0$, $Z = z/L_D$, $\Gamma(Z) = \gamma(z)L_D$ and $\alpha(Z) = \theta(z)k_0\omega_0$, where $\omega_0 = (2k_0^2 n_1/n_0)^{-\frac{1}{4}}$ and $L_D = k_0\omega_0^2$ depict the characteristic transverse scale and the diffraction length, respectively. In dimensionless form Eq. (2.66) can be rewritten as

$$iU_Z + \frac{D(Z)}{2} U_{XX} + \sigma R(Z) |U|^2 U - i\alpha(Z) U_X + \frac{F(Z)}{2} X^2 U = i \frac{\Gamma(Z)}{2} U, \quad (2.67)$$

where $\sigma = \pm 1$ represents the self-focusing (+1) and self-defocusing (-1) nonlinearity of the waveguide. Now we obtain the optical rogon solutions by using the similarity transformation (mentioned in Section 2.4.2) and discuss their controllable propagation through graded-index waveguide in different regimes. In Chapter 3 we shall study the propagation of optical similaritons through the tapered graded-index nonlinear waveguide and reveal their interesting features.

2.7.1 Optical rogons in a tapered graded-index nonlinear waveguide

Here, we work out the rogue wave solutions for Eq. (2.67) with the aid of similarity transformation for the case $\Gamma(Z) = 0$. The case with $\Gamma(Z) \neq 0$ will be dealt in Chapter 3 in the context of optical similaritons.

For $\Gamma(Z) = 0$, Eq. (2.67) becomes

$$iU_Z + \frac{D(Z)}{2}U_{XX} + \sigma R(Z)|U|^2U - i\alpha(Z)U_X + \frac{F(Z)}{2}X^2U = 0. \quad (2.68)$$

The Gauge and similarity transformation as given in Eq. (2.13) can be rewritten in the case of waveguides as follows [17, 29]

$$U(X, Z) = A(Z)\psi[\chi(X, Z), \rho(Z)] e^{i\Phi(X, Z)}, \quad (2.69)$$

with

$$\chi(X, Z) = \frac{X - X_c(Z)}{w(Z)},$$

where $X_c(Z)$ represents the dimensionless position of the rogon wave center. Eq. (2.15) implies that the corresponding quadratically chirped phase is given by

$$\Phi(X, Z) = C(Z)\frac{X^2}{2} + B(Z)X + d_1(Z), \quad (2.70)$$

where the parameters $C(Z)$, $B(Z)$ and $d_1(Z)$ need to be determined.

On substituting Eq. (2.69) along with Eq. (2.70) in Eq. (2.68), it reduces to the standard NLSE, given by Eq. (2.18)

with

$$\rho(Z) = \rho_0 + \int_0^Z R(S)A^2(S)dS, \quad (2.71)$$

and

$$X_c(Z) = w(Z) \left(X_0 + C_{02} \int_0^Z \frac{\alpha(S) - D(S)B(S)}{w(S)} dS \right), \quad (2.72)$$

where X_0 and C_{02} are constants. The conditions among various other equation parameter are the following

$$\begin{aligned} A(Z) &= \frac{1}{\sqrt{w(Z)}}, B(Z) = \frac{\alpha(Z)}{D(Z)}, \\ C(Z) &= \frac{w_Z}{w(Z)D(Z)}, d_1(Z) = I^2 \int D(Z)dZ, \end{aligned} \quad (2.73)$$

The functions $R(Z)$, $w(Z)$, $\alpha(Z)$ and $D(Z)$ are not independent and are related to each other as:

$$R(Z)w(Z) = D(Z), \quad (2.74)$$

$$\alpha(Z) = ID(Z). \quad (2.75)$$

Here I is a constant. The corresponding tapering profile becomes

$$F(Z) = \frac{w_{ZZ}}{wD} - \frac{w_Z D_Z}{wD^2}. \quad (2.76)$$

We can obtain analytical solutions for Eq. (2.68) as it has been reduced to standard NLSE, given by Eq. (2.18) for the certain conditions among the parameters. The explicit expression for the intensity of rogon solutions, possessed by Eq. (2.18) is given as [17]

$$|\psi|^2 = 1 + 8 \frac{1 + 4\rho^2 - 4\chi^2}{(1 + 4\rho^2 + 4\chi^2)^2}. \quad (2.77)$$

ρ and χ can be obtained from Eqs. (2.71) and (2.70). The solutions of Eq. (2.68) can be obtained by using the transformation (2.69) with the conditions (2.71-2.73). The intensity of optical rogons for Eq. (2.68) is given as

$$|U(X, Z)|^2 = \frac{|\Psi|^2}{w(Z)}. \quad (2.78)$$

It is worth mentioning that the various parameters of Eq. (2.68) are spatially dependent and related to each other through Eqs. (2.74)-(2.76). The most important feature is that the coefficients being spatially dependent, can be controlled easily. This provides an insight to managing the optical rogons propagating through an inhomogeneous tapered waveguide.

2.7.2 Management of optical rogons

In order to demonstrate the management of optical rogons in different regimes we divide our study into three parts (*i*) diffraction management, (*ii*) nonlinearity management, and (*iii*) both diffraction and nonlinearity management which are described as follows:

Case I: Optical rogon diffraction management

The effect of $D(Z)$ is studied by considering $R(Z)$ to be constant. For simplicity we are choosing $R(Z) = 1$. In correspondence with the Eq. (2.74-2.76) this choice yields

$$w(Z) = D(Z), \quad (2.79)$$

$$\alpha(Z) = ID(Z), \quad (2.80)$$

and

$$F(Z) = \frac{D_{ZZ}}{D^2(Z)} - \frac{D_Z^2}{D^3(Z)}. \quad (2.81)$$

Clearly, width $w(Z)$, the parameter $\alpha(Z)$ and the tapering function $F(Z)$ can be managed by diffraction parameter $D(Z)$. The intensity profile of rogons for $D(Z) = a \operatorname{sech} Z$ and $D(Z) = 1 + a \cos Z$ with $a = 0.2$ are shown in Fig. 2.11(a) and Fig. 2.11(b), respectively. The reason for these specific choices of the diffraction coefficient lies in their practical applications. The sech type diffraction/dispersion variation is useful as it gets saturated with propagation distance. The importance of periodically varying diffraction has been shown in stabilizing the two-dimensional soliton [71]. It is important to mention here that the tapering function corresponding to hyperbolic diffraction is hyperbolic and for periodic choice is periodic and these choices of tapering function are practically feasible.

Case II: Nonlinearity managed optical rogons

The influence of nonlinearity coefficient $R(Z)$ has been worked out by taking $D(Z)$ to be constant and equal to unity for simplification. Hence following Eq. (2.74) the width of rogons is governed by nonlinearity as

$$w(Z) = \frac{1}{R(Z)}. \quad (2.82)$$

The resulting tapering function is

$$F(Z) = -\frac{R_{ZZ}}{R(Z)} + \frac{2R_Z^2}{R^2(Z)}. \quad (2.83)$$

Here the parameter $\alpha(Z)$ becomes constant $\alpha(Z) = I$, which can be made as small as is practically possible depending upon the design of the system. This in turn proves to be advantageous as for its smaller value, less power will be used to overcome it for pulse propagation in a nonlinear waveguide. Intensity profile of rogons for hyperbolic and trigonometric form of the nonlinearity parameter are

plotted in Fig. 2.12(a) and Fig. 2.12(b), respectively. The motivation of considering trigonometric form of $R(Z)$ came from [67], where similar form has been used to investigate the robustness of solitons in a planar graded-index nonlinear waveguide. The tapering function for the hyperbolic choice of nonlinearity is hyperbolic and for trigonometric form is periodic. The exact form can be worked out by using Eq. (2.83).

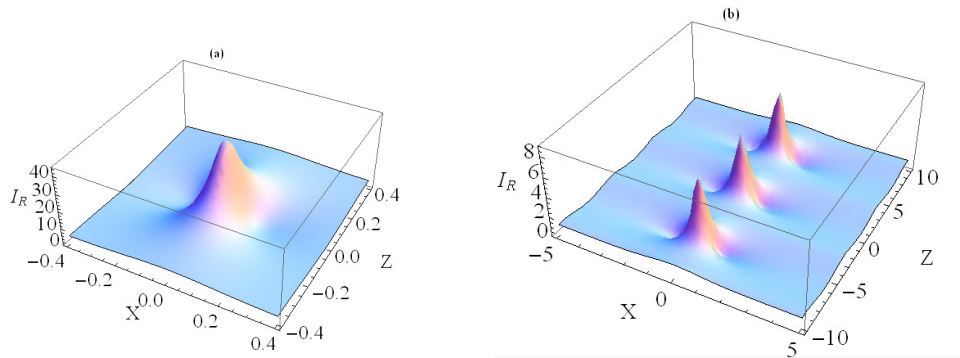


Figure 2.11: Intensity profile of rogons for Eq. (2.68) (a) for $D(Z) = a \operatorname{sech} Z$ (b) for $D(Z) = 1 + a \cos Z$ with $a = 0.2$.

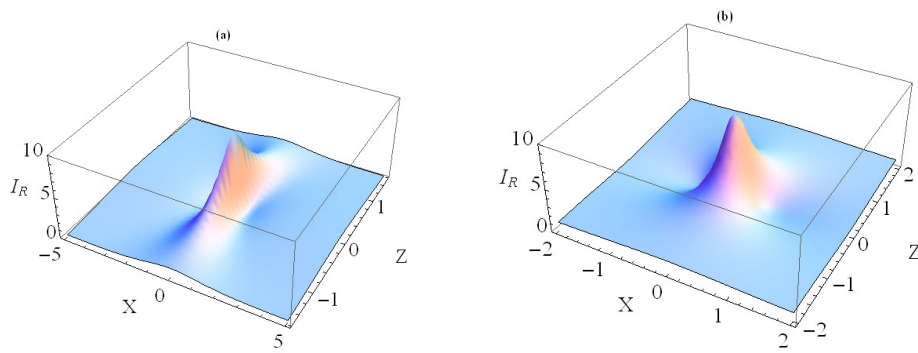


Figure 2.12: Intensity profile of rogons for Eq. (2.68) (a) for $R(Z) = b \cosh Z$ (b) for $R(Z) = 1 + a \cos \Omega Z$ with $b = 1$, $a = 0.1$ and $\Omega = 0.5$.

It is worth noting that the periodic choice of diffraction parameter $D(Z)$ leads to the periodic evolution of rogons (Fig. 2.11(b)). However, the periodic choice of nonlinearity parameter $R(Z)$ does not lead to the periodic evolution of rogons but may cause a periodic background.

Case III: Combined nonlinearity and diffraction managed optical rogons

Here we consider that both the nonlinearity and diffraction have spatial dependence and study the combined effect of their management on the intensity profile of rogons. In Fig. 2.13 we have plotted the intensity profile for different functional forms of the various parameters.

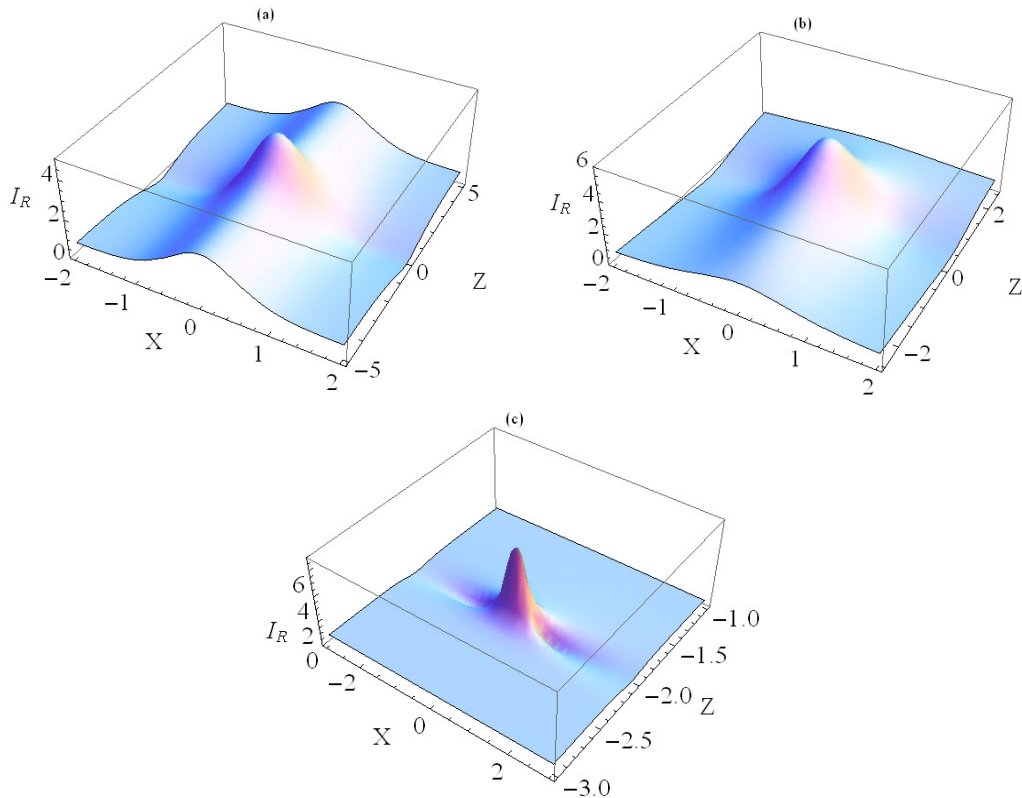


Figure 2.13: Intensity profile of rogons for Eq. (2.68) with $w(Z) = 1 + \text{sech}Z$ (a) for $R(Z) = \text{sech}Z$ (b) for $R(Z) = 1 + c_0 \sin Z$ (c) for $R(Z) = \exp(-c_0 Z) \cosh Z$ with $c_0 = 0.5$.

Now we define the motivation behind the specific forms of the chosen parameters. The first choice of nonlinearity yields the hyperbolic form of $D(Z)$ which gets saturated after an appropriate propagation distance. For the second case, nonlinearity is having a sinusoidal variation which results in sinusoidal $D(Z)$. It has been predicted that these forms of nonlinearity and diffraction parameters stabilize the pulse against decay and provide undisturbed propagation [72]. The last choice

of nonlinearity yields an exponentially varying diffraction and this form of diffraction has been used in [73].

We have analytically predicted the possibility of optical rogons and their management as they propagate through a tapered graded-index nonlinear waveguide. These optical rogons may be used in signal transmission as they are stable against small periodic perturbations and noise and their stability analysis has been shown in [74].

2.7.3 Riccati parameterized optical rogons in a tapered graded-index nonlinear waveguide

So far, we have obtained optical rogons and discussed the various management regimes. In this analysis, we have found that Eq. (2.76) resembles the Schrödinger equation of quantum mechanics for $D(Z) = 1$ and can be written explicitly as

$$F(Z) = \frac{w_{ZZ}}{w(Z)}. \quad (2.84)$$

This allowed us to invoke the isospectral Hamiltonian approach discussed in Section 1.3. As we have discussed earlier by using this formalism we can introduce a Riccati parameter λ which allows us to tune the intensity of the nonlinear pulses and generalize the system parameters. The tapering function $F(Z)$ and the width $w(Z)$ in Eq. (2.84) can be treated as a quantum mechanical analog of potential and wave function, respectively. Since the Schrödinger equation is known to be exactly solvable for a variety of potentials, we can analogously study Eq. (2.68) for a variety of tapering functions. Following Eqs. (1.22) and (1.23), we can generate the class of tapering $\hat{F}(Z)$ and width $\hat{w}(Z)$ as follows

$$\hat{F}(Z) = F(Z) - 2 \frac{d}{dZ} \left(\frac{w^2(Z)}{\lambda + \int_{-\infty}^Z w^2(S) dS} \right), \quad (2.85)$$

$$\hat{w}(Z) = \frac{\sqrt{\lambda(\lambda + 1)} w(Z)}{\lambda + \int_{-\infty}^Z w^2(S) dS}. \quad (2.86)$$

The value of λ has to be chosen so as to avoid singularities in the expression of the modified tapering and the width functions. The corresponding class of the nonlinearity parameter can be obtained by using Eq. (2.82) (for $D(Z) = 1$) and

reads

$$\widehat{R}(Z) = \frac{1}{\widehat{w}(Z)}. \quad (2.87)$$

To demonstrate the importance of invoking isospectral technique we are choosing the width of the rogons $w(Z) = \text{sech}Z$, $\lambda \notin [-2, 0]$. A class of $\widehat{w}(Z)$ can be given as follows by using Eq. (2.86)

$$\widehat{w}(Z) = \frac{\sqrt{\lambda(\lambda + 1)} \text{sech}Z}{\lambda + 1 + \tanh Z}. \quad (2.88)$$

It is straightforward to obtain the explicit expressions of $\widehat{F}(Z)$ and $\widehat{R}(Z)$ corresponding to $\widehat{w}(Z)$ by using Eqs. (2.85) and (2.87). To demonstrate the role of Riccati parameter λ , we have plotted the width, tapering and the nonlinearity profiles for its different values (Fig. 2.14).

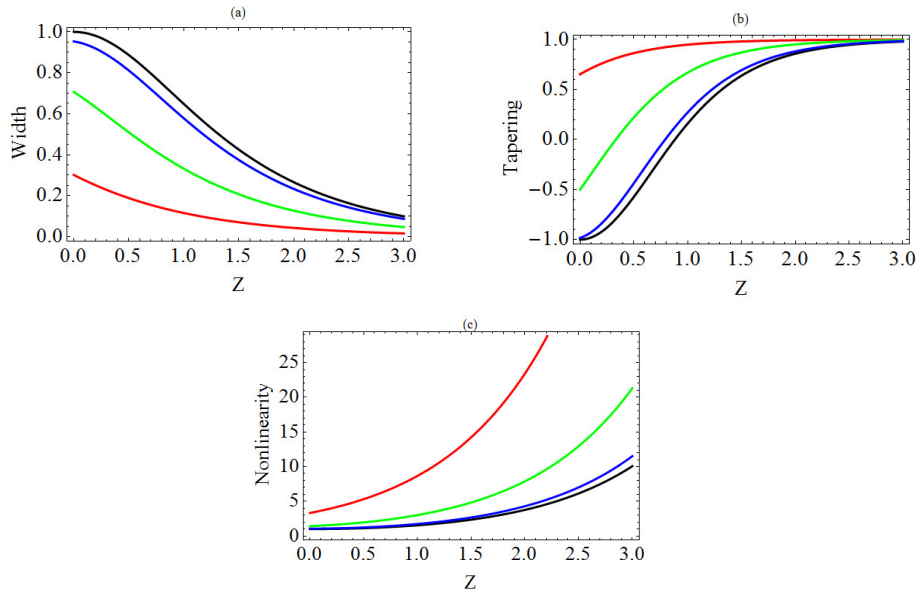


Figure 2.14: The profiles of (a) width (b) tapering (c) nonlinearity parameter. Each plot is drawn for the absence of Riccati generalization (black), for $\lambda = 0.1$ (red), for $\lambda = 1$ (green), for $\lambda = 10$ (blue).

Fig. 2.14 reveals that for a small value of Riccati parameter λ the profiles differ remarkably from the original one but for its higher values they tend to the original ones. It is interesting to note that for the smaller values of $\lambda < 0.414$, $\widehat{F}(Z)$ is always positive which means that tapering of the waveguide is only defocusing

type while in the other cases the nature of the tapering is changing from focusing to defocusing type. The width function is increasing and the nonlinearity parameter is decreasing with increase in λ .

To study the role of λ we compare the intensity profiles of rogons for the case that does not involve the effect of Riccati generalization with the one which contributes its effect. The intensity of rogons corresponding to Riccati generalization can be obtained from Eq. (2.78) by replacing $w(Z)$ with $\hat{w}(Z)$. The intensity profiles of optical rogons with and without Riccati generalization corresponding to different values of λ are plotted in Fig. 2.15.

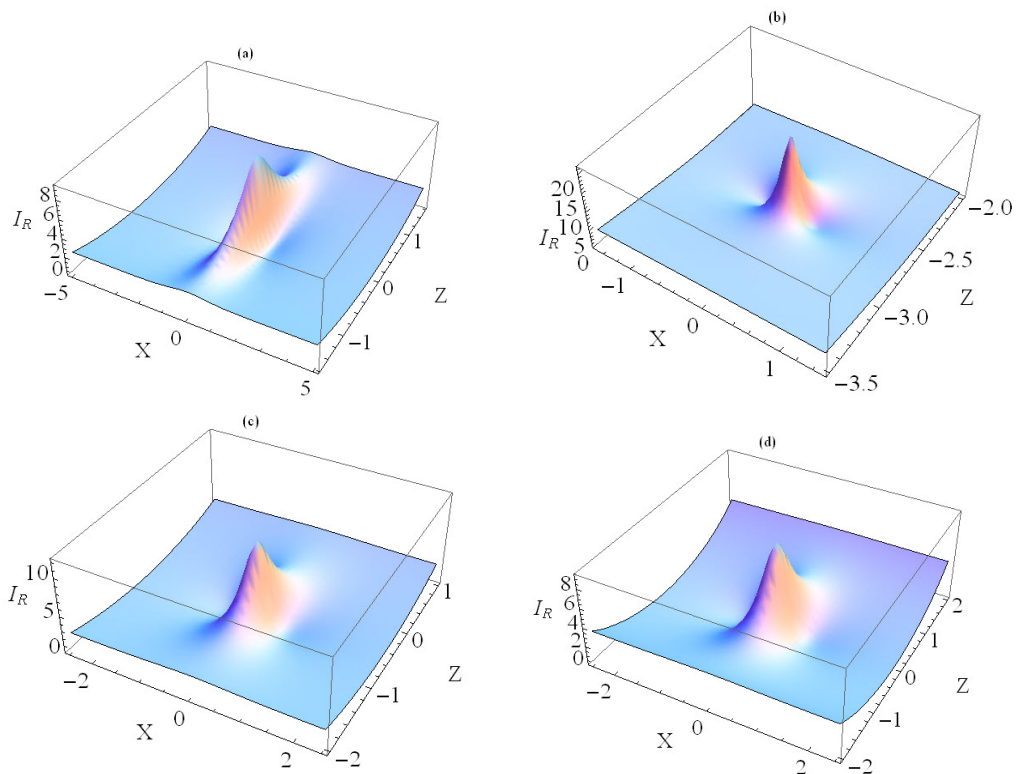


Figure 2.15: The intensity profiles of rogue waves (a) in the absence of Riccati generalization, (b) for $\lambda = 0.1$, (c) for $\lambda = 1$, (d) for $\lambda = 10$.

It is clear from the intensity plots that for a small value of λ the intensity is increased and tends to the original case for a large value. Thus, by invoking the parameter λ we can tune the amplitude of the optical rogons and can get high energy optical rogon pulses which are useful for practical applications. Similar

corroboration has been predicted for the special case of Eq. (2.67) with $D(Z) = R(Z) = 1$ in [75, 76].

2.8 Conclusion

We have obtained the exact analytical rogue wave solutions for the variants of GNLSE corresponding to pulse propagation through different nonlinear fibers and waveguides. The exact solutions have been worked out with the aid of similarity transformation that maps the inhomogeneous model equation to the corresponding constant coefficient model equation. Then by making use of the known results of the constant coefficient model and a transformation we have obtained the exact solutions for the inhomogeneous model. We have found that all the system parameters can, in general, take any functional form depending upon the system under study but all of them can not be chosen independently and certain conditions need to be satisfied. In this chapter we have investigated three models (i) generalized nonautonomous NLSE in the context of fibers including periodically distributed, dispersion increasing and decreasing fibers (ii) NLS-MB model for erbium doped fibers (iii) GNLSE in the context of tapered graded-index waveguide. In the first case we have studied the dynamics of rogue waves for the cases when $W[R, D] = 0$ and $W[R, D] \neq 0$. The former case represents the scenario of periodically distributed fiber system and we have noticed that as the rogue waves propagate through it, they do not suffer any broadening and compression but undergo an overall phase change.

For the latter case we have studied the propagation of rogue waves through dispersion increasing and decreasing fibers and found that the amplitude of the rogue waves increases (decreases) as they travel through dispersion increasing (decreasing) fiber. The second case involves NLS-MB model and represents the pulse propagation through inhomogeneous erbium doped fiber system. We have obtained bright and dark rogue wave solutions and discussed the mechanism which is used to control the propagation of rogue waves. Additionally, we have also shown that by tuning a few parameters we can get the excitation or annihilation of rogue waves at the desired location. The third case involves the study of rogue waves through a tapered graded-index waveguide. We have discussed the differ-

ent management regimes of optical rogons which may be practically achievable through tapering. We have also shown the possibility of producing high energy optical rogons through the coherent control of tapering profile. This is achieved by invoking the concept of isospectral Hamiltonian which allowed us to generate the class of tapering function, which in turn effects the width and the intensity of the optical rogons through the introduction of Riccati parameter λ . The analytical results obtained may prove useful for studying optical rogue waves experimentally.

The work presented here has been published in [77, 78, 74].

Bibliography

- [1] M S Ruderman. Freak waves in laboratory and space plasmas. *The European Physical Journal-Special Topics*, 185(1): 57-66, 2010.
- [2] W M Moslem, P K Shukla, and B Eliasson. Surface plasma rogue waves. *Europhysics Letters*, 96(2): 25002, 2011.
- [3] J M Dudley, G Ú Genty, and B J Eggleton. Harnessing and control of optical rogue waves in supercontinuum generation. *Optics Express*, 16(6): 3644-3651, 2008.
- [4] D R Solli, C Ropers, and B Jalali. Active control of rogue waves for stimulated supercontinuum generation. *Physical Review Letters*, 101(23): 233902, 2008.
- [5] G P Agrawal. *Nonlinear Fiber Optics*, Academic Press, San Diego, 2001.
- [6] A B Shabat, and V E Zakharov. Exact theory of two-dimensional self-focusing and one-dimensional self-modulation of waves in nonlinear media. *Soviet Physics JETP*, 34: 6269, 1972.
- [7] Y S Kivshar, and G P Agrawal. *Optical Solitons: From Fibers to Photonic Crystals*. Academic Press, Boston, 2003.
- [8] A Hasegawa, and Y Kodama. *Solitons in optical communications*, Oxford: Clarendon Press, 1995.
- [9] A D Boardman, and K Xie. Theory of spatial solitons. *Radio Science*, 28(5): 891-899, 1993.
- [10] W J Broad. *Rogue giants at sea*, The New York Times, 2006.

- [11] C Kharif and E Pelinovsky. Physical mechanisms of the rogue wave phenomenon. *European Journal of Mechanics-B*, 22(6): 603-634, 2003.
- [12] P A E M Janssen. Nonlinear four-wave interactions and freak waves. *Journal of Physical Oceanography*, 33(4): 863-884, 2003.
- [13] D R Solli, C Ropers, P Koonath, and B Jalali, Optical rogue waves. *Nature*, 450(7172): 1054-1057, 2007.
- [14] Y Zhenya. Nonautonomous rogons in the inhomogeneous nonlinear Schrödinger equation with variable coefficients. *Physics Letters A*, 374(4): 672-679, 2010.
- [15] S Vergeles, and S K Turitsyn. Optical rogue waves in telecommunication data streams. *Physical Review A*, 83(6): 061801, 2011.
- [16] C Q Dai, G Q Zhou, and J F Zhang. Controllable optical rogue waves in the femtosecond regime. *Physical Review E*, 85 (1): 016603, 2012.
- [17] C Q Dai, Y Y Wang, Q Tian, and J F Zhang. The management and containment of self-similar rogue waves in the inhomogeneous nonlinear Schrödinger equation. *Annals of Physics*, 327(2): 512-521, 2012.
- [18] M Taki, A Mussot, A Kudlinski, E Louvergneaux, M kolobov, and M Douay. Third-order dispersion for generating optical rogue $\langle i \rangle$ solitons $\langle i \rangle$. *Physics Letters A*, 374(4): 691-695, 2010.
- [19] A Ankiewicz, J M Soto-Crespo, M A Chowdhury, and N. Akhmediev. Rogue waves in optical fibers in presence of third-order dispersion, self-steepening, and self-frequency shift. *Journal of the Optical Society of America B*, 30(1): 87-94, 2013.
- [20] Z Yan, and C Q Dai. Optical rogue waves in the generalized inhomogeneous higher-order nonlinear Schrödinger equation with modulating coefficients. *Journal of Optics* 15(6): 064012, 2013.
- [21] J Zamora-Munt, B Garbin, S Barland, M Giudici, J R Leite, C Masoller, and J R Tredicce. Rogue waves in optically injected lasers: Origin, predictability, and suppression. *Physical Review A*, 87(3): 035802, 2013.

- [22] V N Serkin, and A Hasegawa. Exactly integrable nonlinear Schrödinger equation models with varying dispersion, nonlinearity and gain: application for soliton dispersion. *Selected Topics in IEEE, Journal of Quantum Electronics*, 8(3): 418-431, 2002.
- [23] R Ganapathy, K Porsezian, A Hasegawa, and V N Serkin. Soliton interaction under soliton dispersion management. *IEEE, Journal of Quantum Electronics*, 44(4): 383-390, 2008.
- [24] R Ganapathy, Soliton dispersion management in nonlinear optical fibers. *Communications in Nonlinear Science and Numerical Simulation* 17(12): 4544-4550, 2012.
- [25] L H Zhao, and C Q Dai. Self-similar cnoidal and solitary wave solutions of the (1+ 1)-dimensional generalized nonlinear Schrödinger equation. *The European Physical Journal D*, 58(3): 327-332, 2010.
- [26] C Q Dai, Q Yang, J D He, and Y Y Wang. Nonlinear tunneling effect in the (2+ 1)-dimensional cubic-quintic nonlinear Schrödinger equation with variable coefficients. *The European Physical Journal D*, 63(1): 141-148, 2011.
- [27] C Q Dai, C L Zheng, and H P Zhu. Controllable rogue waves in the nonautonomous nonlinear system with a linear potential. *The European Physical Journal D*, 66(4): 1-8, 2012.
- [28] S A Ponomarenko, and G P Agrawal. Optical similaritons in nonlinear waveguides. *Optics Letters*, 32 (12): 1659-1661, 2007.
- [29] C Q Dai, Y J Xu, R P Chen, and S Q Zhu. Self-similar optical beam in nonlinear waveguides. *The European Physical Journal D*, 59(3): 457-461, 2010.
- [30] A Goyal, R Gupta, S Loomba, and C N Kumar. Riccati parameterized self-similar waves in tapered graded-index waveguides. *Physics Letters A*, 376(45): 3454-3457, 2012.
- [31] T S Raju, and P K Panigrahi. Optical similaritons in a tapered graded-index nonlinear-fiber amplifier with an external source. *Physical Review A*, 84(3): 033807, 2011.

- [32] T Kanna, R Babu Mareeswaran, F Tsitoura, H E Nistazakis, and D J Frantzeskakis. Non-autonomous bright-dark solitons and Rabi oscillations in multi-component Bose-Einstein condensates. *Journal of Physics A: Mathematical and Theoretical*, 46(47): 475201, 2013.
- [33] N Akhmediev, A Ankiewicz, and M Taki. Waves that appear from nowhere and disappear without a trace. *Physics Letters A*, 373(6): 675-678, 2009.
- [34] V N Serkin, A Hasegawa, and T L Belyaeva. Nonautonomous solitons in external potentials. *Physical Review Letters*, 98(7): 074102, 2007.
- [35] B Kibler, J Fatome, C Finot, G Millot, F Dias, G Genty, N Akhmediev, and J M Dudley. The Peregrine soliton in nonlinear fibre optics. *Nature Physics*, 6(10): 790-795, 2010.
- [36] S Konar, M Mishra, and S Jana. Dispersion-managed optical solitons with higher-order nonlinearity. *Fiber and Integrated Optics*, 24(6): 537-548, 2005.
- [37] Q Tian, Q Yang, C Q Dai, and J F Zhang. Controllable optical rogue waves: Recurrence, annihilation and sustainment. *Optics Communications*, 284(8): 2222-2225, 2011.
- [38] S Loomba, and H Kaur. Optical rogue waves for the inhomogeneous generalized nonlinear Schrödinger equation. *Physical Review E*, 88(6): 062903, 2013.
- [39] T Li. *Optical Fiber Communications: Fiber fabrication*, Academic Press, San Diego, 1985.
- [40] G A Thomas, B I Shraiman, P F Glodis, and M J Stephen. Towards the clarity limit in optical fibre. *Nature*, 404(6775): 262-264, 2000.
- [41] D Marcuse. *Light Transmission Optics*, Van Nostrand Reinhold, New York, 1982.
- [42] A Hasegawa. *Optical Solitons in Fibers*, Springer, Berlin, 1989.
- [43] G L Lamb Jr. *Elements of Soliton Theory*, New York, Wiley-Interscience, 1980.

- [44] S L McCall, and E L Hahn. Self-induced transparency by pulsed coherent light. *Physical Review Letters*, 18(21): 908, 1967.
- [45] A I Maimistov, and E A Manykin. Prolongation structure for the reduced Maxwell-Bloch equations describing the two-photon self-induced transparency. *Physics Letters A*, 95(5): 216-218, 1983.
- [46] M Nakazawa, Y Kimura, K Kurokawa, and K Suzuki. Self-induced-transparency solitons in an erbium-doped fiber waveguide. *Physical Review A*, 45: 23, 1992.
- [47] M Nakazawa, E Yamada, H Kubota. Coexistence of self-induced transparency soliton and nonlinear Schrödinger soliton. *Physical Review Letters*, 66(20): 2625, 1991.
- [48] M Nakazawa, E Yamada, and H Kubota. Coexistence of a self-induced-transparency soliton and a nonlinear Schrödinger soliton in an erbium-doped fiber. *Physical Review A*, 44(9): 5973, 1991.
- [49] K Porsezian, and K Nakkeeran. Optical soliton propagation in a coupled system of the nonlinear Schrödinger equation and the Maxwell-Bloch equations. *Journal of Modern Optics*, 42(9): 1953-1958, 1995.
- [50] S Kakei, and J Satsuma. Multi-soliton solutions of a coupled system of the nonlinear Schrödinger equation and the Maxwell-Bloch equations. *Journal of the Physical Society of Japan*, 63(3): 885-894, 1994.
- [51] K Nakkeeran. Optical solitons in erbium-doped fibres with higher-order effects and pumping. *Journal of Physics A: Mathematical and General*, 33(23): 4377, 2000.
- [52] K Nakkeeran. Optical solitons in erbium doped fibers with higher order effects. *Physics Letters A*, 275(5): 415-418, 2000.
- [53] K Porsezian, A Mahalingam, and P S Sundaram. Integrability aspects of NLS-MB system with variable dispersion and nonlinear effects. *Chaos, Solitons and Fractals*, 12(6): 1137-1143, 2001.

- [54] A Uthayakumar, A Mahalingam, Y G Han, and S B Lee. Optical soliton propagation in erbium-doped fibre with variable dispersion and nonlinear effects. *Journal of Modern Optics* 53(11): 1619-1626, 2006.
- [55] R Ganapathy, V C Kuriakose, and K Porsezian. Soliton propagation in an erbium-doped fiber with and without a continuous wave background. *Physical Review E*, 68(6): 066615, 2003.
- [56] M Rajan, A Mahalingam, A Uthayakumar, and K Porsezian. Observation of two soliton propagation in an erbium doped inhomogeneous lossy fiber with phase modulation. *Communications in Nonlinear Science and Numerical Simulation* 18(6): 1410-1432, 2013.
- [57] R Guo, B Tian, X L, H Q Zhang, and W J Liu. Darboux transformation and soliton solutions for the generalized coupled variable-coefficient nonlinear Schrödinger-Maxwell-Bloch system with symbolic computation. *Computational Mathematics and Mathematical Physics*, 52(4): 565-577, 2012.
- [58] M S M Rajan, A Mahalingam, and A Uthayakumar. Nonlinear tunneling of nonautonomous optical solitons in combined nonlinear Schrödinger and Maxwell-Bloch systems. *Journal of Optics*, 14(10): 105204, 2012.
- [59] H Zhang, Q Bao, D Tang, L Zhao, and K Loh. Large energy soliton erbium-doped fiber laser with a graphene-polymer composite mode locker. *Applied Physics Letters*, 95(14): 141103, 2009.
- [60] X Wu, D Y Tang, H Zhang, and L M Zhao. Dissipative soliton resonance in an all-normal-dispersion erbium-doped fiber laser. *Optics Express*, 17(7): 5580-5584, 2009.
- [61] H Zhang, D Y Tang, X Wu, and L M Zhao. Multi-wavelength dissipative soliton operation of an erbium-doped fiber laser. *Optics Express*, 17(15): 12692-12697, 2009.
- [62] J He, S Xu, and K Porsezian. New types of rogue wave in an erbium-doped fibre system. *Journal of the Physical Society of Japan*, 81(3): 033002 (2012).

- [63] J He, S Xu, and K Porsezian. N-order bright and dark rogue waves in a resonant erbium-doped fiber system. *Physical Review E*, 86(6): 066603, 2012.
- [64] V A Bogatyrev, M M Bubnov, E M Dianov, A S Kurkov, P V Mamyshev, A M Prokhorov, S D Romyantsev et al. A single-mode fiber with chromatic dispersion varying along the length. *Journal of Lightwave Technology*, 9(5): 561-566, 1991.
- [65] V R Almeida, R R Panepucci, and M Lipson. Nanotaper for compact mode conversion. *Optics Letters*, 28(15): 1302-1304, 2003.
- [66] M Krause, H Renner, and E Brinkmeyer. Efficient Raman lasing in tapered silicon waveguides. *Spectroscopy*, 21(1): 26, 2006.
- [67] L Li, X Zhao, and Z Xu. Dark solitons on an intense parabolic background in nonlinear waveguides. *Physical Review A*, 78(6): 063833, 2008.
- [68] H P Zhu. Nonlinear tunneling for controllable rogue waves in two-dimensional graded-index waveguides. *Nonlinear Dynamics*, 72(4): 873-882, 2013.
- [69] N A R Bhat, and J E Sipe. Optical pulse propagation in nonlinear photonic crystals. *Physical Review E*, 64(5): 056604, 2001.
- [70] K W Chow, K K Y Wong, and K Lam. Modulation instabilities in a system of four coupled, nonlinear Schrödinger equations. *Physics Letters A*, 372(25): 4596-4600, 2008.
- [71] P A Subha, C P Jisha, and V C Kuriakose. Stable diffraction managed spatial soliton in bulk cubic-quintic media. *Journal of Modern Optics*, 54(12): 1827-1835, 2007.
- [72] P A Subha, C P Jisha, and V C Kuriakose. Nonlinearity management and diffraction management for the stabilization of two-dimensional spatial solitons. *Pramana*, 69(2): 229-239, 2007.
- [73] C Dai, and J Zhang. Exact spatial similaritons and rogons in 2D graded-index waveguides. *Optics Letters*, 35(15): 2651-2653, 2010.

-
- [74] S Loomba, R Gupta, C N Kumar, and D Milovic. Optical rogons for inhomogeneous nonlinear Schrödinger equation with inter modal dispersion. *Applied Mathematics and Computation*, 225: 318-325, 2013.
- [75] C N Kumar, R Gupta, A Goyal, S Loomba, T S Raju, and P K Panigrahi. Controlled giant rogue waves in nonlinear fiber optics. *Physical Review A*, 86(2): 025802, 2012.
- [76] A Goyal, R Gupta, S Loomba, and C N Kumar. Riccati parameterized self-similar waves in tapered graded-index waveguides. *Physics Letters A*, 376(45): 3454-3457, 2012.
- [77] S Loomba, R Gupta, H Kaur, and M S Mani Rajan. Self-similar rogue waves in an inhomogeneous generalized nonlinear Schrödinger equation. *Physics Letters A*, 378(30-31): 2137-2141, 2014.
- [78] S Loomba, R Gupta, K De, C N Kumar, T S Raju. *Optical Fiber Technology*, 2014, <http://dx.doi.org/10.1016/j.yofte.2014.07.006>.

Chapter 3

Nonlinear tunneling of optical similaritons in a tapered graded-index nonlinear waveguide

3.1 Introduction

In Chapter 2, we have investigated the self similar rogue waves and their management in a tapered graded-index nonlinear waveguide. Due to the potential applications of tapered graded-index waveguides it is quite interesting to study the dynamical properties of the different kinds of self-similar waves as they propagate through it. The present chapter is devoted to studying the nonlinear tunneling properties of similariton through the tapered graded-index nonlinear waveguide. We begin this chapter by introducing the concept of nonlinear tunneling. Then, we describe the similariton pulses and mention their applications in various areas. Finally, we investigate the nonlinear tunneling of optical similaritons for the constant background and the exponential background case. By making use of the results obtained with exponential background case we extend the analysis and discuss the cascade pulse compression of bright similaritons.

3.2 Nonlinear tunneling

In order to understand the concept of tunneling, one must consider the motion of the pulse in a field which is characterized by the presence of a region known as a potential barrier whose potential energy exceeds the total energy of the parti-

cle. Classically, this potential barrier is impenetrable to the pulse. However, in quantum mechanics the pulse can pass through the potential barrier as the transmission probability of the wave function is non zero. This is known as tunneling effect. Later it was proposed that the soliton pulses also show tunneling effects by treating the localized inhomogeneities in GVD parameter analogous to potential barriers in quantum mechanical tunneling [1]. The tunneling properties exhibited by soliton kind of pulses are known as nonlinear tunneling as they originate from the nonlinear wave equation that leads to a nonlinear dispersion relation in contrast to linear tunneling which follows from the linear wave equation. The propagation of the soliton pulse toward a spatially dependent potential barrier was investigated by Newell, for the first time in 1978 [2]. It was reported that in certain circumstances, depending on the ratio of the soliton amplitude and the barrier height, the soliton can tunnel through a barrier in a lossless manner. The tunneling of sine-Gordon soliton through the impurity potential has been calculated in [3]. Later, the nonlinear tunneling properties of optical solitons through a fiber junction [4], organic thin films and polymeric waveguides [5] have been investigated. The research in this area intensified with the pioneering work of Serkin et al. [6]. Soon afterwards, the utility of nonlinear tunneling in pulse amplification, splitting, compression and cascade compression through nonlinear barriers have been realized and analyzed analytically as well as numerically [7, 8, 9]. Barak and collaborators observed the nonlinear spatial soliton tunneling effects of a paraxial Gaussian beam launched in a potential trap. They found that by increasing the power levels, the dynamics changed from linear tunneling to nonlinear tunneling and then led to the ejection of the soliton through a potential trap [10]. The nonlinear tunneling of nonautonomous solitons through erbium doped fibers [11], birefringent fibers [12, 13] and in the presence of external harmonic potential [14] has also been discussed. Additionally, the tunneling properties of self-similar nonautonomous solitons, known as similaritons [7] and rogue waves [15] have been extensively investigated. It has been revealed that these nonlinear pulses can travel with increasing, unchanged or decreasing amplitude depending on the ratio of the amplitude of the rogue waves and the barrier height. In this chapter we are interested in studying the nonlinear tunneling properties of optical similaritons. We begin with a brief introduction of optical similaritons.

3.3 Optical similaritons

Similaritons are self-similar waves which maintain their overall shapes but change their width and amplitudes with the modulation of system parameters. They have gathered significant attention and have been explored in many fields such as nonlinear optical systems, plasmas, fluid dynamics, Bose-Einstein condensation and condensed matter physics [16]. In the context of nonlinear optics they are termed as optical similaritons and appear due to the co-action of nonlinearity, dispersion/diffraction and gain in a high-power fiber amplifier [17, 18]. Recently they have become a subject of intense research due to their remarkable features and have been investigated in dispersion decreasing fiber [19], nonlinear fibers [20], optical fiber amplifiers [21], inhomogeneous coupled optical fiber [22], nonlinear waveguides [17, 7], tapered graded-index nonlinear waveguides [23, 24], etc. The optical similaritons can be classified into two groups. The first group deals with the asymptotic optical similaritons, which are described by compact parabolic and Hermite Gaussian functions in optical fiber amplifiers [25, 26, 27, 28]. The second group involves exact optical similaritons, which are described by exact soliton solutions [29, 30] and quasi soliton solutions [31]. The exact solitonic similaritons are more intriguing as they are obtained by a process which involves one-to-one correspondence of inhomogeneous NLSE and the standard NLSE, thus ensuring the stability of optical similaritons [21]. We have mentioned in the previous chapter that the self similarity transformation involves the mapping of the inhomogeneous NLSE model to the standard NLSE. Here, we use this transformation along with the Darboux technique to study the nonlinear tunneling properties of the optical similaritons and their pairs for the constant background and the exponential background case.

3.4 Nonlinear tunneling of optical similaritons

These days, a great deal of research is taking place to study the nonlinear tunneling of self-similar waves. In addition to nonautonomous solitons and rogue waves, the nonlinear tunneling properties of optical similaritons have been thoroughly investigated. In [7], Wang et al. have analyzed the tunneling of optical similaritons propagating through an inhomogeneous nonlinear waveguide. The spatiotemporal

self-similar nonlinear tunneling effects in a nonlinear medium in the presence of linear and nonlinear gain have also been discussed [32]. The propagation of bright similaritons in a cubic-quintic nonlinear medium with inhomogeneous dispersion and gain have been studied analytically and their propagation through diffraction barrier and well in the presence of noise has been examined. The numerical analysis revealed the stable propagation of bright similaritons over tens of diffraction lengths [33]. Nonlinear tunneling of similaritons has also been reported in birefringent fibers [13]. Now we study the nonlinear tunneling properties of optical similaritons in a tapered graded-index nonlinear waveguide whose refractive index is given by Eq. (2.65). Using the model Eq. (2.67) from the previous chapter which is used to study the pulse propagation in a tapered graded-index nonlinear waveguide, for the sake of convenience, we are rewriting it here in the normalized coordinates as follows

$$iU_Z + \frac{D(Z)}{2}U_{XX} + \sigma R(Z)|U|^2U - i\alpha(Z)U_X + \frac{F(Z)}{2}X^2U = i\frac{\Gamma(Z)}{2}U. \quad (3.1)$$

Here all the parameters have the same meaning as in section 2.7. First of all, we obtain the exact optical similariton solutions for Eq. (3.1) by using self-similarity transformation and the Darboux technique. After that, we will employ these solutions to investigate the nonlinear tunneling properties through different barriers and wells.

On substituting Gauge and similarity transformation given in Eq. (2.69) along with Eq. (2.70) in Eq. (3.1), collecting similar terms and demanding the coefficients of real and imaginary parts of each term to be separately equal to zero, we obtain the following relations among the various parameters

$$\begin{aligned} A(Z) &= \sqrt{\frac{D}{R}} \frac{1}{w(Z)}, B(Z) = k_1, \\ C(Z) &= \frac{w_Z}{w(Z)D(Z)}, d_1(Z) = k_2^2 \int \frac{D(Z)B^2}{2} dZ, \end{aligned} \quad (3.2)$$

where k_1 and k_2 are constants.

The pulse center $X_c(Z)$ and the tapering function $F(Z)$ read

$$X_c(Z) = w(Z) \left(X_0 + C_{02} \int_0^Z \frac{-\alpha(S) + D(S)B(S)}{w(S)} dS \right), \quad (3.3)$$

$$F(Z) = \frac{w_{ZZ}}{WD} - \frac{w_Z D_Z}{WD^2}. \quad (3.4)$$

Eqs.(3.2,3.3,3.4) are self-consistent only if the gain function $\Gamma(Z)$ satisfies the following condition

$$\Gamma(Z) = \frac{RD_Z - DR_Z}{2RD} - \frac{3w_Z}{2w}. \quad (3.5)$$

Using the transformations given in Eqs. (2.69, 2.70), Eq. (3.1) reduces to the following standard NLSE, for the conditions given in Eqs. (3.2,3.3,3.4,3.5)

$$i \frac{\partial \psi}{\partial \rho} + \frac{1}{2} \frac{\partial^2 \psi}{\partial \chi^2} + \sigma |\psi|^2 \psi = 0, \quad (3.6)$$

where the effective propagation distance $\rho(Z)$ is given as

$$\rho(Z) = \rho_0 + \int_0^Z \frac{D(s)}{w^2} dS. \quad (3.7)$$

Now we construct the bright and dark similaritons and their pairs for Eq. (3.1) by applying Darboux method.

3.4.1 Bright and Dark similariton solutions

The solution of Eq. (3.1) can be obtained from the solution of Eq. (3.6) by using a one-to-one correspondence. By employing the transformation given by Eq. (2.69) and the Darboux transformation (DT) [34], bright multi-similariton solutions of Eq. (3.1) can be given as:

$$U(X, Z) = A(Z) e^{i\Phi} \left[U_0 + 2 \sum_{m=1}^n \frac{(\lambda_m + \lambda_m^*) \phi_{1,m}(\lambda_m) \phi_{2,m}^*(\lambda_m)}{A_m} \right], \quad (3.8)$$

$$\begin{aligned} \Phi_{j,m+1}(\lambda_{m+1}) &= (\lambda_{m+1} + \lambda_m^*) \phi_{j,m}(\lambda_{m+1}) \\ &\quad - \frac{B_m}{A_m} (\lambda_m + \lambda_m^*) \phi_{j,m}(\lambda_m). \end{aligned} \quad (3.9)$$

with

$$A_m = |\phi_{1,m}(\lambda_m)|^2 + |\phi_{2,m}(\lambda_m)|^2. \quad (3.10)$$

$$B_m = \phi_{1,m}(\lambda_{m+1}) \phi_{1,m}^*(\lambda_m) + \phi_{2,m}(\lambda_{m+1}) \phi_{2,m}^*(\lambda_m). \quad (3.11)$$

where, $m = 1, 2, \dots, n$ and $j = 1, 2$. The complex spectral parameter reads

$$\lambda_m = \alpha_m + i\beta_m. \quad (3.12)$$

The parameter λ_m^* is the complex conjugate of λ_m , $A(Z)$ and Φ can be obtained from Eq. (3.2) and Eq. (2.70), respectively.

On substituting the seed solution $U_0 = 0$ into Eq. (3.8) one can obtain 1-similariton solution of Eq. (3.1) and by using 1-similariton solution as a seed solution in Eq. (3.8) we can derive 2-similariton solution. Thus, by recursion, one can generate upto n-similariton solutions. Here, we are presenting 1 and 2-bright similariton solutions of Eq. (3.1) for $\sigma = 1$ as follows:

$$U_{1B}(X, Z) = A(Z)2\alpha_1 \operatorname{sech}(\xi_1) \exp[-i(2\beta_1\chi - 2(\alpha_1^2 - \beta_1^2)\rho - \Phi)]. \quad (3.13)$$

with

$$\xi_1 = 2\alpha_1\chi + 4\alpha_1\beta_1\rho + \xi_{10}, \quad (3.14)$$

where, χ , Φ and ρ are determined by Eq. (2.69), Eq. (2.70) and Eq. (3.7), respectively.

2-bright similariton solution in the explicit form can be given as

$$U_{2B}(X, Z) = 4A(Z)e^{i\Phi} \frac{G_1(Z, X)}{F_1(Z, X)}, \quad (3.15)$$

where

$$\begin{aligned} G_1(Z, X) = & \cosh \xi_2 \exp(-i\chi_1)[(\beta_2 - \beta_1)^2 + 2i\alpha_2(\beta_2 - \beta_1) \\ & \tanh \xi_2 + \alpha_1^2 - \alpha_2^2] + \alpha_2 \cosh \xi_1 \exp(-i\xi_2) \\ & [(\beta_2 - \beta_1)^2 - 2i\alpha_1(\beta_2 - \beta_1) \tanh \xi_1 - \alpha_1^2 + \alpha_2^2]. \end{aligned} \quad (3.16)$$

and

$$\begin{aligned} F_1(Z, X) = & \cosh(\xi_1 + \xi_2)[(\beta_1)^2 + (\alpha_2 - \alpha_1)^2] + \cosh(\xi_1 - \xi_2) \\ & [(\beta_2 - \beta_1)^2 + (\alpha_2 + \alpha_1)^2] - 4\alpha_1\alpha_2 \cos(\chi_2 - \chi_1). \end{aligned} \quad (3.17)$$

The arguments and the phases are

$$\xi_j(\chi, \rho) = 2\alpha_j\chi + 4\alpha_j\beta_j\rho + \xi_{j0}, \quad (3.18)$$

$$\chi_j(\chi, \rho) = 2\beta_j\chi + 2(\beta_j^2 - \alpha_j^2)\rho + \chi_{j0}, \quad (3.19)$$

where α_j and β_j are the spectral parameters. The functions χ , Φ and ρ are determined by Eq. (2.69), Eq. (2.70) and Eq. (3.7), respectively.

Due to the one-to-one correspondence between the model equation (3.1) and the standard NLSE, one can derive gray (dark) multi-similariton solutions of Eq. (3.1). The exact 1- dark similariton solution for $\sigma = -1$ is given as:

$$U_{1D}(X, Z) = 2A(Z)\beta_1[\sqrt{1-a^2} + ia \tanh(2a\beta_1\chi + 4a\beta_1^2\sqrt{1-a^2}\rho)] \exp[-4i\beta_1^2\rho], \quad (3.20)$$

where the parameter $0 < a < 1$ defines the depth of modulation which means the blackness of gray similariton. It becomes black for $a = 1$.

The 2-dark similariton solution is given as:

$$U_{2D}(X, Z) = A(Z)\mu e^{i(\Phi+\zeta(\rho,\chi))} \left(1 + \frac{G_2}{F_2}\right), \quad (3.21)$$

where

$$G_2 = 4\mu(\omega_1 + \omega_2 - 2\mu) - 4i \frac{\lambda_1 + \lambda_2}{(\beta_1 + \beta_2)} \eta \quad (3.22)$$

$$F_2 = 4\mu^2 \left(\frac{\lambda_1 + \lambda_2}{\beta_1 + \beta_2}\right)^2 \eta, \quad \eta = (\omega_1 - \mu)(\omega_2 - \mu),$$

$$\omega_j = \frac{(\alpha_j - i\beta_j)(\alpha_j + i\beta_j \tanh(\delta_j))}{\mu},$$

$$\delta_j = \beta_j[\chi - \chi_{j0} - (\Omega + \alpha_j)\rho],$$

$$\zeta = -\left(\mu^2 + \frac{\Omega^2}{2}\right)\rho - \Omega\chi - \zeta_0, \quad \mu = |\lambda_j|.$$

From the expressions of ξ_j and δ_j for bright and dark similaritons pairs, one can clearly see that their velocities are determined by $\beta_j \int_0^Z \frac{D(s)}{w^2} ds$ and $(\Omega + \alpha_j) \frac{D(s)}{w^2} ds$, which are associated with the parameters α_j , β_j and $D(Z)$. Therefore, by assigning appropriate system parameters, we can control the interactions of similariton pairs by managing their velocities. The initial position and initial phase are related to the parameters ξ_{j0} and χ_{j0} for bright similariton pairs and the parameters χ_{j0} and ζ_0 for dark similariton pairs. The evolutionary behaviour of similaritons can be controlled by the spectral parameters α_j and β_j . To demonstrate this we are studying the nonlinear tunneling of similaritons in the coming section.

3.4.2 Nonlinear tunneling of optical similaritons with constant background

In order to study the optical similaritons behaviour through diffraction and nonlinear barriers with constant background we consider the following two examples.

The first one is diffraction barrier(DB) or diffraction well (DW). For this we are choosing the parameters as [6]

$$D(Z) = 1 + h\text{sech}^2[\epsilon(Z - Z_0)], \quad R(Z) = R_0, \quad (3.23)$$

The second one is nonlinearity barrier (NB) or nonlinearity well (NW). For this we are choosing the parameters as [7]

$$R(Z) = 1 + h\text{sech}^2[\epsilon(Z - Z_0)], \quad D(Z) = D_0, \quad (3.24)$$

where h denotes the barrier's height, ϵ represents the barrier (well) width and Z_0 signifies the location of the barrier (well). If $h = 0$ it represents the similariton propagation through a homogeneous waveguide, $h > 0$ represents barrier and $-1 < h < 0$ indicates well. The parameters $R_0, D_0 > 0$ are associated with the nonlinearity and diffraction parameters of the system.

Case(i) The nonlinear tunneling of similaritons through DB (DW) has been investigated by choosing pulse width $w(Z) = \text{sech}(0.1Z)$. The corresponding tapering function $F(Z)$ and the gain function $\Gamma(Z)$ comes out to

$$F(Z) = \frac{p}{(1 + h\text{sech}^2[\epsilon(Z - Z_0)])^2}, \quad (3.25)$$

where

$$p = (0.01\text{sech}(0.1Z))^2(-1.5 + 0.5 \cosh(0.2Z) + h\text{sech}^2[\epsilon(Z - Z_0)]^2(-1 + \sinh^2(0.1Z) - 10\epsilon \sinh(0.2Z) \tanh[\epsilon(Z - Z_0)])).$$

The gain function $\Gamma(Z)$ is as follows:

$$\Gamma(Z) = 0.15 \tanh(0.1Z) - \frac{4\epsilon h \tanh[\epsilon(Z - Z_0)]}{1 + 2h + \cosh[2\epsilon(Z - Z_0)]}. \quad (3.26)$$

The tapering and gain profile is plotted in Fig. 3.1. It is clear from Eq. (3.23) that the diffraction barrier/well is formed at $Z = Z_0$, resulting in the behavioural change of $F(Z)$ and $\Gamma(Z)$ at Z_0 , which is evident in Fig. 3.1. The tapering function $F(Z)$ changes its sign from positive to negative for DB case implying that

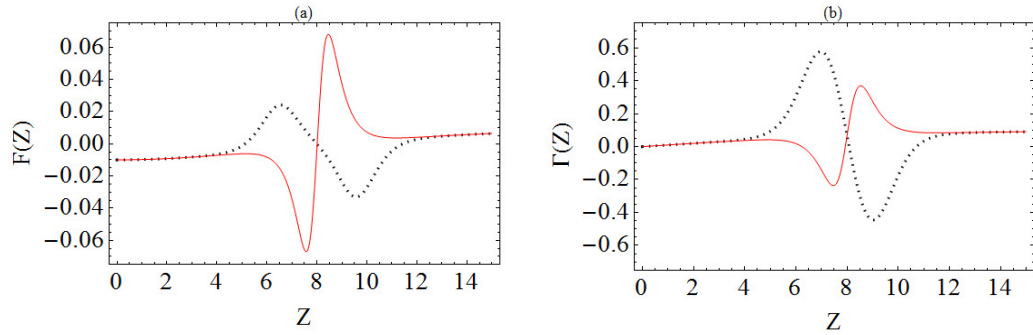


Figure 3.1: (a) The tapering profile $F(Z)$ given by Eq. (3.25) (b) The gain profile $\Gamma(Z)$ given by Eq. (3.26) solid line (for DW) and dashed (for DB). The chosen parameters are $\epsilon = 1$, $R_0 = 1$, $h = 5$ for DB and $h = -0.5$ for DW, $Z_0 = 8$.

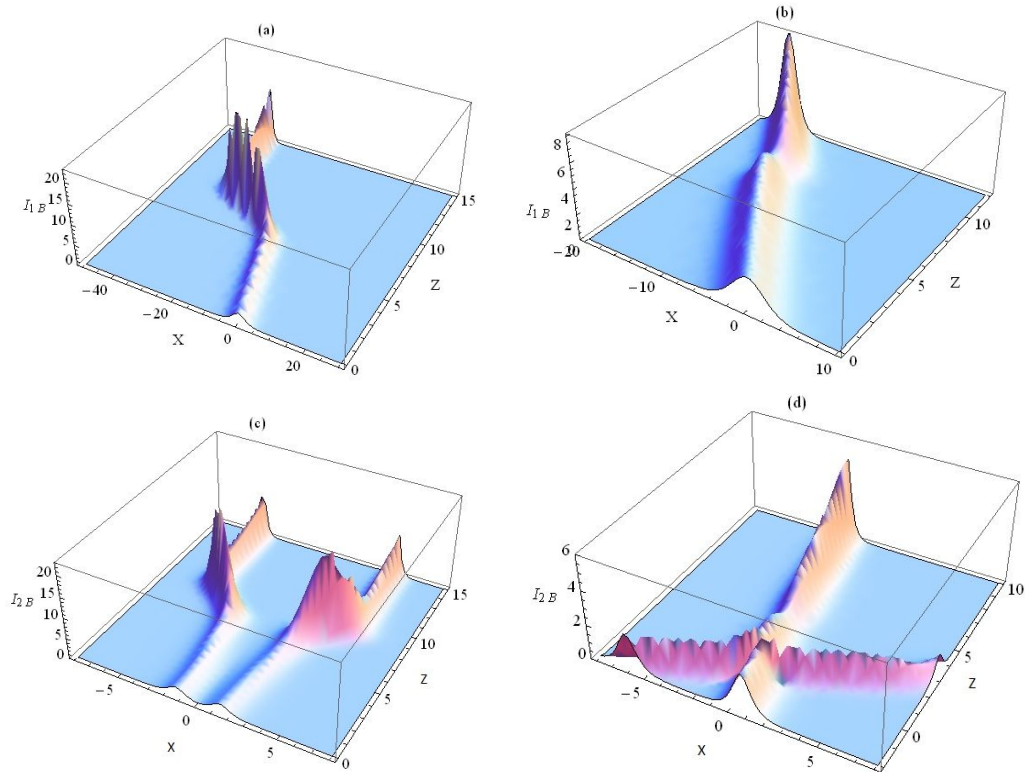


Figure 3.2: Intensity plots of (a) bright similariton For DB (b) DW with $\alpha_1 = -0.8$, $\beta_1 = 0.2$ (c) Intensity plot for 2-bright similariton for DB with $\beta_2 = -0.1$ (d) For DW with $Z_0 = 8$, $\beta_2 = -1.5$. The other parameters are $\beta_1 = 0.1$, $\alpha_1 = -1.1$, $\alpha_2 = 1$. The remaining parameters are same as in Fig. 3.1

the inhomogeneity of the waveguide should change from defocusing to focusing type. The gain function $\Gamma(Z)$ forms a convex part and then undergoes a change at the barrier location, forming a concave part after crossing the barrier. The reverse occurs for the well case. This kind of gain distribution can be realized in erbium doped waveguide by suitably adjusting the density of the dopants [35].

Fig. 3.2 and Fig. 3.3 depict the dynamical evolutionary scenarios of the nonlinear tunneling of the bright similariton (3.2(a),3.2(b)), 2-bright similariton (3.2(c),3.2(d)), dark similariton (3.3(a),3.3(b)) and 2-dark similariton (3.3(c),3.3(d)) as they pass through the diffraction barrier (DB) and diffraction well (DW) given by Eq. (3.23). When the similaritons pass through the DB, the pulses are amplified and form the peaks in the vicinity of the barrier and then get attenuated. In the case of DW, the pulses form dips at well location, then propagate in accordance with the system parameters. It is worth mentioning here that we can control the interactions between the similariton pairs by controlling their velocities through the proper assignment of the system and spectral parameters. This is depicted for 2-bright similariton case in Fig. 3.2(c) and 3.2(d) where the separating or interacting evolutionary behaviour of similaritons have been obtained by suitably choosing spectral parameters α_j and β_j .

We have also investigated the nonlinear tunneling properties of rogue waves for the form of dispersion barrier given by Eq. (3.23) as they propagate through an erbium doped optical fiber. We have found that as the rogue waves reaches in the vicinity of the barrier they get amplified and after crossing the barrier they restore their original shape. Moreover, we have predicted that the presence of erbium atoms causes the phase shifting of the rogue waves in the vicinity of the barrier [36].

Case(ii) The evolution of optical similaritons through nonlinearity barrier (NB) and well (NW) has been studied by choosing pulse width $w(Z) = \cosh(0.1Z)$. The corresponding tapering function $F(Z)$ comes out to be

$$F(Z) = \frac{0.01}{D_0}, \quad (3.27)$$

The gain function $\Gamma(Z)$ reads

$$\Gamma(Z) = -0.15 \tanh(0.1Z) + \frac{2\epsilon h \tanh[\epsilon(Z - Z_0)]}{1 + h + \cosh[2\epsilon(Z - Z_0)]}. \quad (3.28)$$

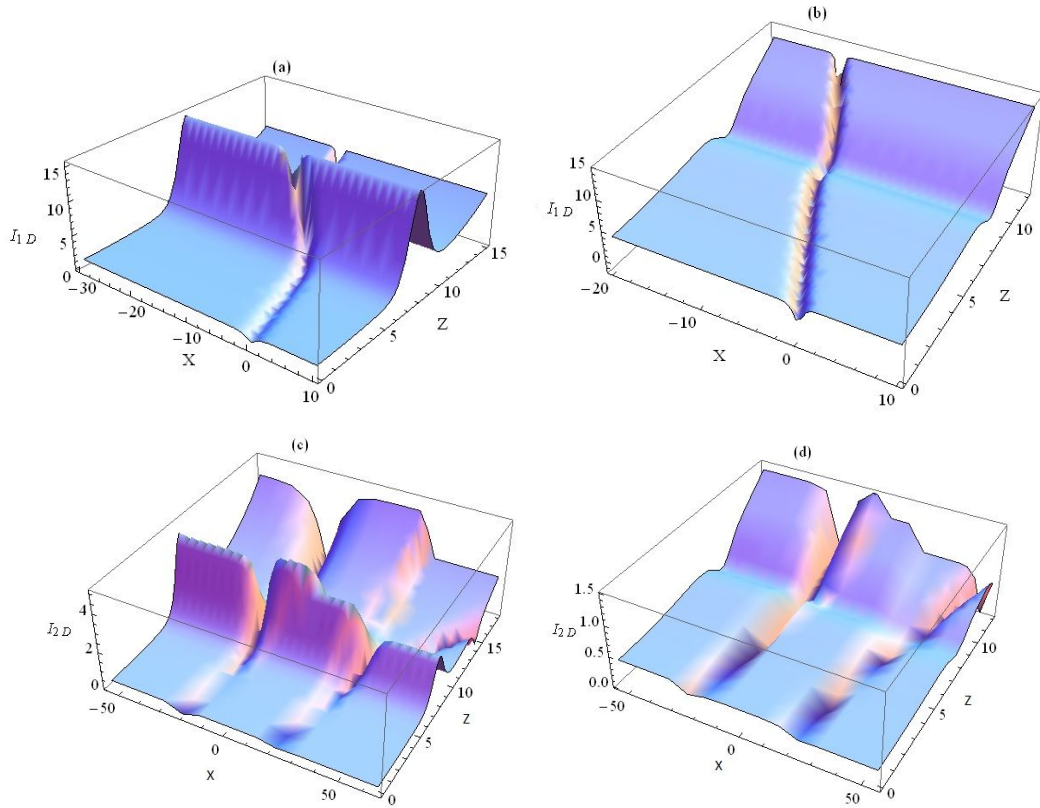


Figure 3.3: Intensity plots of (a) dark similariton for DB with $\alpha_1 = \beta_1 = 0.6$ (b) DW with $\alpha_1 = 0.8, \beta_1 = 0.2$, (c) Intensity plot for 2-dark similariton for DB (d) For DW $\chi_{10} = -\chi_{20} = 20, \beta_1 = 0.45, \beta_2 = 0.35, \alpha_1 = -.01, \alpha_2 = 0.6$. The remaining parameters are same as in Fig. 3.1

Fig. 3.4 shows the dynamical behaviour of 1-and 2-bright similaritons as they propagate through NB and NW. Unlike DB the amplitude of the bright similaritons decreases as they propagate through NB and forms a dip (Figs. 3.4(a),3.4(c)). The optical similaritons form peaks through NW (Figs. 3.4(b),3.4(d)). Similar dynamical behaviour is observed for 1 and 2-dark similaritons which is depicted in Fig. 3.5.

It should be noted that the tapering becomes constant as can be seen from Eq. (3.27). By choosing different values of tapering parameter $F(Z)$ (through the choice of D_0) we can control the amplitude of similaritons to such an extent that they can even be annihilated. This is in general true for both bright and dark similaritons and their pairs. We have depicted this behaviour for bright similaritons

pairs with different D_0 in Fig. 3.6.

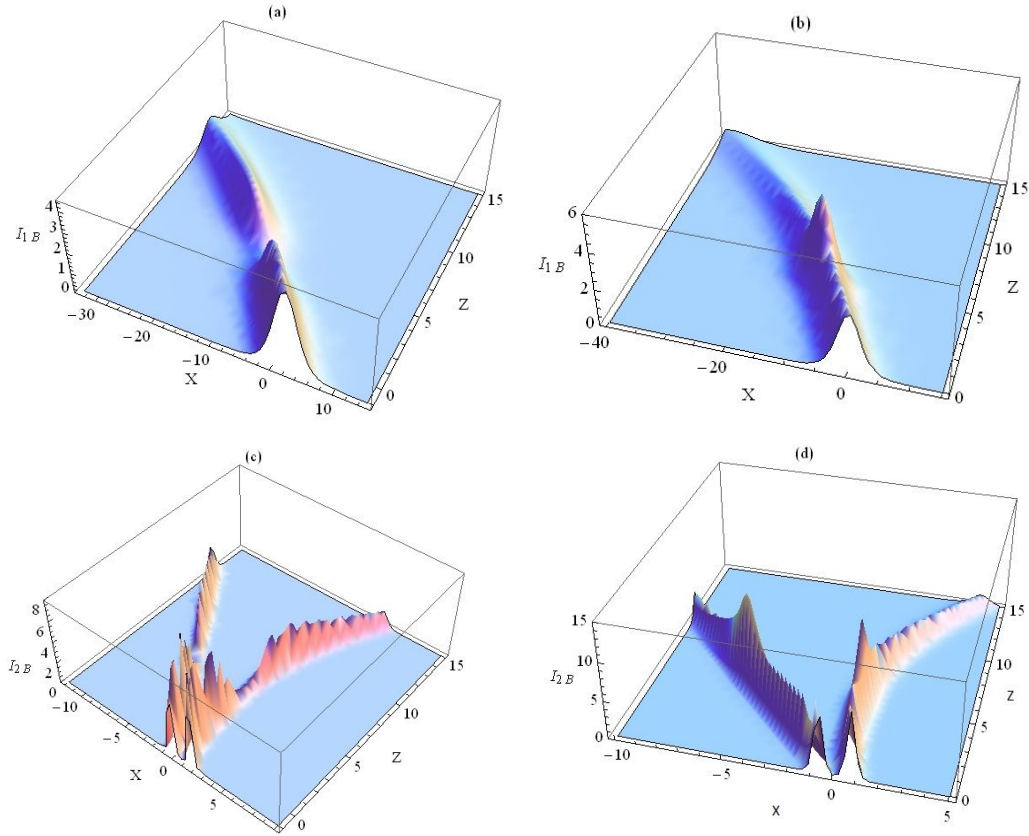


Figure 3.4: Intensity plots of (a) bright similariton for NB (b) NW with $\alpha_1 = 1$, $\beta_1 = 0.2$ (c) Intensity plot for 2-bright similariton for NB with $D_0 = 0.5$ (d) For NW $D_0 = 1$. The other parameters are $\beta_1 = -0.9$, $\beta_2 = -0.5$, $\alpha_1 = 2$, $\alpha_2 = -2.1$, $Z_0 = 5$. The remaining parameters are same as in Fig. 3.1.

3.4.3 Nonlinear tunneling of optical similaritons with exponential background

We choose the following diffraction and nonlinearity parameters to study the optical similaritons propagation behaviour [14, 11, 33]

$$\begin{aligned} D(Z) &= D_0 \exp(-r_0 Z) + h \operatorname{sech}^2[\epsilon(Z - Z_0)], \\ R(Z) &= R_0 \exp[-r_0 Z]. \end{aligned} \quad (3.29)$$

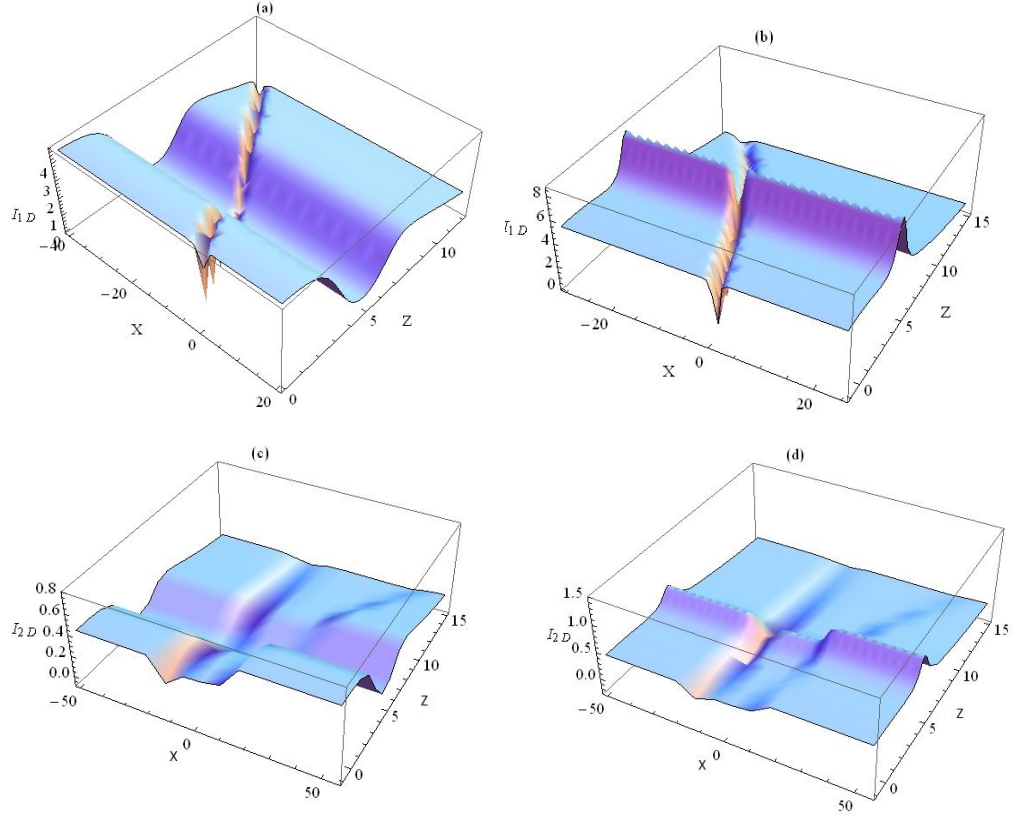


Figure 3.5: Intensity plots of (a) dark similariton for NB (b) NW with with $\epsilon = \beta_1 = 1, \alpha_1 = 0.8$ (c) Intensity plot for 2-dark similariton for DB (d) For DW $\chi_{10} = -\chi_{20} = 10, \beta_1 = -0.5, \beta_2 = -0.4, \alpha_1 = -0.58, \alpha_2 = 0.38, Z_0 = 5$. The remaining parameters are same as in Fig. 3.1.

where the parameter r_0 is decaying ($r_0 > 0$) or increasing ($r_0 < 0$). We are choosing the pulse width $w(Z) = \text{sech}(0.1Z)$ and the corresponding tapering and gain functions come out to be

$$F(Z) = \frac{p_1}{(D_0 + \exp(r_0 Z) h \text{sech}^2[\epsilon(Z - Z_0)])^2}, \quad (3.30)$$

where

$$p_1 = \exp(r_0 Z) \text{sech}^2(0.1Z) (D_0 (-0.015 - 0.015r_0 + (0.005 + 0.05r_0) \cosh(0.2Z) + \exp(r_0 Z) h \text{sech}^2[\epsilon(Z - Z_0)] (-0.01 - 0.02\epsilon \tanh[\epsilon(Z - Z_0)] + \sinh^2[0.1Z] (0.01 + 0.02\epsilon \tanh[\epsilon(Z - Z_0)])))).$$

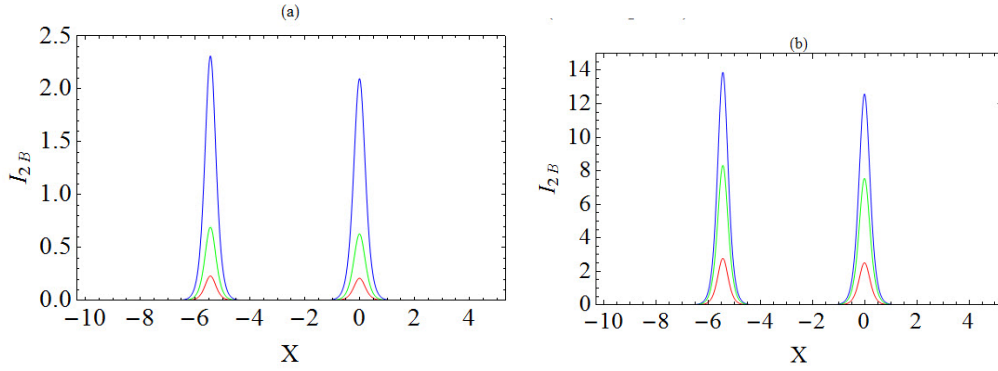


Figure 3.6: Intensity profile of 2-bright similariton (a) for nonlinearity barrier case (b) for nonlinearity well case for $D_0 = 1$ (Blue), $D_0 = 0.3$ (Green), $D_0 = 0.1$ (Red). The other parameters are the same as depicted in Fig. 3.4

$$\Gamma(Z) = \frac{p_2}{D_0 + \exp[r_0 Z] h \operatorname{sech}^2[\epsilon(Z - Z_0)]}, \quad (3.31)$$

where

$$p_2 = 0.1D_0 \tanh(0.1Z) + \exp(r_0 Z) h \operatorname{sech}^2[\epsilon(Z - Z_0)] \\ (0.5r_0 + 0.1 \tanh(0.1Z) - \epsilon \tanh[\epsilon(Z - Z_0)]).$$

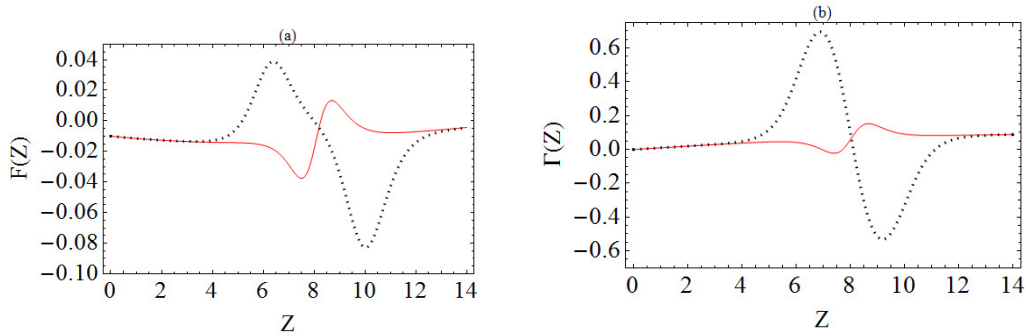


Figure 3.7: (a) The tapering profile $F(Z)$ given by Eq. (3.30) (b) The gain profile $\Gamma(Z)$ given by Eq. (3.31) solid line (for DW) and dashed (for DB). The chosen parameters are $\epsilon = 1$, $R_0 = 1$, $h = 5$ for DB and $h = -0.1$ for DW, $Z_0 = 8$.

The tapering and gain profile is plotted in Fig. 3.7. Now we are concentrating on the dynamics of bright similaritons and ignoring dark similaritons. Fig. 3.8 shows the evolution of the 1 and 2-bright similaritons as they pass through the diffraction barrier and well with decaying r_0 . We have found that for the chosen

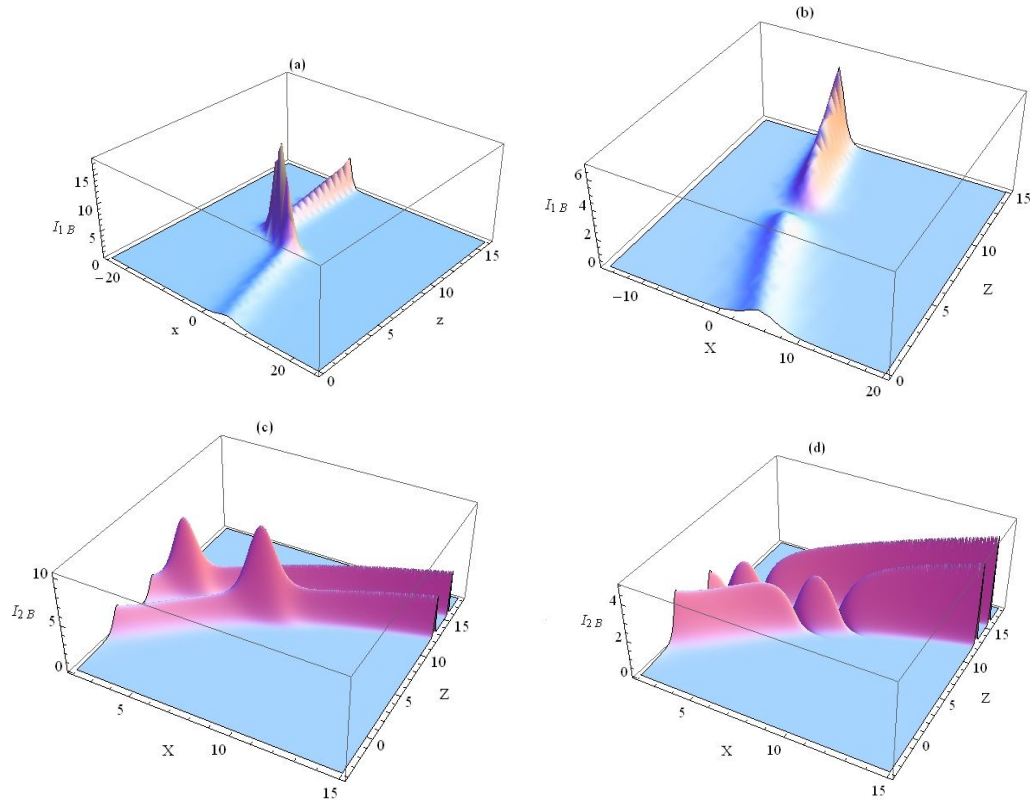


Figure 3.8: Intensity plots of 1-bright similariton (a) DB with $h = 5$ (b) DW with $h = -0.5$, $\alpha_1 = 0.5$, $\beta_1 = 0.2$. Intensity plots of 2-bright similaritons with (c)DB (d) DW with $\alpha_1 = 1.21, \alpha_2 = 1.19$, $\beta_1 = -0.2, \beta_2 = -0.3$. The remaining parameters are $r_0 = 0.08$, $\epsilon = 2$, $Z_0 = 8$.

value of r_0 , the amplitude and the width of similaritons remain invariant before they cross the DB/DW and their amplitude is changed at barrier or well location due to the exchange of energy between the similariton and the barrier/well. In case of DB, their amplitude is increased as they gain energy from barrier while in case of DW their amplitude is decreased as they lose their energy to the well and after crossing the barrier/well they get compressed. This energy exchange feature between the pulse and the barrier/well is very useful in an optical communication system to improve the channel capacity. Additionally, by suitably choosing the value of r_0 we can control the propagation of similaritons. We have depicted this behaviour for 1-bright similariton case in Fig. 3.9 as they propagate through DB. For increasing parameter r_0 , after crossing the barrier pulse width is compressed

and it gets amplified (Fig. 3.9(a)), while for decaying parameter the pulse width is compressed and amplitude is reduced as depicted in Fig. 3.9(b). Similar behaviour has been observed for the DW case. Thus, by the proper management of barrier or well height, location and r_0 we can change the amplitude of the pulse to an extent so that it vanishes. Hence, the transmission will not take place after the barrier/well. This concept can be applied in constructing logic gate devices to achieve ultrafast switches.

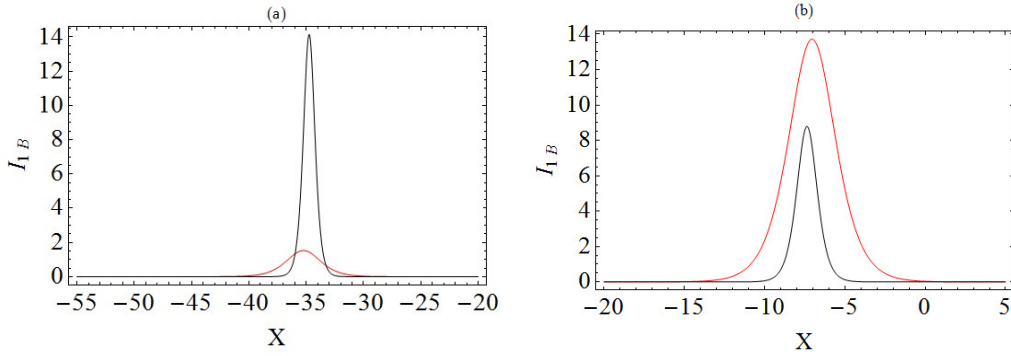


Figure 3.9: Intensity plots of 1-bright similariton through DB (a) $r_0 = -0.014$ (b) $r_0 = 0.164$. The evolution of the pulse before (red) at $Z = 7$ and after crossing (blue) the barrier at $Z = 20$. The other parameters are the same as depicted in Fig. 3.8.

3.4.4 Cascade compression

We have observed that the bright similariton pairs get compressed after undergoing tunneling in the presence of exponential background. This property can be extended to successive compressions by allowing the similaritons to pass through successive potential barriers or wells. This process is termed as cascade compression. To investigate the behaviour of similaritons the diffraction and nonlinearity parameters are chosen as [9]

$$D(Z) = D_o \exp(-r_0 Z) + h \sum_{j=1}^n \text{sech}^2[\epsilon(Z - jZ_0)],$$

$$R(Z) = R_0 \exp(-r_0 Z), \quad (3.32)$$

where n is a natural number and Z_0 denotes the spacing between two consecutive barriers. The corresponding form of tapering function $F(Z)$ and gain $\Gamma(Z)$ can

be worked out by using Eqs.(3.4) and (3.5). In Fig. 3.10 we have plotted the profile of 2-bright similaritons crossing two successive diffraction barriers and wells. On closely observing the plots we infer that at barrier (well) location similaritons amplitude is increased (decreased) and after crossing the first barrier (well) it get compressed. When it reaches the second barrier (well) their amplitude is increased (decreased) even further and after crossing the second barrier the pulses are even more compressed. Thus, we can conclude that by allowing the similaritons to pass through number of barriers we can get the similaritons of desired width and intensity.

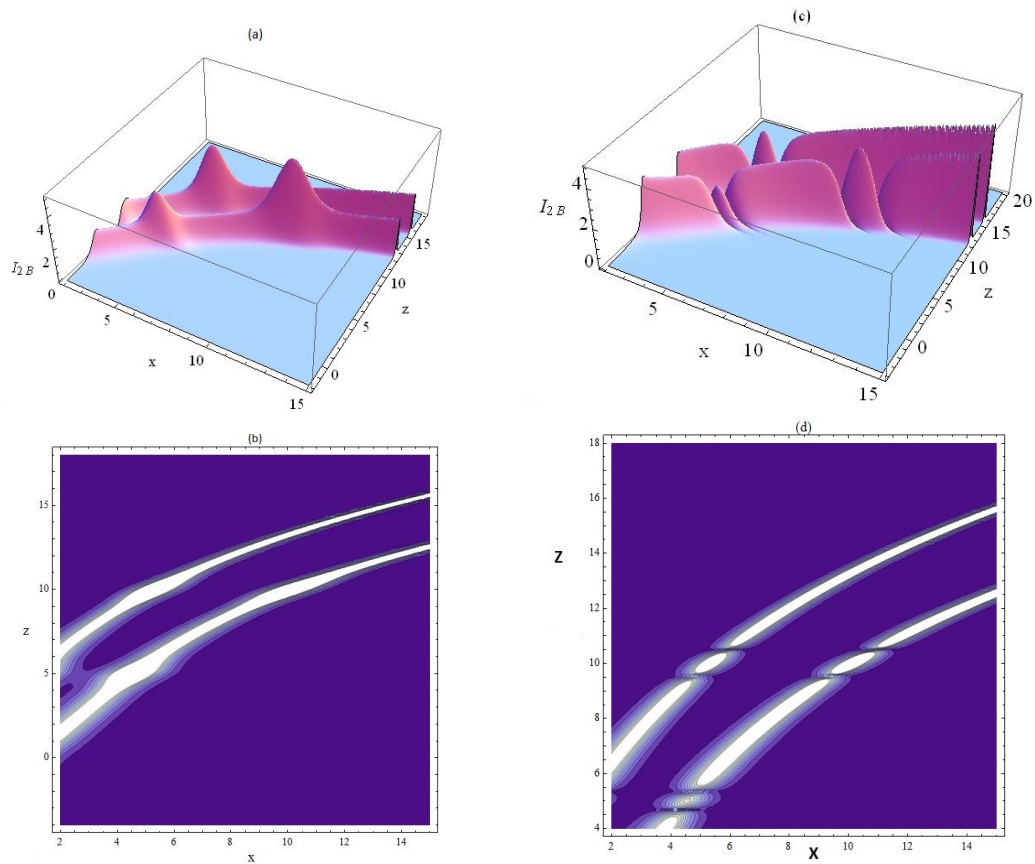


Figure 3.10: (a) Intensity plot 2-bright similariton profile through DB (b) The corresponding contour plot with $h = 3$. (c) Intensity plot 2-bright similariton profile through DW (d) The corresponding contour plot with $h = -1$. The other parameters are $\alpha_1 = 1.21$, $\beta_1 = -0.2$, $\alpha_2 = 1.19$, $\beta_2 = -0.3$, $\epsilon = 2 r_0 = 0.08$.

3.5 Conclusion

We have obtained 1 and 2-bright and dark similariton solutions for inhomogeneous generalized NLSE, which governs the propagation of optical similaritons through a tapered graded-index nonlinear waveguide. The exact analytical optical similariton solutions have been worked out by using gauge-similarity transformation and Darboux technique. Upon obtaining the similariton solutions, we have investigated the nonlinear tunneling for two cases (i) constant background (ii) exponential background. For the former, we have found that the amplitude of the similaritons is increased or decreased at barrier location, depending upon whether they are propagating through DB (DW) or NB (NW). For the latter case, pulse compression is achieved. This feature is extended to cascade pulse compression by allowing the pulse to propagate through multiple barriers. As a result of cascade compression, we can get similaritons of desired amplitudes and widths at the desired propagation distance. We expect our results to find applications in nonlinear optical devices based on optical similaritons.

The work presented here has been published in [37].

Bibliography

- [1] V N Serkin, V A Vysloukh, and J R Taylor. Soliton spectral tunnelling effect. *Electronics Letters*, 29(1): 12-13, 1993.
- [2] A C Newell. Nonlinear tunnelling. *Journal of Mathematical Physics*, 19, 1126, 1978.
- [3] A I Larkin, and P A Lee. Tunneling of solitons and charge-density waves through impurities. *Physical Review B*, 17(4): 1596, 1978.
- [4] D Anderson, M Lisak, B Malomed, and M Q Teixeira. Tunneling of an optical soliton through a fiber junction. *Journal of the Optical Society of America B*, 11(12): 2380-2384, 1994.
- [5] V N Serkin, V M Chapela, J Percino, and T L Belyaeva. Nonlinear tunneling of temporal and spatial optical solitons through organic thin films and polymeric waveguides. *Optics Communications*, 192(3): 237-244, 2001.
- [6] V N Serkin, and T L Belyaeva. High-energy optical Schrödinger solitons. *Journal of Experimental and Theoretical Physics Letters*, 74(12): 573-577, 2001.
- [7] J Wang, L Li, and S Jia. Nonlinear tunneling of optical similaritons in nonlinear waveguides. *Journal of the Optical Society of America B*, 25(8): 1254-1260, 2008.
- [8] R Yang, and X Wu. Spatial soliton tunneling, compression and splitting. *Optics Express*, 16(22): 17759-17767, 2008.

- [9] G Yang, R Hao, L Li, Z Li, and G Zhou. Cascade compression induced by nonlinear barriers in propagation of optical solitons. *Optics Communications*, 260(1): 282-287, 2006.
- [10] A Barak, Or Peleg, C Stucchio, A Soffer, and M Segev. Observation of soliton tunneling phenomena and soliton ejection. *Physical Review Letters*, 100(15): 153901, 2008.
- [11] M S M Rajan, A Mahalingam, A Uthayakumar. Nonlinear tunneling of nonautonomous optical solitons in combined nonlinear Schrödinger and MaxwellBloch systems. *Journal of Optics*, 14(10): 105204, 2012.
- [12] M S M Rajan, J Hakkim, A Mahalingam, and A Uthayakumar. Dispersion management and cascade compression of femtosecond nonautonomous soliton in birefringent fiber. *The European Physical Journal D*, 67(7): 1-8, 2013.
- [13] C Dai, Y Y Wang, and J F Zhang. Nonlinear similariton tunneling effect in the birefringent fiber. *Optics Express*, 18(16): 17548-17554, 2010.
- [14] W P Zhong, and M R Beli. Soliton tunneling in the nonlinear Schrödinger equation with variable coefficients and an external harmonic potential. *Physical Review E*, 81(5): 056604, 2010.
- [15] C Q Dai, Y Y Wang, Q Tian, and J F Zhang. The management and containment of self-similar rogue waves in the inhomogeneous nonlinear Schrödinger equation. *Annals of Physics*, 327(2): 512-521, 2012.
- [16] G I Barenblatt. *Scaling, Self-similarity and Intermediate Asymptotics*, Cambridge University Press, 1996.
- [17] S A Ponomarenko and G P Agrawal. Optical similaritons in nonlinear waveguides. *Optics Letters*, 32(12): 1659-1661, 2007.
- [18] V I Kruglov, A C Peacock, and J D Harvey. Exact self-similar solutions of the generalized nonlinear Schrödinger equation with distributed coefficients. *Physical Review Letters*, 90(11): 113902, 2003.

- [19] C Dai, Y Wang, and J Chen. Analytic investigation on the similariton transmission control in the dispersion decreasing fiber. *Optics Communications*, 284(13): 3440-3444, 2011.
- [20] M E Fermann, V I Kruglov, B C Thomsen, J M Dudley, and J D Harvey. Self-similar propagation and amplification of parabolic pulses in optical fibers. *Physical Review Letters*, 84(26): 6010, 2000.
- [21] S A Ponomarenko, and G P Agrawal. Interactions of chirped and chirp-free similaritons in optical fiber amplifiers. *Optics Express*, 15(6): 2963-2973, 2007.
- [22] R Gupta, A Goyal, T S Raju, and C N Kumar. Symbiotic multimode spatial similaritons and rogons in inhomogeneously coupled optical fibers. *Journal of Modern Optics*, 60(18): 1569-1575, 2013.
- [23] A Goyal, R Gupta, C N Kumar, T S Raju, and P K Panigrahi. Controlling optical similaritons in a graded-index nonlinear waveguide by tailoring of the tapering profile. *Optics Communications*, 300: 236-243, 2013.
- [24] A Goyal, R Gupta, S Loomba, and C N Kumar. Riccati parameterized self-similar waves in tapered graded-index waveguides. *Physics Letters A*, 376(45): 3454-3457, 2012.
- [25] J M Dudley, C Finot, D J Richardson, and G Millot. Self-similarity in ultrafast nonlinear optics. *Nature Physics*, 3(9): 597-603, 2007.
- [26] V I Kruglov, A C Peacock, J D Harvey, and J M Dudley. Nonlinear wave phenomena in confined structures-Nonlinear effects in fibers-self-similar propagation of parabolic pulses in normal-dispersion fiber amplifiers. *Journal of the Optical Society of America B: Optical Physics*, 19(3): 461-469, 2002.
- [27] V I Kruglov, A C Peacock, J M Dudley, and J D Harvey. Self-similar propagation of high-power parabolic pulses in optical fiber amplifiers. *Optics Letters*, 25(24): 1753-1755, 2000.
- [28] L Wu, J F Zhang, L Li, Q Tian, and K Porsezian. Similaritons in nonlinear optical systems. *Optics Express*, 16(9): 6352-6360, 2008.

- [29] C Dai, Y Wang, and C Yan. Chirped and chirp-free self-similar cnoidal and solitary wave solutions of the cubic-quintic nonlinear Schrödinger equation with distributed coefficients. *Optics Communications*, 283(7): 1489-1494, 2010.
- [30] C Q Dai, Y Y Wang, and X G Wang. Ultrashort self-similar solutions of the cubic-quintic nonlinear Schrödinger equation with distributed coefficients in the inhomogeneous fiber. *Journal of Physics A: Mathematical and Theoretical*, 44(15): 155203, 2011.
- [31] Y Ozeki, and T Inoue. Stationary rescaled pulse in dispersion-decreasing fiber for pedestal-free pulse compression. *Optics Letters*, 31(11): 1606-1608, 2006.
- [32] Y Y Wang, J D He, and C Q Dai. Spatiotemporal self-similar nonlinear tunneling effects in the (3+ 1)-dimensional inhomogeneous nonlinear medium with the linear and nonlinear gain. *Optics Communications*, 284(19): 4738-4744, 2011.
- [33] C Q Dai, Q Yang, J D He, and Y Y Wang. Nonlinear tunneling effect in the (2+ 1)-dimensional cubic-quintic nonlinear Schrödinger equation with variable coefficients. *The European Physical Journal D*, 63(1): 141-148, 2011.
- [34] Lu Li, Z Li, S Li, and G Zhou. Modulation instability and solitons on a cw background in inhomogeneous optical fiber media. *Optics Communications*, 234(1): 169-176, 2004.
- [35] J R He, and L Yi. Exact optical self-similar solutions in a tapered graded-index nonlinear-fiber amplifier with an external source. *Optics Communications*, 320: 129-137, (2014).
- [36] S Loomba, R Gupta, K De, C N Kumar, T S Raju. *Optical Fiber Technology*, 2014, <http://dx.doi.org/10.1016/j.yofte.2014.07.006>.
- [37] S Loomba, M S M Rajan, R Gupta, H Kaur, and C N Kumar. Nonlinear tunneling of optical similaritons in a tapered graded-index nonlinear waveguide. *Optics Communications*, 324: 286-295, 2014.

Chapter 4

Controlling self-similar matter waves in Bose-Einstein condensates

4.1 Introduction

So far we have discussed self-similar waves including rogue waves and optical similaritons in the context of nonlinear fiber optics. Now we study these waves in the context of Bose-Einstein condensates (BECs) by using similar mathematical tools. This can be done as the generalized nonlinear Schrödinger equation (GNLSE) which is the model equation governing the pulse dynamics in two different nonlinear media is the same. Firstly, we give a brief introduction of BECs and then obtain the rogue wave solutions for the cigar shaped BEC in the presence of space and time dependent trap. We shall then exemplify their management for different choices of the parameters and reveal their interesting features. Later, we shall study self-similar waves solutions including bright solitons and their pairs, dark solitons, Akhmediev breathers (ABs) and rogue waves, for the special case of GNLSE with time dependent parabolic trap and scattering length, by using similarity transformation. Then we shall generate the class of nonlinearity parameter by invoking isospectral Hamiltonian procedure and introduce a free parameter λ , known as the Riccati parameter. After generating the class of the Feshbach nonlinearity parameter for a given trapping potential, we investigate the role of parameter λ on the intensity profiles of the self-similar matter waves.

4.2 Bose-Einstein condensate (BEC)

We are aware that even though matter pervades the entire universe, it is found in just a few admissible forms such as solid, liquid and gas. It is possible to make a transition between different states of matter by changing the temperature or pressure. When a gas composed of bosonic atoms is cooled below a certain critical temperature at which the de Broglie wavelength becomes comparable to the interatomic spacing, the atomic wave packets overlap and the gas starts to become a quantum soup of indistinguishable particles. It means that a large fraction of the atoms occupy the lowest quantum state of the external potential and this state of matter is known as Bose-Einstein condensate (BEC). The concept of BEC was first predicted in 1925 by Albert Einstein, but was experimentally realized only in 1995. Anderson and his co-workers created the first pure BEC by cooling a dilute vapor consisting of approximately two thousand ^{87}Rb atoms to 170 nK by using a process of laser cooling and magnetic evaporative cooling [1]. Subsequently, BEC has also been realized in ^{23}Na and ^7Li [2, 3]. The experimental realization of quasi-one-dimensional BECs in a parabolic trap provides an ideal laboratory for studying solitons in a controlled environment. The dynamics of BECs can be described by the effective mean field equation, known as Gross-Pitaevskii (GP) equation which satisfies both the theoretical stand point as well as experimentally relevant conditions [4]. This is a generalized form of NLSE and is given as

$$i\hbar \frac{\partial}{\partial t} \Psi(r, t) = -\frac{\hbar^2}{2m} \nabla^2 \Psi(r, t) + U_0 |\Psi(r, t)|^2 \Psi(r, t) + V_{ext}(r) \Psi(r, t), \quad (4.1)$$

where $\Psi(r, t)$, $r = (x, y, z)$ is the macroscopic wave function of condensate, $V_{ext}(r)$ is the external trapping potential and U_0 describes the strength of interatomic two body interactions. The (3+1)-dimensional GP equation is non-integrable and possesses the solitary wave solutions under specific conditions. For cigar shaped BEC of relatively low density, which corresponds to the case when the kinetic energy in the transverse direction is much greater than the energy of the two body interactions, the three-dimensional GP equation reduces to quasi-one-dimensional GP equation. This implies that for understanding the dynamics of BECs, one should work out the analytical solutions of GP equation and then study their behaviour for the different choices of nonlinearity parameter and trapping potential. Recently, a great deal of research took place in this regard and several

works have been reported that involve study of GP equation with space and/or time modulated potentials [5, 6, 7, 8, 9, 10].

4.3 Controlling matter rogue waves in BEC

Here we are focusing on cigar shaped BEC of relatively low density which corresponds to the case when the kinetic energy in the transverse direction is much greater than the energy of the two body interactions i.e $N|a_s| \ll a_\perp$ where N represents the total number of atoms, a_s is the time dependent s-wave scattering length and $a_\perp = \sqrt{\frac{\hbar}{m\omega_\perp}}$ [11]. The evolution of the condensate is governed by the quasi one-dimensional GP equation [11, 12]

$$i\hbar \frac{\partial Q}{\partial t} + D_1(t) \frac{\hbar^2}{2m} \frac{\partial^2 Q}{\partial x^2} + \sigma R_1(t) |Q|^2 Q + V(x, t) Q = 0, \quad (4.2)$$

where $Q(x, t)$ represents the macroscopic condensate density, m is the atomic mass, $D_1(t)$ denote the dispersion coefficient, $R_1(t)$ is a measure of nonlinear two body interactions and is associated with the scattering length a_s that can be modulated by Feshbach resonance and $V(x, t)$ is the space and time dependent potential.

Upon normalizing the density $|Q|^2$, length, time and energy in Eq. (4.2) in units of $2a_s$, $a_\perp = \sqrt{\frac{\hbar}{m\omega_\perp}}$, ω_\perp^{-1} , and $\hbar\omega_\perp$ where ω_\perp is the transverse trapping frequency; we get the following effective one-dimensional GP equation with time dependent dispersion ($D(t)$) and nonlinearity ($R(t)$) and time and space dependent potential ($v(x, t)$)

$$i \frac{\partial Q}{\partial t} + \frac{D(t)}{2} \frac{\partial^2 Q}{\partial x^2} + \sigma R(t) |Q|^2 Q + v(x, t) Q = 0. \quad (4.3)$$

The nonlinearity parameter $R(t)$ can be tuned experimentally through the Feshbach resonance [13, 14, 15]. We will obtain the rogue wave solutions for Eq. (4.3) and then we exemplify their management for the different choices of the parameters. This analysis reveals the interesting properties of rogue waves and shows how to get the desired rogue waves at a desired location.

4.3.1 Methodology and rogue wave solutions

In order to obtain the rogue wave solution for Eq. (4.3) we are substituting the following ansatz

$$Q(x, t) = [S(x, t) + iG(x, t)] \exp i\phi(x, t), \quad (4.4)$$

into Eq. (4.3) and on separating the real and imaginary parts we get the set of coupled equations with variable coefficients as

$$\begin{aligned} -G_t - S\phi_t + \frac{D(t)}{2}[S_{xx} - 2\phi_x G_x - \phi_{xx}G - \phi_x^2 S] \\ + R(t)(S^2 + G^2)S + vS = 0. \end{aligned} \quad (4.5)$$

$$\begin{aligned} S_t - G\phi_t + \frac{D(t)}{2}[G_{xx} + 2\phi_x S_x + S\phi_{xx} - \phi_x^2 G] + \\ R(t)(S^2 + G^2)G + vG = 0. \end{aligned} \quad (4.6)$$

Here functions $S(x, t)$, $G(x, t)$ and $\phi(x, t)$ are real.

We introduce new variables $\eta(x, t)$, $\chi(x, t)$ and $\tau(t)$ and employ the similarity transformation for the real functions S , G and ϕ as

$$S(x, t) = M(t)[1 + nP(\eta, \tau)]. \quad (4.7)$$

$$G(x, t) = lM(t)Q(\eta, \tau). \quad (4.8)$$

$$\phi(x, t) = \chi(x, t) + \mu(\tau). \quad (4.9)$$

Here n and l are constants. Substituting these transformations in Eq. (4.5) and Eq. (4.6), we deduce the following conditions

$$\eta_{xx} = 0. \quad (4.10)$$

$$\eta_t + D\chi_x\eta_x = 0. \quad (4.11)$$

$$-\chi_t - \frac{\chi_x^2}{2}D + v = 0. \quad (4.12)$$

$$2M_t + D\chi_{xx}M = 0. \quad (4.13)$$

$$\begin{aligned} -lMQ_\tau\tau_t - M(1 + nP)\mu_\tau\tau_t + n\frac{D}{2}\eta_x^2MP_{\eta\eta} \\ + R(t)[(1 + nP)^2 + l^2Q^2]M^3(1 + nP) = 0. \end{aligned} \quad (4.14)$$

$$\begin{aligned}
& nMP_\tau\tau_t - lMQ\mu_\tau\tau_t + l\frac{D}{2}\eta_x^2MQ_{\eta\eta} \\
& + R(t)[(1+nP)^2 + l^2Q^2]lM^3Q = 0,
\end{aligned} \tag{4.15}$$

where the functions $\eta(x, t)$, $\chi(x, t)$, $M(t)$, $P(\eta, \tau)$, $Q(\eta, \tau)$ need to be determined. Solving Eqs.(4.10-4.13) we obtain

$$\eta = k_1(t)x + k_2(t). \tag{4.16}$$

$$\chi = -\frac{k_{1t}}{2Dk_1}x^2 - \frac{k_{2t}}{Dk_1}x + \chi_0(t). \tag{4.17}$$

$$v = \chi_t + \frac{\chi_x^2}{2}D. \tag{4.18}$$

$$M(t) = k_{10}\sqrt{k_1}, \tag{4.19}$$

where k_{10} is a constant, $k_1(t)$ can be associated with the inverse of pulse width, $k_2(t)$ represents the position of its center of mass and $\chi_0(t)$ is a free function of t . Eq. (4.18) in the explicit form can be written as

$$v = v_2(t)x^2 + v_1(t)x + v_0(t), \tag{4.20}$$

where v_2 , v_1 and v_0 are real functions of time and are given as

$$\begin{aligned}
v_2 &= -\frac{k_{1tt}}{2Dk_1} + \frac{k_{1t}^2}{Dk_1^2} + \frac{k_{1t}D_t}{2D^2k_1}, \\
v_1 &= -\frac{k_{2tt}}{Dk_1} + 2\frac{k_{2t}k_{1t}}{Dk_1^2} + \frac{k_{2t}D_t}{D^2k_1}, v_0 = \frac{k_{2t}^2}{2Dk_1^2}.
\end{aligned} \tag{4.21}$$

Eq. (4.14) and Eq. (4.15) reduce to a set of constant coefficient coupled partial differential equations which are given as:

$$nP_\tau - lQ\mu_0 + lQ_{\eta\eta} + GlQ[l^2Q^2 + (1+nP)^2] = 0. \tag{4.22}$$

$$-lQ_\tau + nP_{\eta\eta} - (1+nP)\mu_0 + G(1+nP)[l^2Q^2 + (1+nP)^2] = 0. \tag{4.23}$$

under the following constraints on $\tau(t)$, $R(t)$ and μ

$$\tau(t) = \int \frac{D}{2}k_1^2 dt, \quad R(t) = \frac{R_0k_1D}{2k_{10}^2}, \tag{4.24}$$

$$\mu = \mu_0 \int \frac{D}{2}k_1^2 dt, \tag{4.25}$$

where μ_0 and R_0 are constants.

Following the approach given in [16, 17] we obtain the simultaneous rational solution of Eq. (4.22) and Eq. (4.23) for $R_0 = 1$ and $\mu_0 = 1$ as

$$\begin{aligned} P(\eta, \tau) &= -\frac{4}{n(1 + 2\eta^2 + 4\tau^2)}, \\ Q(\eta, \tau) &= -\frac{8\tau}{l(1 + 2\eta^2 + 4\tau^2)}. \end{aligned} \quad (4.26)$$

Using Eq. (4.26) in Eqs. (4.7-4.9), the exact rogue wave solution of Eq. (4.3) following Eq. (4.4), can be given as

$$Q = k_{10} \sqrt{k_1} \left[1 - \frac{4 + 8i\tau}{1 + 2\eta^2 + 4\tau^2} \right] \exp[i(\chi + \mu)], \quad (4.27)$$

where η , χ , τ and μ are given by Eqs.(4.16), (4.17), (4.24) and (4.25), respectively.

4.3.2 Management of matter rogue waves

The dynamics of rogue waves can be controlled by suitably managing the parameters k_1 and k_2 . This can be understood by considering the following three examples

(A) If we choose $k_1 = 1.1$, $k_2 = \sin^2 t$ and $D(t) = 3 \cos t$, it represents the propagation of rogue waves on a constant background. The periodic choice of dispersion parameter $D(t)$ results in periodic nonlinearity $R(t)$ and is given as

$$R(t) = 3 \frac{R_0 k_1 \cos t}{2k_{10}^2}. \quad (4.28)$$

The corresponding potential can be worked out by using Eq. (4.18)

$$v(x, t) = -\frac{2x \cos t}{3k_1} + \frac{2 \cos t \sin^2 t}{3k_1}. \quad (4.29)$$

The profile of potential is shown in Fig. 4.1(a), which reveals the quasiperiodic nature of potential. Fig. 4.1(b) reveals that the rogue waves evolve periodically in the presence of linear (in space) potential whose amplitude is sinusoidally modulated in time. Clearly, rogue waves reoccur periodically and propagate without changing their width. The recurrence of rogue waves is due to the periodic functional form of the parameters R , D and k_2 . The rogue wave maintains the constant

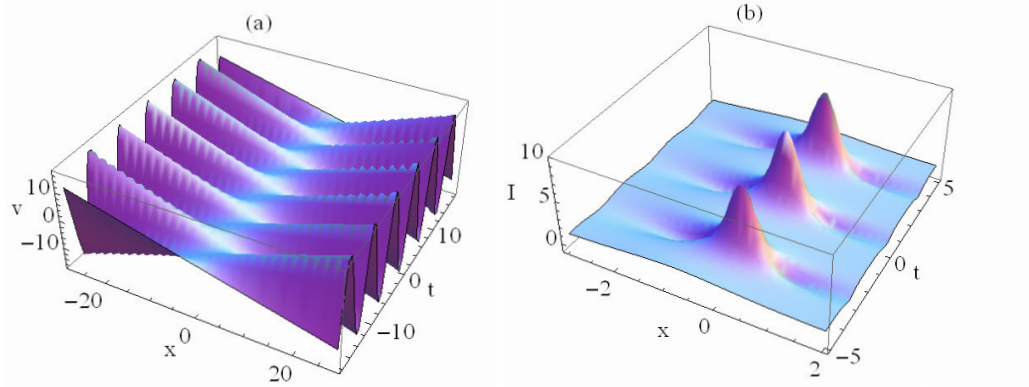


Figure 4.1: (a) The profile of potential for Eq. (4.29) (b) Intensity profile of first-order rogue wave for the parameters $D = 3 \cos t$, $k_1 = 1.1$, $k_2 = \sin^2 t$, $\mu_0 = k_{10} = 1$, $\chi_0 = 0$.

width and amplitude during propagation because of the absence of atomic feeding from the thermal cloud. It is evident that the nonlinearity $R(t)$ is periodic in nature and this variation can be achieved experimentally by using a periodic magnetic or optical field near Feshbach resonance [18, 19, 13]. To be specific, nonlinearity can be positive or negative corresponding to attractive interactions (as in ^7Li [20], ^{85}Rb [21] in the BECs) or repulsive interactions (as in ^{87}Rb , ^{23}Na in the BECs) [11, 22] between the atoms.

(B) If we choose k_1 to be periodic and both the parameters k_2 and β as constants, then it represents the propagation of rogue waves on a periodic background. For $k_1 = 1.1 + \cos t$, $k_2 = D = 1$, the nonlinearity parameter $R(t)$ and potential v read

$$R(t) = \frac{R_0(1.1 + \cos t)}{2k_{10}^2}. \quad (4.30)$$

$$v(x, t) = v_2(t)x^2, \quad (4.31)$$

with

$$v_2(t) = \frac{0.5(1.1 \cos t + \cos^2 t + 2 \sin^2 t)}{(1.1 + \cos t)^2}.$$

For the chosen parameters the intensity profile of rogue wave is plotted in Fig. 4.2. Here, like the previous case, the nonlinearity parameter $R(t)$ is periodic in nature and possesses only the positive value which leads to attractive interactions as in ^7Li or ^{85}Rb case. The potential given by Eq. (4.31) is also time periodic and

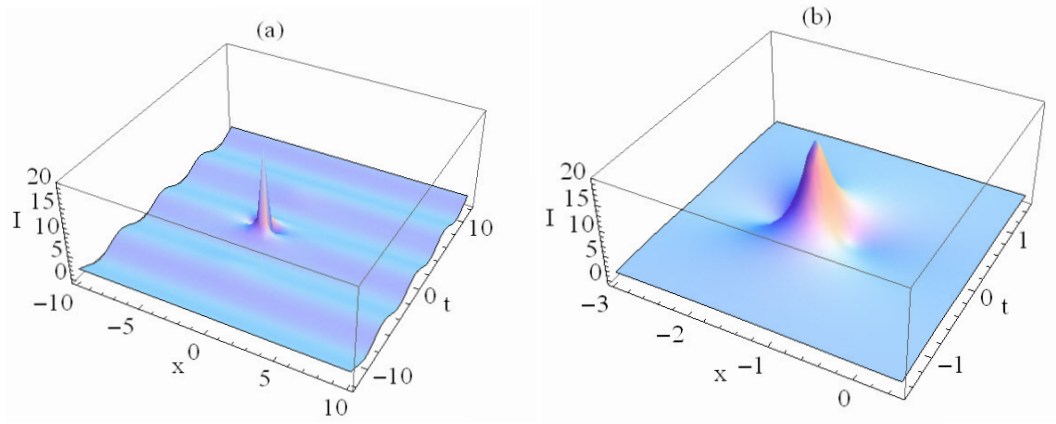


Figure 4.2: Intensity profile of rogue waves with a periodic background (a) shows the periodic background and the rogue wave (b) Detailed local profile of rogue wave. The parameters are $k_1 = 1.1 + \cos t$, $k_2 = 1$, $D = 1$, $\mu_0 = k_{10} = 1$, $\chi_0 = 0$.

can either be confining ($v_2 < 0$) or expulsive ($v_2 > 0$).

(C) If we choose $k_1 = \frac{0.5}{2+h \sin^2(\epsilon(t-t_0))}$ and $k_2 = \sin t$, then they lead to the following form of dispersion and nonlinearity parameters

$$D = 2 + h \sin^2(\epsilon(t - t_0)), \quad R = R_0, \quad (4.32)$$

where $R_0 = \frac{0.25}{k_{10}^2}$.

This specific choice of dispersion and nonlinearity represents the case of non-linear tunneling through periodic dispersion barrier with h as the barrier height ($h > -2$) and ϵ as the barrier width. It should be noted that the condensate is subject to linear potential (in x) for (A) and quadratic potential (in x) for (B) while (C) deals with the scenario when the condensate is subject to the combination of linear and quadratic trapping potential. The exact form of the potential can be worked out by using Eq. (4.20) with

$$v_2 = \epsilon^2 h \frac{1 - 2 \sin^2[\epsilon(t - t_0)]}{(2 + h \sin^2[\epsilon(t - t_0)])^2} - \epsilon^2 h^2 \frac{\sin^2[2\epsilon(t - t_0)]}{(2 + h \sin^2[\epsilon(t - t_0)])^3} + \frac{1}{2} \epsilon^2 h^2 (2 + h \sin^2[\epsilon(t - t_0)]) \frac{\sin^2[2\epsilon(t - t_0)]}{(2 + h \sin^2[\epsilon(t - t_0)])^4},$$

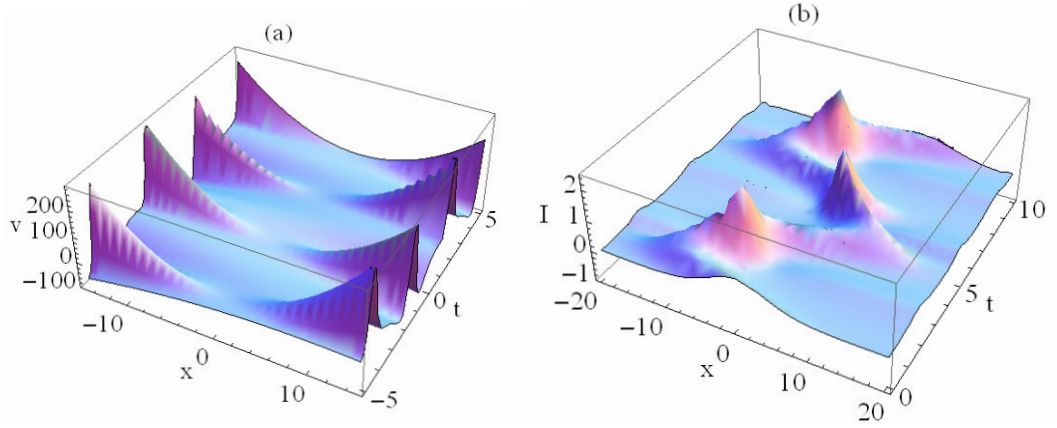


Figure 4.3: (a) The profile of periodic potential (b) Intensity plot of rogue wave for the parameters $k_2 = \sin t$, $\mu_0 = k_{10} = 1$, $\chi_0 = 0$.

$$v_1 = 2 \sin t - 2(2 + h \sin^2[\epsilon(t - t_0)]) \frac{\epsilon h \cos t \sin[2\epsilon(t - t_0)]}{(2 + h \sin^2[\epsilon(t - t_0)])^2}, \quad (4.33)$$

$$v_0 = 2 \cos^2 t (2 + h \sin^2[\epsilon(t - t_0)]).$$

Its profile is plotted in Fig. 4.3(a). For the choice of parameters R , D and k_1 , the condensate is subject to an external quadratic potential which is periodic in nature and gains maximum amplitude whenever it encounters the barrier. With these modulations, the system acquires maximum energy at all the barrier locations and the rogue waves exchanges the energy with the barriers and get amplified whenever it passes through the barrier. This behaviour is depicted in Fig. 4.3(b). The propagation of rogue waves in the presence of quadratic potential is governed by the parameter v_1 which contributes the effect of frequency shift and central positioning term, i.e. through k_1 and k_2 . The choice of k_1 is fixed in order to get the specific dispersion barrier while the rogue waves behaviour will be different for different choices of k_2 , resulting in different functional form of v_1 . Thus, by appropriately managing the location and the height of the barrier, we can get the desired amplitude of the rogue waves at the desired location. Moreover, their propagation can be controlled by suitably choosing the parameter k_2 .

Additionally, we have also investigated the propagation of the rogue waves through the conventional hyperbolic nonlinearity and dispersion barrier through the appro-

appropriate choices of k_1 and k_2 . In case of nonlinearity barrier, the rogue waves are localized while the propagating rogue waves have been predicted for the dispersion barrier case. Moreover, their amplitude management at the barrier location has also been discussed in [23].

4.4 Controlling matter waves by tailoring nonlinearity parameter

In the above section, we have discussed the rogue waves for the NLSE with time varying dispersion and nonlinearity in the presence of space and time dependent trap. Now we consider the case which involves the study of NLSE with time varying scattering length and harmonic trap as it provides the manipulation of matter rogue waves and nonlinear excitations via Feshbach resonance management [24]. In 2005 the dynamics of bright solitons in BECs with time dependent scattering length in an expulsive parabolic trap was studied [25]. If we substitute $D(t) = 1$ and $v(x, t) = \Omega^2(t)x^2$ in Eq. (4.3), it reduces to NLSE with a time varying scattering length and a parabolic trap governing the dynamics of one-dimensional BEC confined by a harmonic potential and given as:

$$i\frac{\partial Q}{\partial t} + \frac{1}{2}\frac{\partial^2 Q}{\partial x^2} + \sigma R(t)|Q|^2Q - \frac{1}{2}\Omega^2(t)x^2Q = 0, \quad (4.34)$$

where the last term $\Omega^2(t)$ is the real valued time dependent parabolic trapping potential. The $\sigma = \pm 1$ corresponds to the attractive or repulsive nonlinear interaction. Eq. (4.34) has been explored by Serkin et al. to study the matter wave solitons in a one-dimensional BEC confined by harmonic trap [7, 8].

In general, it is more difficult to deal with the nonlinear equations with variable coefficients than with the constant coefficients nonlinear equations. To make the analysis simpler, the next step is to reduce the variable coefficient NLSE to the standard NLSE. To do so, we use the following transformation [26]

$$Q(x, t) = A(t)u(X, T) \exp(i\phi(X)), \quad (4.35)$$

It reduces Eq. (4.34) to the following standard NLSE

$$i\frac{\partial u}{\partial T} + \frac{1}{2}\frac{\partial^2 u}{\partial X^2} + |u|^2u = 0, \quad (4.36)$$

with the identifications of

$$\begin{aligned} A(t) &= \sqrt{R(t)}, X = R(t)x, \\ T(t) &= \int_0^t R^2(\tau)d\tau, \phi = -\frac{R'(t)}{2R^3(t)}X^2. \end{aligned} \quad (4.37)$$

Here the nonlinearity control parameter and trapping potential can not be chosen independently. They are related to each other by the relation

$$\Omega^2(t) = \frac{R''(t)}{R(t)} - 2\frac{R'(t)^2}{R^2(t)}, \quad (4.38)$$

where $R'(t)$ and $R''(t)$ represent the first and second-order time derivative of $R(t)$, respectively. Eq. (4.38) is the integrability condition for Eq. (4.34) [7]. The functions $R(t)$ and $\Omega^2(t)$ are real valued and can take positive as well as negative values. The positive (negative) value of $R(t)$ and $\Omega^2(t)$ characterise the attractive (repulsive) nature of the bosonic interactions and the harmonic trap, respectively. Eq. (4.38) is equivalent to defining $\Omega^2(t)$ and $R(t)$ as [7]

$$R(t) = \exp \int_0^t \Gamma(t')dt', \quad (4.39)$$

$$\Omega^2(t) = \frac{\partial \Gamma(t)}{\partial t} - \Gamma^2(t), \quad (4.40)$$

where $\Gamma(t)$ is an arbitrary function of time.

4.4.1 Analytical solutions

Since Eq. (4.34) is reduced to the standard NLSE given by Eq. (4.36) whose 1-soliton, 2-soliton, ABs and rogue wave solutions solutions are well known (discussed in Section 1.1), hence the exact analytical solutions of Eq. (4.34) can be obtained by making use of the transformation given in Eq. (4.35) along with the conditions given in Eqs. (4.37) and (4.38):

1-soliton solutions

For $\sigma = +1$ ($\sigma = -1$), Eq. (4.34) posses the bright (dark) soliton of the form

(i) Bright soliton

$$Q_{1b}(x, t) = 2\sqrt{R(t)}f_0 \operatorname{sech}[2f_0R(t)x + 4v_0f_0 \int_0^t R^2(\tau)d\tau] \exp[-i(2v_0R(t)x + 2(v_0^2 - f_0^2) \int_0^t R^2(\tau)d\tau - i\frac{R'(t)}{2R(t)}x^2)], \quad (4.41)$$

where v_0 and f_0 are constants.

(ii) Dark soliton

$$Q_{1d}(x, t) = 2\sqrt{R(t)}\eta_0(\sqrt{1 - a^2} + ia \tanh[2a\eta_0R(t)x + 4a\eta_0^2\sqrt{1 - a^2} \int_0^t R^2(\tau)d\tau]) \exp[-4i\eta_0^2 \int_0^t R^2(\tau)d\tau - i\frac{R'(t)}{2R(t)}x^2], \quad (4.42)$$

where the parameter $0 < a < 1$ defines the depth of modulation i.e the blackness of gray soliton and its velocity against the background. When $a = 1$, it becomes black.

2-soliton solution

$$Q_{2b}(x, t) = 4\sqrt{R(t)}\frac{N(x, t)}{D(x, t)} \exp[-i\frac{R'(t)}{2R(t)}x^2]. \quad (4.43)$$

with

$$N(x, t) = \cosh \xi_2 \exp(-i\chi_1)[(\kappa_2 - \kappa_1)^2 + 2i\eta_2(\kappa_2 - \kappa_1) \tanh \xi_2 + \eta_1^2 - \eta_2^2] + \eta_2 \cosh \xi_1 \exp(-i\xi_2)[(\kappa_2 - \kappa_1)^2 - 2i\eta_1(\kappa_2 - \kappa_1) \tanh \xi_1 - \eta_1^2 + \eta_2^2]. \quad (4.44)$$

and

$$D(x, t) = \cosh(\xi_1 + \xi_2)[(\kappa_2 - \kappa_1)^2 + (\eta_2 - \eta_1)^2] + \cosh(\xi_1 - \xi_2)[(\kappa_2 - \kappa_1)^2 + (\eta_2 + \eta_1)^2] - 4\eta_1\eta_2 \cos(\chi_2 - \chi_1). \quad (4.45)$$

The arguments and the phases are

$$\xi_i(x, t) = 2\eta_iR(t)x + 4\eta_i\kappa_i \int_0^t R^2(\tau)d\tau, \quad (4.46)$$

$$\chi_i(x, t) = 2\kappa_iR(t)x + 2(\kappa_i^2 - \eta_i^2) \int_0^t R^2(\tau)d\tau,$$

where η_i and κ_i define the amplitude and the velocity of the i^{th} soliton ($i = 1, 2$), respectively.

Akhmediev Breathers

$$Q_{AB}(x, t) = \sqrt{R(t)} \left(\frac{\cos \sqrt{2}R(t)x + i\sqrt{2} \sinh \int_0^t R^2(\tau) d\tau}{\cos \sqrt{2}R(t)x - \sqrt{2} \cosh \int_0^t R^2(\tau) d\tau} \right) \exp \left[i(-R'(t) \frac{x^2}{2R(t)} + \int_0^t R^2(\tau) d\tau) \right]. \quad (4.47)$$

Rogue waves

$$Q_r(x, t) = \sqrt{R(t)} \left(1 - 4 \frac{1 + 2i(\int_0^t R^2(\tau) d\tau)}{1 + 4(\int_0^t R^2(\tau) d\tau)^2 + 4(R(t)x)^2} \right) \exp \left[i(-R'(t) \frac{x^2}{2R(t)} + \int_0^t R^2(\tau) d\tau) \right]. \quad (4.48)$$

4.4.2 Construction of a family of $R(t)$ ($\widehat{R}(t)$) through Riccati parameterization

Identifying Eq. (4.40) as a Riccati equation enables us to generate the class for $R(t)$. To construct the family, we choose

$$\widehat{\Gamma}(t) = \Gamma(t) + \nu(t). \quad (4.49)$$

Demanding that $\widehat{\Gamma}(t)$ gives rise to the same trapping potential, substituting Eq. (4.49) in Eq. (4.40) yields

$$\nu'(t) - \nu^2 - 2\Gamma\nu = 0. \quad (4.50)$$

In order to work out the solution for ν , we introduce the function $y(t) = \frac{1}{\nu}$ which results in the following equation

$$y' + 2\Gamma y + 1 = 0, \quad (4.51)$$

whose solution is given as [27]

$$y(t) = (\exp \int -2\Gamma(t) dt \left[-1 \int \left(\exp \int 2\Gamma(t) dt \right) dt + \lambda \right]). \quad (4.52)$$

The resulting expression for $\nu(t)$ is given as follows

$$\nu(t) = \left(\exp \int -2\Gamma(t) dt \left[-1 \int \left(\exp \int 2\Gamma(t) dt \right) dt + \lambda \right] \right)^{-1}. \quad (4.53)$$

where λ is a constant of integration, also known as the Riccati parameter, has to be chosen in such a way so as to avoid singularities.

It should be noted that for $\widehat{\Gamma}(t)$ a class of the nonlinearity parameter $\widehat{R}(t)$ can be generated by using Eq. (4.39). The integrability condition Eq. (4.38) is still satisfied, hence the analytical solutions of Eq. (4.34) for $\widehat{R}(t)$ is given by Eqs. (4.41-4.48) by replacing $R(t)$ with $\widehat{R}(t)$. The introduction of the Riccati parameter λ allows us to tune the intensity profiles of matter waves. We demonstrate this in the next section.

4.4.3 Riccati parameterized self-similar matter waves in BEC

We demonstrate the role of Riccati parameter λ by considering the following example

$$\Gamma = -n\gamma_3 \tanh \gamma_3 t, \quad (4.54)$$

where γ_3 is a constant. We shall illustrate for the cases $n = 1, 2$.

Case I For $n = 1$, Eqs. (4.39) and (4.40) yield nonlinearity control parameter and the corresponding trapping potential as

$$R(t) = \operatorname{sech} \gamma t, \quad (4.55)$$

$$\Omega^2(t) = -\gamma^2. \quad (4.56)$$

Eq. (4.56) implies that the condensate is subjected to constant expulsive harmonic potential which has been used to study the dynamics of bright solitons and matter rogue waves in BEC [25, 28]. Following Eqs. (4.49)-(4.53), the $\widehat{\Gamma}(t)$ and $\widehat{R}(t)$ can be given as

$$\widehat{\Gamma}(t) = -\gamma \tanh\left(\gamma t - \tanh^{-1} \frac{1}{\lambda\gamma}\right), \quad (4.57)$$

$$\widehat{R}(t) = \operatorname{sech}\left(\gamma t - \tanh^{-1} \frac{1}{\lambda\gamma}\right). \quad (4.58)$$

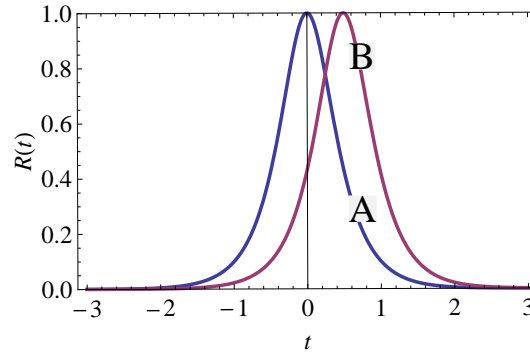


Figure 4.4: Profile of nonlinearity control parameter: Curve A is for $R(t)$ given by Eq. (4.55). Curve B is for $\widehat{R}(t)$ given by Eq. (4.58) and $\lambda = 0.37$. $\gamma = 3$ for both the curves.

Clearly $\widehat{R}(t)$ is translated, which is demonstrated in Fig. 4.4. Similar corroborations have been inferred, even from the stability analysis of sine-Gordon model [29]. We have plotted the intensity profiles of all the solutions in Fig. 4.5 corresponding to $R(t)$. In this case, $\widehat{R}(t)$ is the translated form of $R(t)$ so the presence of λ is not lending any change in the intensity profiles of solitons, ABs and rogue waves. Consequently, the intensity plots corresponding to $\widehat{R}(t)$ will be similar to the ones as shown in Fig. 4.5.

Case II For $n = 2$, Eqs. (4.39) and (4.40) yield the nonlinearity control parameter and the corresponding trapping potential as

$$R(t) = \text{sech}^2 \gamma t, \quad (4.59)$$

$$\Omega^2(t) = -2\gamma^2(2 - \text{sech}^2 \gamma t). \quad (4.60)$$

Eq. (4.60) refers to the time dependent expulsive nature of the harmonic trap and such a trap has been realized in [30].

The class for $\widehat{\Gamma}(t)$ by using Eq. (4.49) and Eq. (4.53) is given as

$$\widehat{\Gamma}(t) = -2\gamma \tanh \gamma t + \frac{\gamma \text{sech}^4 \gamma t}{\lambda \gamma - \tanh \gamma t + \frac{\tanh^3 \gamma t}{3}}. \quad (4.61)$$

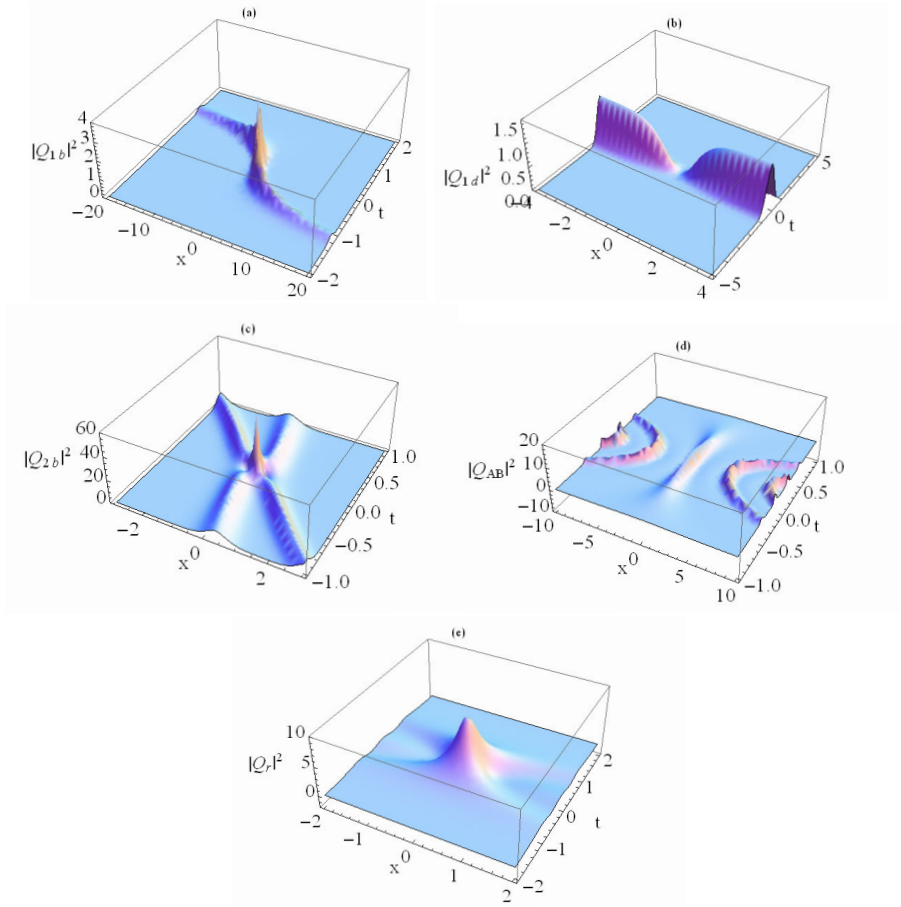


Figure 4.5: Intensity plots corresponding to $R(t)$ for (a) bright soliton (b) dark soliton (c) 2-soliton (d) AB (e) rogue waves. The parameter $\gamma = 3$ for all of these plots.

Hence, $\widehat{R}(t)$ is defined as

$$\widehat{R}(t) = \frac{k \operatorname{sech}^2 \gamma t}{\lambda \gamma - \tanh \gamma t + \frac{\tanh^3 \gamma t}{3}}, \quad (4.62)$$

where $k = \frac{-\tanh(\gamma t_0) + \frac{\tanh^3(\gamma t_0)}{3} + \lambda \gamma}{\operatorname{sech} \gamma t_0}$ and $\lambda \gamma \notin [-0.67, 0.67]$.

The effect of λ on the varying in time nonlinearity is incorporated in Fig. 4.6(a) and the parabolic potential is shown in Fig. 4.6(b).

Unlike the first case, the amplitude of $R(t)$ can be controlled through λ here. To understand its role we have plotted the Figs. 4.7 and 4.8 which depict the intensity profiles of solitons, ABs and rogue waves corresponding to $R(t)$ as well as

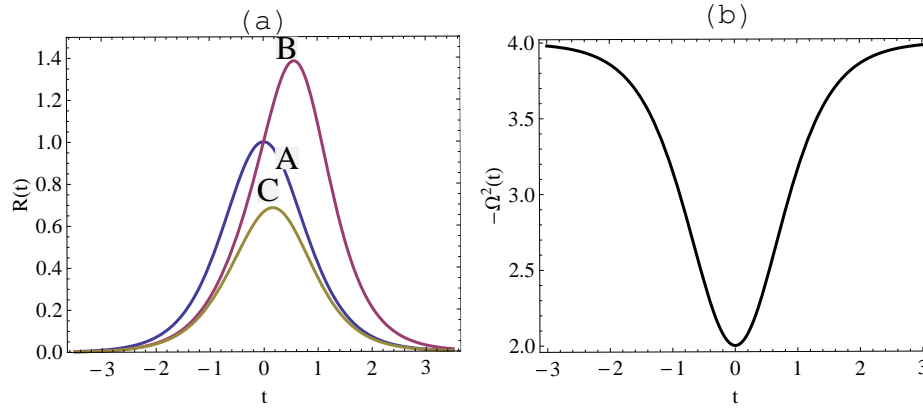


Figure 4.6: (a) Variation of nonlinearity control parameter: Curve A shows $R(t)$ given by Eq. (4.59), Curve B and C are the plots for $\widehat{R}(t)$ given by Eq. (4.62) with $\lambda = 0.8$ and $\lambda = 2$, respectively (b) plot of trapping potential, given by Eq. (4.60), of both the plots, $\gamma = 2$.

$\widehat{R}(t)$. Figs. 4.7 and 4.8 infer that the amplitude of the solitons and rogue waves can be tuned through λ while in the case of breathers, presence of λ enables us to control their frequency with a slight variation in their amplitude. To understand the reason beyond it one needs to consider the analytical expressions of the various solutions given in Eqs. (4.41)-(4.48). The analytical treatment of the solutions of solitons and rogue waves corresponding to $\widehat{R}(t)$ reveals that the amplitude tuning is taking place due to the presence of $\widehat{R}(t)$ and $\int_0^t \widehat{R}^2(\tau) d\tau$ that in turn depend on $\lambda\gamma$. The magnitude of $\widehat{R}(t)$ and $\int_0^t \widehat{R}^2(\tau) d\tau$ will be larger at a finite positive value of t for the smaller value of the product $\lambda\gamma$, and vice-versa. So the small value of the product $\lambda\gamma$ leads to the large amplitude of the intensity profile of the pulse in comparison to the case without Riccati generalization. On the other hand the in case of ABs, we consider the expression given in Eq. (4.47) by replacing $R(t)$ with $\widehat{R}(t)$ which shows that the intensity $|Q_{AB}|^2$ is comprised of two terms, one containing the trigonometric part and the other one containing the hyperbolic part. The argument in the cosine term is dependent on $\widehat{R}(t)$ which in turn depends on λ and γ that are responsible for the frequency/number of peaks appearing in the finite range of x . The remaining hyperbolic part and the nonlinearity parameter, appearing explicitly in the expression of intensity of breathers Eq. (4.47), are responsible for their slight amplitude variation. Clearly Eq. (4.62) reveals that the

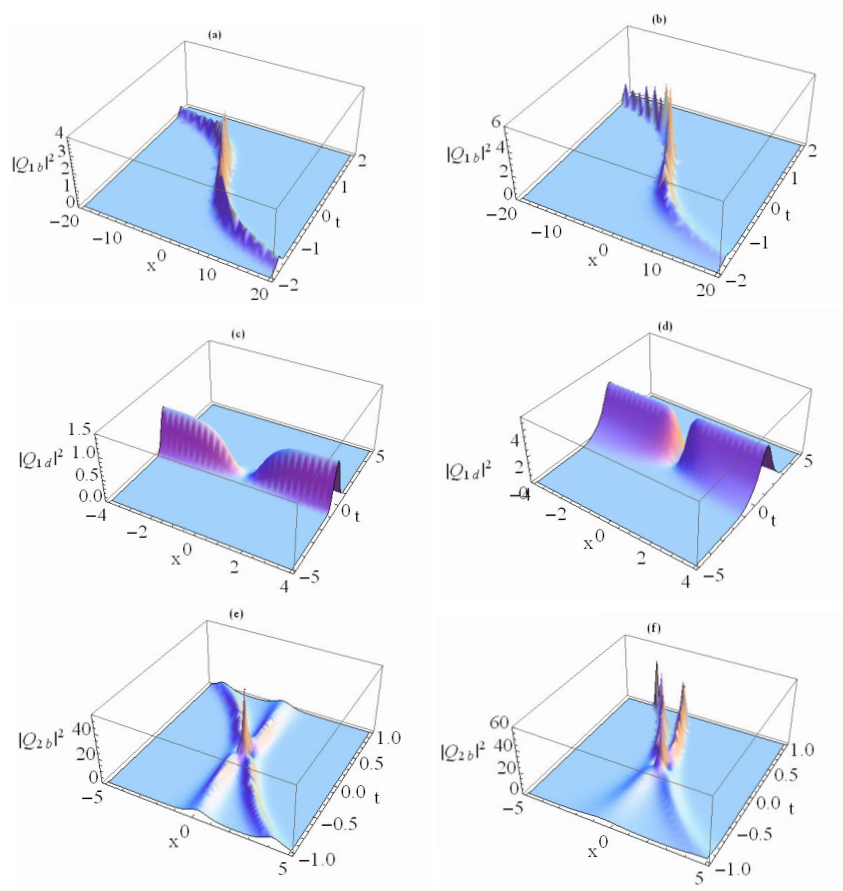


Figure 4.7: Intensity profiles corresponding to $R(t)$ are shown in (a),(c),(e) for bright soliton, dark soliton, 2-solitons, respectively. Profiles corresponding to $\widehat{R}(t)$ for bright ((b) with $\lambda = 0.9$), dark ((d) with $\lambda = 0.7$), 2-soliton ((f) with $\lambda = 0.7$, $\eta_1 = 2$, $\eta_2 = 1.8$, $\kappa_1 = 1$, $\kappa_2 = 0.5$). The parameter $\gamma = 1$ in all these plots.

higher the value of $\lambda\gamma$, the smaller will be $\widehat{R}(t)$ at a fixed finite positive t and vice-versa. This in turn implies that for large value of $\lambda\gamma$ the magnitude of the intensity profile and the argument of cosine term will be smaller for a finite positive value of t because of the small value of $\widehat{R}(t)$ as compared to the small value of $\lambda\gamma$ which results in a lesser number of peaks with slightly less amplitude. Moreover, if we kept on increasing the value of $\lambda\gamma$, the $\widehat{R}(t)$ will tend to approach to $R(t)$ and the intensity profiles corresponding to $\widehat{R}(t)$ case will tend to become as if there is no Riccati generalization.

It is worthy to mention that the similar results as discussed for $n = 2$ case has been

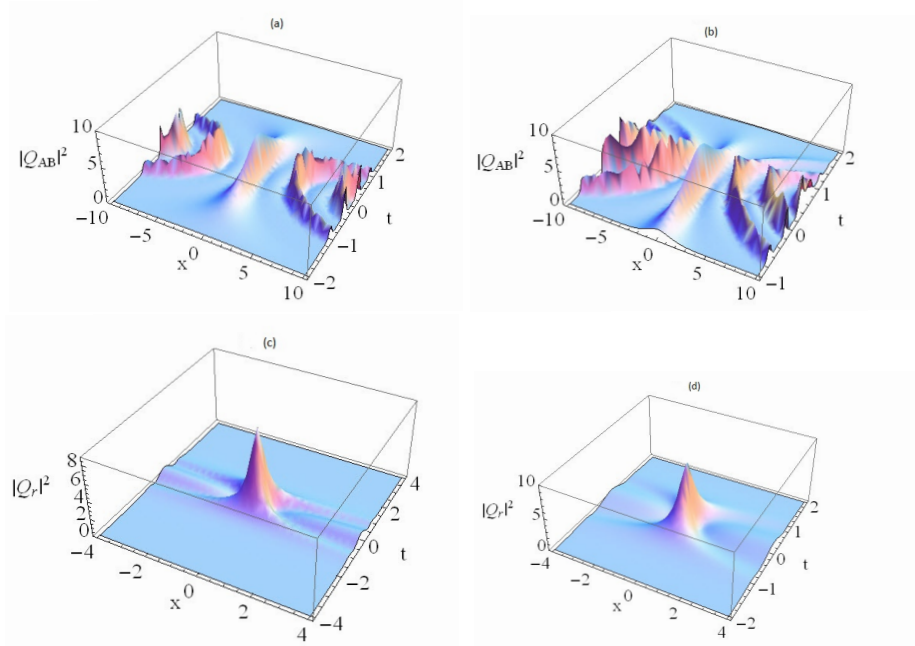


Figure 4.8: Intensity profiles corresponding to $R(t)$ are shown in (a),(c) (i) for ABs and rogue wave. Profiles corresponding to $\widehat{R}(t)$ for AB ((b) with $\lambda = 1$), rogue waves ((d) with $\lambda = 0.7$). The parameter $\gamma = 1$ in all these plots.

obtained for $n = 3$ case. The detailed analysis for $n = 3$ case has been shown in [10].

4.5 Conclusion

The whole chapter has been divided into two parts. In the first part we have obtained the matter rogue wave solution for quasi-one-dimensional GP equation which describes the evolution of cigar shaped BECs. The solution has been obtained by using a direct ansatz and similarity transformation. Here, we have demonstrated through three examples that the matter rogue waves can be controlled by suitably choosing the parameters k_1 and k_2 . For the first one BECs have been studied in the presence of linear in space potential whose amplitude is modulated in time, while for the second example the potential is quadratic in space and can either be confining or expulsive. The rogue waves evolve periodically on

a constant background for the former and the localized rogue waves on the periodic background has been obtained for the later. The third example comprises of the study of BECs in the presence of linear and quadratic external potential. The choice of the parameter k_1 made in this scenario corresponds to the nonlinear tunneling of rogue waves through the periodic dispersion barrier. We have shown that by suitably choosing the location and the height of the barrier, the rogue waves of desired amplitude at the desired location can be obtained. The second half of the chapter dealt with the special case of quasi-one-dimensional GP equation ($D(t) = 1, v(x, t) = \Omega^2(t)x^2$). Here, we have obtained the class of Riccati generalized self-similar matter wave solutions by using self-similarity transformation and isospectral Hamiltonian technique. The class of analytical solutions have been obtained by generating the class of nonlinearity parameter within the integrability framework for the same trapping potential, by introducing Riccati parameter λ . We have demonstrated that presence of λ allows us to control the intensity profiles of the self-similar matter waves. Since, the control on the intensity profiles has been obtained by creating the class of nonlinearity parameter, which in turn associated with the interatomic interactions in BEC and can be easily manipulated experimentally through Feshbach resonance. Hence, our results can be amenable to experimentalists too.

The work presented here has been published in [23, 10].

Bibliography

- [1] M H Anderson, J R Ensher, M R Matthews, C E Wieman, and E A Cornell. Observation of Bose-Einstein condensation in a dilute atomic vapor. *Science*, 269(5221): 198-201, 1995.
- [2] K B Davis, M O Mewes, M R Andrews, N J V Druten, D S Durfee, D M Kurn, and W Ketterle. Bose-Einstein condensation in a gas of sodium atoms. *Physical Review Letters*, 75(22): 3969, 1995.
- [3] C C Bradley, C A Sackett, J J Tollett, and R G Hulet. Evidence of Bose-Einstein condensation in an atomic gas with attractive interactions. *Physical Review Letters*, 75(9): 1687, 1995.
- [4] G R Carretero, D J Frantzeskakis, and P G Kevrekidis. Nonlinear waves in Bose-Einstein condensates: physical relevance and mathematical techniques. *Nonlinearity*, 21(7): R139, 2008.
- [5] J Belmonte-Beitia, V M Pérez-Garcia, V Vekslerchik, and V V Konotop. Localized nonlinear waves in systems with time-and space-modulated nonlinearities. *Physical Review Letters*, 100(16): 164102, 2008.
- [6] Z Yan, X F Zhang, and W M Liu. Nonautonomous matter waves in a waveguide. *Physical Review A*, 84(2): 023627, 2011.
- [7] V N Serkin, A Hasegawa, and T L Belyaeva. Nonautonomous matter-wave solitons near the Feshbach resonance. *Physical Review A*, 81(2): 023610, 2010.
- [8] V N Serkin, A Hasegawa, and T L Belyaeva. Solitary waves in nonautonomous nonlinear and dispersive systems: nonautonomous solitons. *Journal of Modern Optics*, 57(14-15): 1456-1472, 2010.

- [9] R Radha, V R Kumar, and K Porsezian. Remote controlling the dynamics of Bose-Einstein condensates through time-dependent atomic feeding and trap. *Journal of Physics A: Mathematical and Theoretical*, 41(31): 315209, 2008.
- [10] R Gupta, S Loomba, and C N Kumar. Class of nonlinearity control parameter for bright solitons of non-autonomous NLSE with trapping potential. *IEEE Journal of Quantum Electronics*, 48(7): 847-851, 2012.
- [11] F Kh Abdullaev, A M Kamchatnov, V V Konotop, and V A Brazhnyi. Adiabatic dynamics of periodic waves in Bose-Einstein condensates with time dependent atomic scattering length. *Physical Review Letters*, 90(23): 230402, 2003.
- [12] D J Frantzeskakis. Dark solitons in atomic Bose-Einstein condensates: from theory to experiments. *Journal of Physics A: Mathematical and Theoretical*, 43(21): 213001, 2010.
- [13] S L Cornish, N R Claussen, J L Roberts, E A Cornell, and C E Wieman. Stable ^{85}Rb Bose-Einstein condensates with widely tunable interactions. *Physical Review Letters*, 85(9): 1795, 2000.
- [14] J Stenger, S Inouye, M R Andrews, H J Miesner, D M Stamper-Kurn, and W Ketterle. Strongly enhanced inelastic collisions in a Bose-Einstein condensate near Feshbach resonances. *Physical Review Letters*, 82(12): 2422, 1999.
- [15] J L Roberts, N R Claussen, J P Burke, C H Greene, E A Cornell, and C E Wieman. Resonant magnetic field control of elastic scattering in cold ^{85}Rb . *Physical Review Letters*, 81(23): 5109, 1998.
- [16] N Akhmediev, A Ankiewicz, and J M Soto-Crespo. Rogue waves and rational solutions of the nonlinear Schrödinger equation. *Physical Review E*, 80(2): 026601, 2009.
- [17] N Akhmediev, A Ankiewicz, and M Taki. Waves that appear from nowhere and disappear without a trace. *Physics Letters A*, 373(6): 675-678, 2009.

- [18] S Inouye, M R Andrews, J Stenger, H J Miesner, D M Stamper-Kurn, and W Ketterle. Observation of Feshbach resonances in a Bose-Einstein condensate. *Nature*, 392(6672): 151-154, 1998.
- [19] F K Fatemi, K M Jones, and P D Lett. Observation of optically induced Feshbach resonances in collisions of cold atoms. *Physical Review Letters*, 85(21): 4462, 2000.
- [20] K E Strecker, G B Partridge, A G Truscott, and R G Hulet. Formation and propagation of matter-wave soliton trains. *Nature*, 417(6885): 150-153, 2002.
- [21] S L Cornish, S T Thompson, and C E Wieman. Formation of bright matter-wave solitons during the collapse of attractive Bose-Einstein condensates. *Physical Review Letters*, 96(17): 170401, 2006.
- [22] P G Kevrekidis, D J Frantzeskakis, and R Carretero-Gonzalez. *Emergent Nonlinear Phenomena in Bose-Einstein Condensates: Theory and Experiment*. Springer, New York, 2008.
- [23] S Loomba, H Kaur, R Gupta, C N Kumar, and T S Raju. Controlling rogue waves in inhomogeneous Bose-Einstein condensates. *Physical Review E*, 89(5): 052915, 2014.
- [24] D E Pelinovsky, P G Kevrekidis, and D J Frantzeskakis. Averaging for solitons with nonlinearity management. *Physical Review Letters*, 91(24): 240201, 2003.
- [25] Z X Liang, Z D Zhang, and W M Liu. Dynamics of a bright soliton in Bose-Einstein condensates with time-dependent atomic scattering length in an expulsive parabolic potential. *Physical Review Letters*, 94(5): 050402, 2005.
- [26] T L Belyaeva, and V N Serkin. *Hydrodynamics-Advanced Topics*, edited by Harry Schulz. Intech, Rijeka, Croatia, 2011.
- [27] C N Kumar. Isospectral Hamiltonians: generation of the soliton profile. *Journal of Physics A: Mathematical and General*, 20(15): 5397, 1987.

- [28] L Wen, L Li, Z D Li, S W Song, X F Zhang, and W M Liu. Matter rogue wave in Bose-Einstein condensates with attractive atomic interaction. *The European Physical Journal D-Atomic, Molecular, Optical and Plasma Physics*, 64(2): 473-478, 2011.
- [29] B Dey, and C N Kumar. New sets of kink-bearing Hamiltonians. *International Journal of Modern Physics A*, 9(15): 26992705, 1994.
- [30] V R Kumar, R Radha and P K Panigrahi. Matter wave interference pattern in the collision of bright solitons. *Physics Letters A*, 373(47): 4381-4385, 2009; V R Kumar, R Radha and P K Panigrahi. Dynamics of Bose-Einstein condensates in a time-dependent trap. *Physical Review A*, 77(2): 023611, 2008; A Khan, R Atre and P K Panigrahi. Complex envelope soliton in Bose-Einstein condensate with time dependent scattering length. *arXiv preprint cond-mat/0612436*, 2006.

Chapter 5

Summary and conclusions

This thesis comprises of the study of the family of soliton solutions such as bright and dark solitons, similaritons and their pairs, Akhmediev breathers, Peregrine solitons (rogue waves) and their generalization in two different areas, namely nonlinear fiber optics and Bose-Einstein condensates (BECs). These systems are modelled by the nonlinear Schrödinger equation (NLSE) and its variants, irrespective of the origin of the nonlinear and the dispersive terms. In general, the various nonlinear systems governed by the constant-coefficient NLSE and its variants are highly idealized. In realistic conditions, there are several factors like density fluctuations, manufacturing defects, environmental fluctuations, interatomic interactions, etc. which causes the deviation from the actual system. Therefore, the variable-coefficient NLSE, termed as generalized NLSE (GNLSE) are more realistic than their constant-coefficient counterparts in understanding the dynamics of a nonlinear physical system. Here, we have studied the possible localized nonlinear excitations for the variants of GNLSE which correspond to different nonlinear systems. In the field of nonlinear optics, the coefficients are Z (propagation distance) dependent and in BECs they are t (time) dependent. All the systems modelled by GNLSE may not be integrable but a few cases have been reported in literature where the integrability conditions for the variable coefficient NLSE or GNLSE have been mentioned. For instance, it has been shown that the relation between the trapping potential and the nonlinearity parameter represents the integrability condition for the nonautonomous NLSE [Serkin *et al.*, Phys. Rev. A 81 (2010) 023610].

Chapter 2 involves the study of rogue waves in the context of nonlinear optics

and has been divided into two parts. The first part deals with various nonlinear optical fibers and the second part deals with the tapered graded-index nonlinear waveguide. The rogue wave solutions for the different GNLSE models have been obtained by using similarity transformation. We have revealed that these waves can appear with constant, increasing, or decreasing amplitude depending upon the choices of the system parameters corresponding to periodically distributed fiber, dispersion increasing and dispersion decreasing fiber, respectively. However, in all these cases, the rogue waves preserve their width. As the nonlinear pulses propagate through optical fibers, they suffer losses due to absorption and scattering. For the effective signal transmission these losses need to be compensated. It was predicted that these losses can be surmounted by doping the fiber core with erbium atoms. This system is modelled by the coupled nonlinear Schrödinger equation and Maxwell-Bloch equations (NLS-MB). We have studied the rogue waves for the variable-coefficient NLS-MB model and predicted a mechanism that enables us to get the recurrence and annihilation characteristics of rogue waves at the desired propagation distance for the periodic choices of the system parameters. After that, we have exploited the analogy between “dispersion in time” (for fibers) and “diffraction in space” (for waveguides) and worked out the optical rogons for the tapered graded-index nonlinear waveguide. Upon obtaining the analytical solutions, we have depicted the various management regimes of optical rogons for the periodic and the hyperbolic tapering and revealed their interesting properties. While studying the nonlinearity management case, we have found that the tapering and the width function relation resembles with the Schrödinger equation of quantum mechanics. This observation allows us to identify a large manifold of allowed tapering profiles by invoking the isospectral Hamiltonian technique. These tapering profiles are governed by a free Riccati parameter λ which enables us to tune the amplitude and the width of optical rogons. It is realized that the modulation of the tapering profile through Riccati parametrization imposes a significant effect on the intensity profile of rogue waves which paves the way for the experimental realization of highly energetic pulses for various practical applications. The analytical studies of rogue waves made in this chapter through different nonlinear systems helps in enhancing the experimental investigation of rogue waves.

In Chapter 3 we have further extended the study of tapered graded-index nonlinear

waveguides for optical similaritons. We have investigated their nonlinear tunneling properties for two cases (i) constant background (ii) exponential background. For the former, we have found that the amplitude of the similaritons is increased or decreased at barrier location, depending upon whether they are propagating through dispersion barrier (well) or nonlinearity barrier (well). For the latter case, we have shown that the optical similariton pulses get compressed after crossing the barrier. This pulse compression feature of optical similaritons have been extended to cascade pulse compression by letting the pulses to propagate through multiple barriers. We have noticed that at the barrier (well) location, the amplitude of similaritons is increased (decreased) and after crossing the first barrier (well) they get compressed. When they reach the second barrier (well), their amplitude is increased (decreased) even further and after crossing the second barrier the pulses are even more compressed. Thus, by allowing the similaritons to pass through a number of barriers we can get the similaritons of desired width and intensity. This can find applications in optical devices based on optical similaritons.

In Chapter 4, we have investigated the propagation of self-similar matter waves for nonautonomous quasi-one-dimensional Gross-Pitaevskii (GP) equation with space and time dependent external potential, governing the dynamics of waves in a cigar shaped BEC. We have demonstrated the interesting features of controllable rogue waves for three cases. For the first case, the condensate is subjected to a linear trapping potential with periodic nonlinearity that can be positive or negative, characterizing the attractive interactions in ^7Li or repulsive interactions in ^{87}Rb , resulting in the periodic evolution of rogue waves on the constant background. For the second case, the condensate is subjected to a quadratic trapping potential with positive periodic nonlinearity which leads to attractive interactions and results in the localized rogue waves on a periodic background. For the third case, the condensate is considered to be under the combined effect of linear and quadratic potential. It corresponds to the case of nonlinear tunneling through periodic barrier and upon appropriately choosing the location and the height of the barrier we can get the desired amplitude of rogue waves at the desired location. We have then dealt with the special case of quasi-one-dimensional GP equation which describes

the scenario in which the condensate is trapped in an expulsive harmonic trap. By using similarity transformation within the integrability framework, we have obtained the self-similar matter wave solutions involving bright and dark solitons, 2-solitons, Akhmediev breathers (ABs) and rogue waves. In the process of solving the equation analytically, we have found that the structure of expulsive parabolic trap equation is of Riccati type, which allows us to invoke the isospectral Hamiltonian approach to generate a class of nonlinearity parameter for a given trapping potential. This Riccati generalization enables us to control the intensity profiles of various self-similar matter waves by tuning the Riccati parameter. A direct application of this is in the generation of highly energetic self-similar waves in BEC by tuning the interatomic interactions which are experimentally feasible through Feshbach resonance.

Apart from the above mentioned works, we have also studied the soliton propagations in negative index materials (NIMs). These materials have been designed to possess unique properties that are not present in naturally occurring materials, thus offering entirely new prospects in manipulating light. Recently, a great deal of research has taken place to study the propagation of electromagnetic waves in NIMs because of the realization of NIMs in infrared and optical frequency regime. We have presented the bright soliton and 2-soliton solutions for NLSE by including self-steepening effect with dispersive permittivity and permeability in NIMs. The exact solutions have been worked out by using Lax pair and Darboux transformation technique and have been explicitly investigated the role of self-steepening parameter on the intensity profile of solitons [Loomba *et al.*, Eur. Phys. J. D 68 (2014) 1-6]. Being artificially constructed materials, NIMs give us the flexibility to control the pulse propagation through them. The analytical solutions obtained here will be advantageous in experimentally studying the soliton propagation through NIMs.

To conclude, this thesis presents the analytical study of the localized solutions and their management for the variable coefficient GNLSE and its variants which finds applications in studying the pulse dynamics through different nonlinear systems. In general, the rogue waves, obtained for constant coefficient NLSE, are

high intensity waves which are localized in space and time and have been associated with supercontinuum generation. Here, we have demonstrated that by suitably controlling the system parameters we can get the controllable rogue waves which can be localized in one co-ordinate and reoccur in the other co-ordinate. In the context of nonlinear fiber optics, we have found that the rogue waves are localized in time and appear periodically with propagation distance Z along the fiber or waveguide, while, in the context of BECs, these waves are localized in space and appear periodically with time. Thus, the analytical results discussed in this thesis for rogue waves in different nonlinear optical fibers and tapered graded-index nonlinear waveguide may be implemented to investigate these waves experimentally. The study presented on optical similaritons which are self-similar waves may find applications in nonlinear devices where communication is based on these kind of pulses. We have also discussed the propagation and the management of self-similar waves in the context of BEC and expect that these results can be realized experimentally with the advancement in experimental techniques that enable us to control the effective interaction in BEC via Feshbach resonance.

List of publications

Papers in refereed journals

1. **S. Loomba**, M. Rajan, R. Gupta, H. Kaur and C. N. Kumar, Nonlinear tunneling of optical similaritons in a tapered graded-index nonlinear waveguide, *Optics Communications* 324 (2014) 286.
2. **S. Loomba**, R. Gupta, H. Kaur and M. S. M. Rajan, Self-similar rogue waves in an inhomogeneous generalized nonlinear Schrödinger equation, *Physics Letters A* 378 (2014) 2137.
3. **S. Loomba**, M. S. M. Rajan, R. Gupta and A. Mahalingam, Soliton propagation in negative-index materials with self-steepening effect, *The European Physical Journal D* 68 (2014)1.
4. **S. Loomba**, H. Kaur, R. Gupta, C. N. Kumar and T. S. Raju, Controlling rogue waves in inhomogeneous Bose-Einstein condensates, *Physical Review E* 89 (2014) 052915.
5. **S. Loomba** and H. Kaur, Optical rogue waves for the inhomogeneous generalized nonlinear Schrödinger equation, *Physical Review E* 88 (2013) 062903.
6. **S. Loomba**, R. Gupta, C. N. Kumar and D. Milovic, Optical rogons for inhomogeneous nonlinear Schrödinger equation with inter modal dispersion, *Applied Mathematics and Computation* 225 (2013)318.
7. R. Gupta, **S. Loomba** and C. N. Kumar, Class of nonlinearity control parameter for bright solitons of non-autonomous NLSE with trapping potential, *IEEE Journal of Quantum Electronics* 48 (2012) 847.
8. A. Goyal, R. Gupta, **S. Loomba** and C. N. Kumar, Riccati parameterized self-similar waves in tapered graded-index waveguides, *Physics Letters A* 376 (2012) 3454.
9. C. N. Kumar, R. Gupta, A. Goyal, **S. Loomba**, T. S. Raju and P. K. Pani-grahi, Controlled giant rogue waves in nonlinear fiber optics, *Physical Review A* 86 (2012) 025802.

10. **S. Loomba**, H. Kaur, R. Gupta and C. N. Kumar, Chirped bright and dark solitons for NLSE with localized dissipation, *Journal of Mathematics and System Science* 4 (2014) 491.
11. **S. Loomba**, R. Gupta, K. De, C. N. Kumar and T.S.Raju, Controllable bright and dark rogue waves in inhomogeneous erbium doped fibers, *Optical Fiber Technology* (2014), DOI: 10.1016/j.yofte.2014.07.006.
12. **S. Loomba**, R. Gupta, C. N. Kumar, T. S. Raju and P. K. Panigrahi, Combined control of Akhmediev breather frequency and rogue wave amplitude: an analytical approach, Manuscript submitted to *Chaos, Solitons and Fractals*, 2014.

Papers in conferences and workshops

1. **S. Loomba**, H. Kaur and R. Gupta, Bright and Dark solitons for NLSE with self steepening and localized dissipation, *8th conference on nonlinear systems and dynamics*, Indian Institute of Technology, Indore, December 11-14, 2013.
2. **S. Loomba**, R. Gupta and C. N. Kumar, Solitons and periodic solutions of nonlinear Schrödinger equation for negative-index materials *37th National Symposium of Optical Society of India*, Pondicherry University, Puducherry, January 23-25, 2013.
3. R. Gupta, **S. Loomba** and C. N. Kumar, Analytical solutions of Nonlinear Schrödinger Equation for Negative Index Metamaterials, *6th Chandigarh Science Congress*, Panjab University, Chandigarh, February 26-28, 2012.
4. R. Gupta, **S. Loomba** and C. N. Kumar, Controlling nonautonomous 1-and 2-soliton solutions in Bose-Einstein Condensates, *DAE-BRNS Symposium on Atomic, Molecular and Optical Physics*, IISER, Kolkata, December 14-17, 2012.

5. R. Gupta, **S. Loomba** and C. N. Kumar, Solitary wave solutions of nonlinear reaction-diffusion equations with variable coefficients, 5th **Chandigarh Science Congress**, Panjab University, Chandigarh, February 26-28, 2011.
6. A. Goyal, **S. Loomba** and C. N. Kumar, Solutions of sine-Gordon-type equations using algebraic method, 4th **Chandigarh Science Congress**, Panjab University, March 19-20, 2010.

Selected Reprints